Physical chemical properties of selected pharmaceutical co-crystals
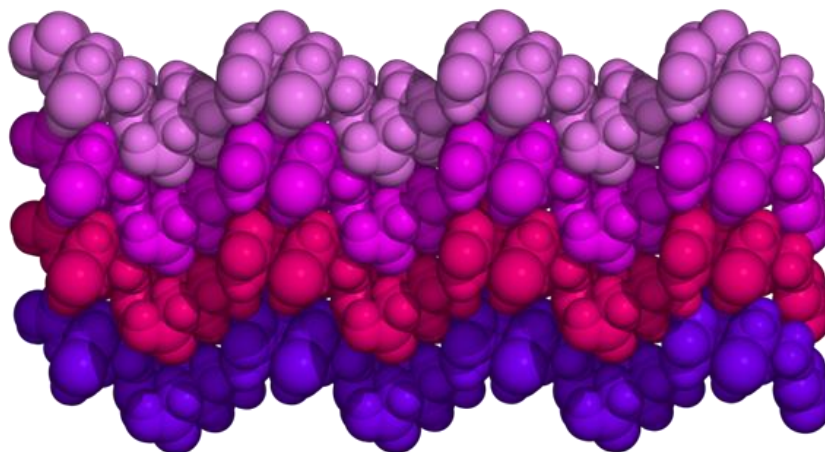
by

ORNELLA EDLYNE YOUDAGA KILINKISSA

Thesis submitted in fulfilment of the requirements for the degree

Magister Technologiae: Chemistry

in the Faculty of Applied Sciences at the

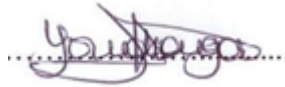## CAPE PENINSULA UNIVERSITY OF TECHNOLOGY

Supervisor: Dr Nikoletta B. Báthori
Co-supervisor: Prof Luigi R. Nassimbeni

Cape Town
May 2014

DECLARATION

I, ORNELLA EDLYNE YOUDAGA KILIKISSA, declare that the contents of this thesis represent my own unaided work, and that the thesis has not previously been submitted for academic examination towards any qualification. Furthermore, it represents my own opinions and not necessarily those of the Cape Peninsula University of Technology.

Signed .... **Date**   **28 July 2014**

ABSTRACT

The solid state modification of a given active pharmaceutical ingredient is a desired way to alter its physicochemical properties, such as solubility or bioavailability. The solubility-melting point relationship of the ensuing co-crystal or salt is not fully understood.

In this thesis, a series of model co-crystals and pharmaceutical co-crystals and salts of baclofen were investigated. The model co-crystals were prepared from 4,4'-bipyridine (BIPY) and 1,2-bis(4-pyridyl)ethane (ETBIPY) used as host compounds which were combined with a series of carboxylic acids as co-formers, such as p-toluic acid (PTA), rac-phenylbutyric acid (racPBA), racemic and S-phenylsuccinic acid (racPSA and S-PSA, respectively). In the second part, six new multicomponent crystals of baclofen (BAC, (RS) 4-amino-3-(4-chlorophenyl)-butanoic acid), were prepared with mono- and dicarboxylic acids: two pharmaceutical co-crystals obtained with benzoic acid (BAC•BA) and p-toluic acid (BAC•PTA) and four pharmaceutical salts with 1-hydroxy-2-naphthoic acid, $(BAC^+)(HNA^-)$, oxalic acid, $2(BAC^+)(OA^{2-})$, maleic acid, $(BAC^+)(MA^-)$ and p-toluene sulfonic acid, $(BAC^+)(PTSA^-)•IPA$. The compounds prepared were analysed by single crystal and powder X-ray diffractometry, differential scanning calorimetry and their solubility was measured in water and ethanol.

From the analysis of the model co-crystals it was concluded that their aqueous solubility is inversely related to the melting point values and this can be explained by packing features. Also, the introduction of a chiral building block, compared to its racemic counterpart, is a valuable way to limit the formation of the intermolecular interactions in the new multicomponent crystal and thus decrease the efficiency of the packing which eventually leads to lower melting points and better solubility.

The analysis of the baclofen crystals suggests that a strong, robust and predictable hydrogen bonding network with a combination of molecular building blocks which show acceptable molecular flexibility is a good recipe for successful co-crystal design.

ACKNOWLEDGEMENTS

I wish to thank:

- My family, friends and colleagues for their support and encouragement
- My supervisors, Dr Nikoletta N. Báthori and Prof Luigi R. Nassimbeni for their willingness to help, advices and support
- The Staff of the Department of Chemistry , CPUT

DEDICATION

I dedicated my thesis to my family.

TABLE OF CONTENTS

CHAPTER 1: Introduction

CHAPTER 2: Experimental methods and materials

CHAPTER 3: Analysis of model co-crystals

CHAPTER 4: Multicomponent crystals of baclofen

CHAPTER 5: Summary and conclusion

LIST OF FIGURES

LIST OF TABLES

GLOSSARY

Terms/Acronyms/Abbreviations	Definition/Explanation
Rf	Ratio of frequency of occurrence
CSD	Cambridge Structural Database
pKa	-log(acid ionisation constant)
API	Active pharmaceutical ingredient
P'	Polarity index
ε	Dielectric constant
TGA	Thermogravimetric analysis
DSC	Differential Scanning Calorimetry
PXRD	Powder X-ray Diffraction
a, b, c	Unit cell axes
α	Angle between b and c unit cell axes
β	Angle between a and c unit cell axes
γ	Angle between a and b unit cell axes
V	Unit cell volume
Z	Number of formula units per cell
T_{on}	Onset temperature
T_{peak}	Peak temperature
BIPY	4,4'-bipyridine
ETBIPY	1,2-bis(4-pyridyl)ethane
PTA	p-toluic acid
racPBA	racemic phenylbutyric acid
racPSA	racemic phenylsuccinic acid
S-PSA	S-phenylsuccinic acid
BAC	Baclofen
BA	benzoic acid
MA	maleic acid
HNA	1-hydroxy-2-naphthoic acid
OA	oxalic acid
PTSA	p-toluene sulfonic acid
DMSO	dimethyl sulfoxide
IPA	isopropanol
N_{arom}	aromatic nitrogen
S_w	Solubility for water
S_e	Solubility for ethanol
ρ	Density
PI	Packing index
$C_{aromatic}$	Aromatic carbon

Atom colours

Carbon

Oxygen

Nitrogen

Hydrogen

Hydrogen for Crystal Explorer figures

Chlorine

Sulphur
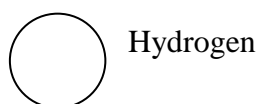
Chapter 1

Introduction

1 Introduction

1.1 Supramolecular chemistry

The history of early supramolecular systems started in 1810 by Sir Humphrey Davy with the discovery of chlorine hydrate clathrate, the inclusion of chlorine within a solid water lattice (**Table 1.1**). In 1978, supramolecular chemistry was introduced by Jean-Marie Lehn and has been described as 'chemistry of molecular assemblies and of the intermolecular bond'. Supramolecular chemistry can be defined as the study of molecules which are connected by non-covalent bonds such as electrostatic interactions, hydrogen bonding, dispersion forces and hydrophobic effects between two or more covalent molecules or ions to form a supramolecular system. **(Figure 1.1)** There are two main subsets of supramolecular chemistry, namely (i) host-guest chemistry and (ii) self-assembly. In host-guest systems the smaller molecule 'guest' becomes enveloped by the larger molecule called 'host' in a binding region, while in a self-assembled system two or more species with no significant difference in size are joined together by non-covalent bonds. These intermolecular interactions are typically hydrogen bonds, ion-ion, ion-dipole, dipole-dipole interactions, cation-π, π-π stacking and *van der Waals* interactions. [1] Also, supramolecular chemistry may be classified into subdivisions, such as organic, inorganic and physical chemistry.
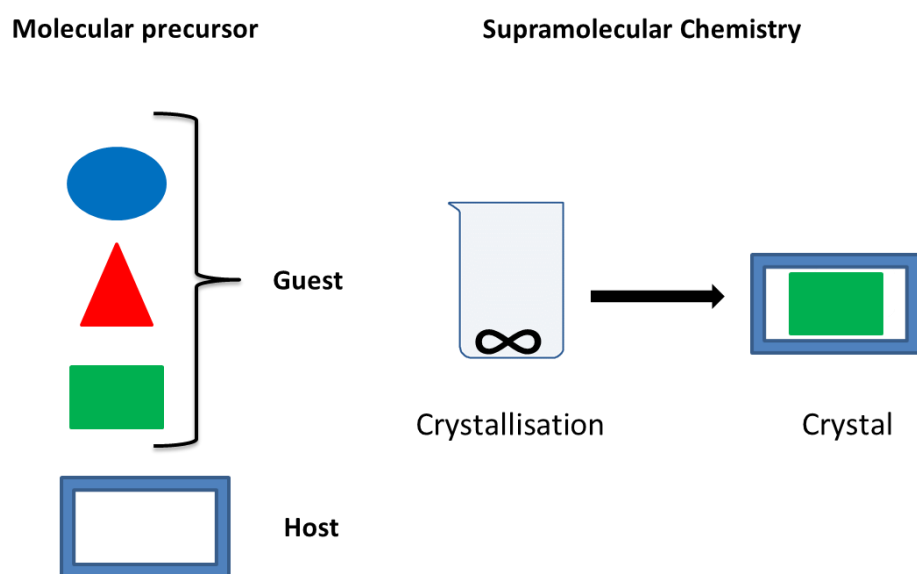
Figure 1.1 Comparison between molecular and supramolecular chemistry showing the phenomenon of selectivity.

Table 1.1 History of supramolecular chemistry[2]

Year	Event
1810	Sir Humphrey Davy**:** discovery of chlorine hydrate
1823	Michael Faraday**:** formula of chlorine hydrate
1841	C. Schafhäutl**:** study of graphite intercalates
1849	F. Wöhler: β-quinol H_2S clathrates
1891	Villiers and Hebd: cyclodextrin inclusion compounds
1893	Alfred Werner: Co-ordination chemistry
1894	Emil Fischer introduced the lock and key concept
1906	Paul Ehrlich introduced the concept of a receptor
1937	K. L. Wolf: the term Übermolecüle is coined to describe organised entities arising from the association of co-ordinately saturated species, e.g. the acetic acid dimer.
1939	Linus Pauling: hydrogen bonds are included in the groundbreaking book "The nature of the chemical bond"
1940	M. F. Bengen: urea channel inclusion compounds
1948	H. M. Powell: X-ray structures of β-quinol inclusion compounds; coins the term 'clathrate' to describe compounds where one component is enclosed within the framework of the other
1949	Brown and Farthing synthesize [2,2]paracyclophane
1953	Watson and Crick discover the structure of DNA
1956	Dorothy Crowfoot Hodgkin: X-ray crystal structure of vitamin B_{12}
1959	Donald Cram attempted the synthesis of cyclophane charge transfer complexes with $(NC)_2C=C(CN)_2$
1961	N. F. Curtis: first Schiff's base macrocycle from acetone and ethylenediamine
1964	Busch and Jäger: Schiff's base macrocycles
1967	Charles Pedersen: crown ethers
1968	Park and Simmonds: katapinand anion hosts
1969	Jean-Marie Lehn: synthesis of the first cryptands
1969	Jerry Atwood: liquid clathrate from alkyl aluminium salts
1973	Donald Cram: spherands hosts produced to test the importance of pre-organisation
1978	Jean-Marie Lehn: introduction of the term supramolecular chemistry
1979	Gokel and Gokahara developed the lariat ethers.
1981	Vögtle and Weber: podand host and developing of nomenclature
1987	Donald J. Cram, Jean-Marie Lehn and Charles J. Pedersen received the Nobel prize for chemistry for their contributions to supramolecular chemistry.
1996	Atwood, Davies, MacNicol and Vögtle: publication of Comprehensive Supramolecular Chemistry containing contributions from almost all the key groups and summarising the development of the discipline.
1996	Kroto, Smalley and Curly: Nobel Prize for chemistry for their work on the fullerenes
2012	Steed and Gale: Supramolecular Chemistry: From Molecules to Nanomaterials

1.2 Intermolecular interactions

Non-covalent interactions, also known as intermolecular interactions, are forces with electrostatic origin. Their general properties are the strength, direction and distance dependence. Intermolecular interactions can be classified as ion-ion, ion-dipole, dipole-dipole, hydrogen bonding, cation-π, π-π stacking and *van der Waals*. Ion-ion interactions are the strongest and they are non-directional, while the strength of the ion-dipole and the dipole-dipole interactions is maximised when the geometry is optimal. Hydrogen bonds vary in strength from strong to the weaker interactions similarly to the π-type interactions (cation-π, π-π stacking). The strength of the *van der Waals* interactions (e. g. London forces) heavily depends on the polarisability of the species and their distance from each other. Hydrophobic effects arise from solvent-solvent or non-polar groups and solvent interaction energy and play an important role in macromolecular biological assemblies. A salient question when designing solid crystalline materials is which of these interactions play significant role in the crystal packing. Recently it has been shown that the occurrence of these interactions is not only dependent on their energy, but some of them occur more often in crystalline materials than statistically expected.[3] The ratios of frequency of occurrence was defined, R_f, and its meaning is that the given "interaction with $R_f = x$ occurs x times more often than expected by chance." Some of the highest R_f values are assigned to the different type of O⋯H bonds, such as $R_{f\,\text{O⋯H[polar]}} = 5.8$ and $R_{f\,\text{C-H⋯O}} = 2.0$. Also, the hydrogen bonds between an acceptor N and H occurs more often than expected by chance, $R_{fN[\text{acc}]⋯\text{H}} = 5.7$ **Table 1.2** shows the intermolecular interactions and their strengths in kJ mol^{-1}.

Table 1.2 Summary of the main intermolecular interactions[1]

Interactions	Strength (kJ mol^{-1})	Example
Ion-ion	200-300	Tetrabutylammonium chloride
Ion dipole	50-200	Sodium [15]crown-5
Dipole-dipole	5-50	Acetone
Hydrogen bonding	4-120	Amino acids
Cation-π	5-80	K$^+$ in benzene
π-π	0-50	Benzene and graphite
van der Waals	<5 kJ mol^{-1} but variable depending on surface area	Argon; packing in molecular crystals
Hydrophobic effects	Related to solvent-solvent interaction	Cyclodextrin inclusion compounds

1.3 Hydrogen bond

Hydrogen bonding is one of the most important and most often occurring intermolecular interactions in organic crystalline materials. In supramolecular chemistry, hydrogen bonding has been described as the 'master key interaction' because of its strength (up to 120 kJ mol^{-1}) and highly directional nature.[4] Jeffrey's definition for hydrogen bond is "when a hydrogen atom attached to an electronegative atom (or electron withdrawing group) is attracted to a neighbouring dipole on an adjacent molecule or functional group". According to the IUPAC definition, "the hydrogen bond is an attractive interaction between a hydrogen atom from a molecule or a molecular fragment X-H in which X is more electronegative than H, and an atom or a group of atoms in the same or different molecule, in which there is evidence of bond formation".[5] The latter definition is more precise from that aspect that includes the intramolecular hydrogen bonds also. They can be represented as D-H⋯A where D is a donor and A is the acceptor.[6] Hydrogen bonds may be described by the distances of D⋯A ($d_{D⋯A}$) and H⋯A ($d_{H⋯A}$), and also the angle defined between D-H⋯A atoms (θ). Hydrogen bonding occurs most commonly between donor groups such as C-H, N-H, O-H, F-H, P-H, S-H, Cl-H, Br-H, I-H and acceptors groups of N, O, P, S, Cl, Br, I, alkenes, alkynes, aromatic π-systems and transitions metals.[4]

The angle between D-H⋯A atoms (θ) inclines toward 180° for most of the hydrogen bonds. The reason for this is that the energy between the positively charged H atom and the electronegative acceptor atom is maximised in this geometry.[7] However, it is common to observe bent hydrogen bonds in crystal structures ($\theta \sim 165°$) because the hydrogen atom can be attracted by multiple acceptors in the same time. According to Taylor and Kennard[8], $d_{D⋯A}$ can be determined by the properties of the donor and the acceptor and the length is related to the number of bonds to which the acceptor is attached. For example, if a hydrogen bond acceptor is involved in single bonds the distance will be shorter than when it is involved in multiple bonds. The charge of the species plays a role in the bond lengths and they deduced that shorter bonds are formed for charged species and longer ones for uncharged groups.[9] The strength of the hydrogen bond is greatly dependent on its environment and the adopted geometry may vary. **Figure 1.2** shows various types of hydrogen bonding between the donor group, D and the acceptor group(s), A. Linear and bent hydrogen bonds are primary interactions, a direct contact between the donor and acceptor group. Bifurcated arrangements are hydrogen bonds between a single donor and two acceptors
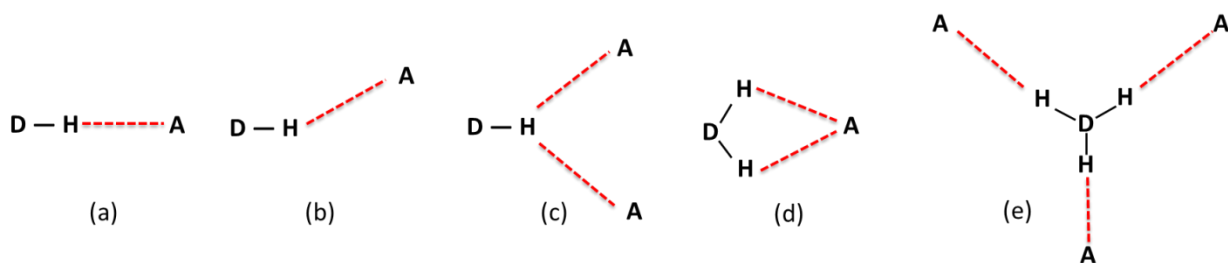
Figure 1.2 Typical types of hydrogen bonding geometries, such as (a) linear, (b) bent, (c) donating bifurcated, (d) accepting bifurcated and (e) trifurcated.

(bifurcated donor), two donors and a single acceptor (bifurcated acceptor) or a single donor and three acceptors (trifurcated).[10]

Hydrogen bonds are classified into three categories: very strong (F-H-F⁻), strong (O-H···O or N-H···O) and weak (C-H···O) according to the energy of the interactions.[11] **Table 1.3** shows the parameters of these hydrogen bonds.[12]

- ❖ **Very strong hydrogen bonds**: They are characterized by a D-H···A (A and D = F, O, N) where D···A= 2.2-2.5Å and the angle (θ) close to 180° (linear). The short $d_{D···A}$ accompanied by a lengthening of the covalent D-H distance where the proton is shared almost equally between the two electronegative atoms. They have bond energies in the range of 60-120 kJ mol^{-1}. For example, these very strong hydrogen bonds are observed in the linear HF$_2^-$ ion with the hydrogen atom between the two fluorine atoms, [F-H-F]⁻.[10]

- ❖ **Strong hydrogen bonds**: This hydrogen bond is the most common type for a hydrogen attached to an electronegative atom, like oxygen. The $d_{D···A}$ vary from 2.6-3.1Å and the θ range is between 135 to 180° with bond energies ranging from 16-60 kJ mol^{-1}. They are formed between neutral donor and neutral acceptor groups via lone pair electrons, for example O-H···O-H.

- ❖ **Weak hydrogen bonds**: These interactions can be found between poor donors, such as C-H moieties, and poor acceptors, like π-electron clouds. Donor and acceptor atoms in weak hydrogen bonds are less electronegative in contrast to strong hydrogen bonds, the $d_{D···A}$ is longer and the θ values can be found in a wide range (110-180°).[10]

Table 1.3 Parameters of hydrogen bonds[12]

Strength	Examples	D$\cdots$A ($d_{D\cdots A}$, Å)	H$\cdots$A ($d_{H\cdots A}$, Å)	D-H$\cdots$A ($\theta°$)	Bond energy (kJ mol^{-1})
Very strong	[F-H-F]$^-$	2.2-2.5	1.2-1.5	175-180	60-120
Strong	O-H$\cdots$O-H	2.6-3.0	1.6-2.2	145-180	16-60
	O-H$\cdots$N-H	2.6-3.0	1.7-2.3	140-180	
	N-H$\cdots$O=C	2.8-3.0	1.8-2.3	150-180	
	N-H$\cdots$O-H	2.7-3.1	1.9-2.3	150-180	
	N-H$\cdots$N-H	2.8-3.1	2.0-2.5	135-180	
Weak	C-H$\cdots$O	3.0-4.0	2.0-3.0	110-180	<12

1.4 Supramolecular synthon

In 1995, a review article by Desiraju introduced the formal literature definition of the supramolecular synthon, based on analogy with the definition of synthons for covalent synthesis by Corey.[13] Supramolecular synthons are defined as structural units within supermolecules which can be formed and/or assembled by known or conceivable synthetic operations involving intermolecular interactions.[13] According to Desiraju "in a crystal, we can identify various patterns of interacting groups and functionalities. These patterns may repeat in other crystal structures composed of molecules that contain similar functional groups". Also, supramolecular synthons are helpful for understanding and designing co-crystals. Two main types of supramolecular synthons can be identified in crystals; the homosynthon and the heterosynthon. (**Figure 1.3**) The homosynthon composed of identical functional groups while the heterosynthon built from different functional groups or complementary donor and acceptor groups.[10] Carboxylic acids, one of the most commonly studied functional groups in crystal engineering, are favorable for supramolecular homosynthons. An example of a supramolecular heterosynthon is the carboxylic acid-pyridine interaction through O-H$\cdots$N hydrogen bonding. According to statistical CSD studies, supramolecular heterosynthons are more reliable for the preparation of co-crystals than supramolecular homosynthons.[14]

Homosynthon   Heterosynthon
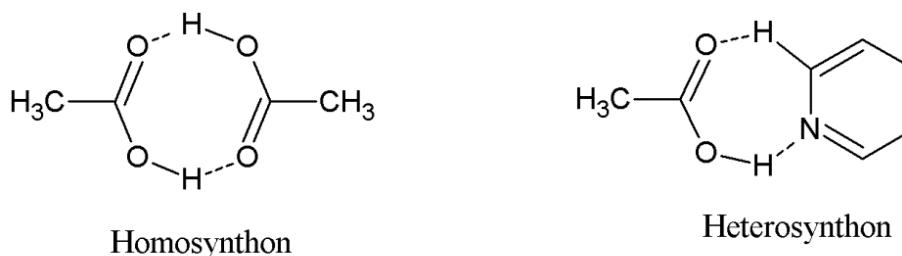
Figure 1.3 Representation of a supramolecular homosynthon and heterosynthon.

1.5 Graph set analysis

The interaction of an H atom with multiple donors can result in a complex geometry. For simplifying the description of the occasionally difficult H-bond network in a crystal, Etter[15] formulated a new nomenclature for describing hydrogen bonding motifs, the so called 'graph set notation'. Applying the graph set notation, all hydrogen bonded crystal structures can be reduced to a combination of four simple patterns, such as designated chains (C), rings (R), intramolecular hydrogen bonded patterns (S for 'self') and others finite patterns (D for 'discrete') which are represented as G, the pattern designator. G is combined with the number of hydrogen bond donors in the pattern (subscript, d) and the number of acceptors (superscript, a). Also, the total number of atoms (n), including H, in the pattern is termed the degree of the pattern. Therefore, a typical total graph set descriptor is $G_d^a(n)$. These kinds of designators are termed first level graph sets and form the unitary graph set, symbolised N_1. In additional to the first-level, graph sets describing two hydrogen bonds (a and b), we also have a binary graph set N_2 involving both a and b interactions. In a system involving three hydrogen bonds a, b and c there will be three binary graph sets containing more than one kind of hydrogen bond forming the second-level, $N_2(ab)$, $N_2(ac)$ and $N_2(bc)$. Then, the third-level graph set, $N_3(abc)$, and so on.[16] Some examples are illustrated in **Figure 1.4**.

$$R_2^2(8) \qquad D_1^1(3) \qquad R_2^2(7)$$
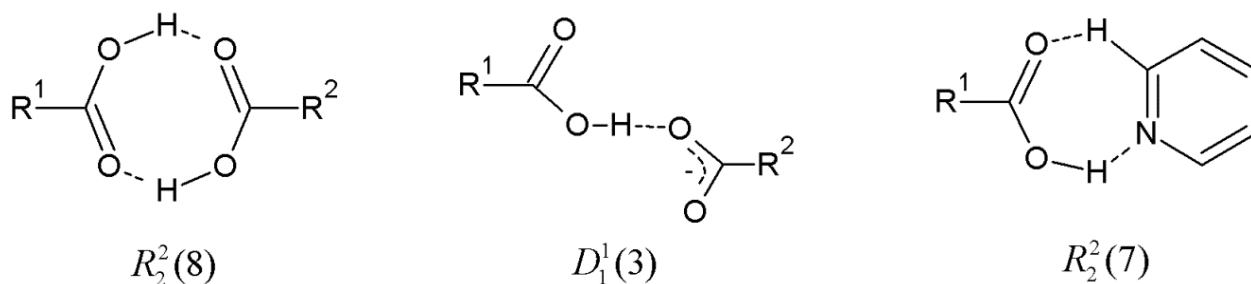
Figure 1.4 Examples of supramolecular synthons with their graph set notations.

1.6 Crystal engineering

Crystal engineering, a sub-discipline of supramolecular chemistry, is the study of the recognition of molecules by one another during crystallization. It consists of designing, synthesizing, determining and analysing crystal structures with required properties. In 1962, this field was identified by von Hippel[16] as "molecular engineering" and then was implemented by Schmidt[17] for the preparation or supramolecular synthesis[18] of new compounds with tailor-made properties. Back to the early 1960s, firstly 'modern crystal engineering' was developed as a method for understanding a field called topochemistry.[19] Two most common strategies are used by exploiting either hydrogen bonds[20] which is central to this study, or coordination bonds[21] which occur between metal centers and ligand compounds. Desiraju defined crystal engineering as "the study of intermolecular interactions, the study of packing modes in the context of these interactions with the aim of designing a strategy for construction and the study of crystal properties".[22] This field is also important in the study of molecular assemblies and compounds other than crystals, such as polymers. It can also be applied in organic chemistry, inorganic chemistry, physical chemistry, materials sciences and computational chemistry.

1.7 Multicomponent crystals

In the 1844, the first multicomponent crystal made by Wöhler[23] was quinhydrone which is a 1:1 co-crystal of benzoquinone and hydroquinone. When other multicomponent crystals were reported, different terms were applied to them, such as "addition compounds"[24] (early 1900s), "organic molecular compounds"[25] (1937), "complexes"[26] (1960s) and "heteromolecular crystal"[27] (2005). The main types of multicomponent crystals are the solvates, the hydrates, the co-crystals and the salts. Also polymorphism is an important phenomenon of solid crystalline materials. (**Figure 1.5**) Polymorphs are defined as the different crystalline phases of the given compound. Solvates are multicomponent crystals in which one component is a solvent. When this solvent is water, the crystal is called a hydrate. Co-crystals generally may be defined as stoichiometric multicomponent crystals formed between two neutral compounds while in salts the building blocks may be organic or inorganic ionic species.
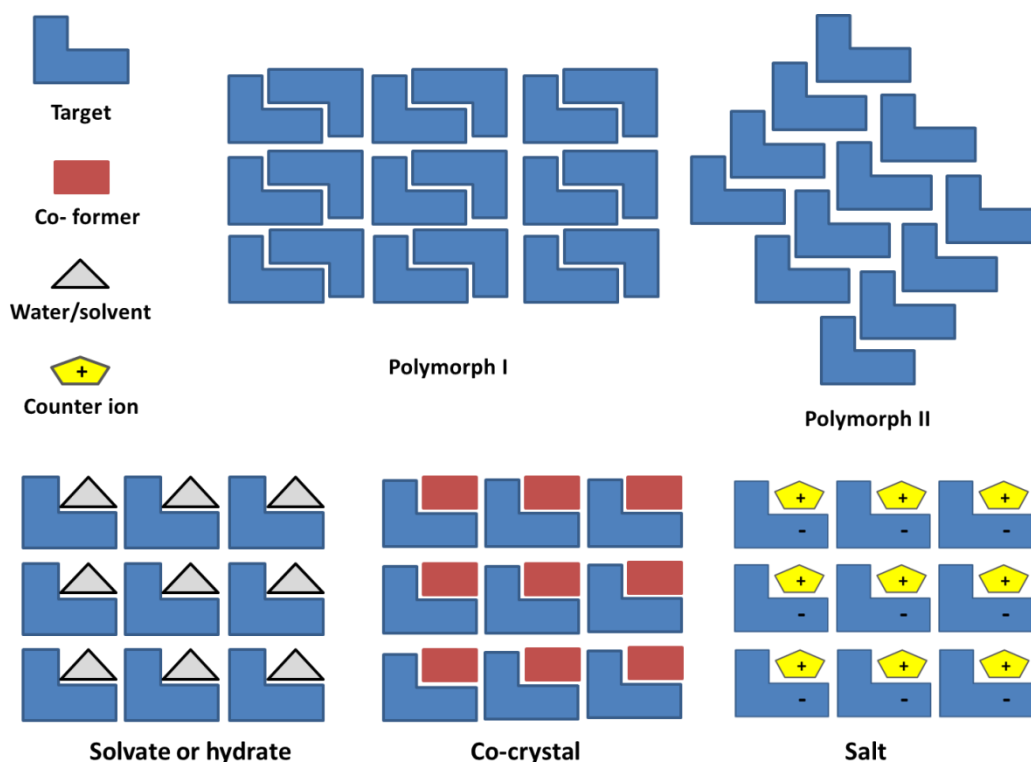
Figure 1.5 Schematic representations of a polymorph, solvate or hydrate, co-crystal and salt.

1.8 Differentiation between co-crystals and salts

The differentiation between a salt and a co-crystal is difficult. However, for intellectual property purposes and regulatory issues, the differentiation is important.[28] Over the last several years the definitions of co-crystals and salts have been discussed quite vigorously. A salt, according to the Compendium of Chemical Terminology produced by the International Union of Pure and Applied Chemistry (the IUPAC "Gold Book") is a "*chemical compound comprising an assembly of cations and anions*". A universal definition of what constitutes a co-crystal is still uncertain. The term co-crystal is not included in the IUPAC Gold Book but it is used to describe the presence of neutral molecular components within a crystalline compound in a definite stoichiometric ratio. A draft guidance proposed by the United States Food and Drug Administration (FDA) defines co-crystals as follows: *"cocrystals are solids that are crystalline single phase materials composed of two or more different molecular and/or ionic compounds generally in a stoichiometric ratio which are neither solvates nor simple salts".[29]* Several scientists, such as Zaworotko and co-workers[30] stated that a co-crystal is a multiple component crystal in which all components when pure are solids

under ambient conditions. The composition of a co-crystal is generally stoichiometric while salts must have stoichiometric compositions because of their charged nature. The differentiation between a salt and a co-crystal is based on the positioning of the acidic H atom. (**Figure 1.6**) To allocate the accurate position of an H atom in the electron density map obtained with X-ray radiation is difficult because the diffracting power of the H is based on only one electron. Thus the allocation of the H atoms should be verified with the careful analysis of the neighbouring bond length of the heavy atoms. Childs and co-workers[31] suggested that the distinction between a co-crystal and a salt must also be viewed as a continuum between the two limiting structures based on the position of the hydrogen.

Figure 1.6 An example of a co-crystal and a salt.

Formation of a co-crystal or a salt from a given molecular system might be dependent on different conditions, such as temperature[32] but most important can be predicted by the acid ionisation constant, the pKa values of the acidic (A) and the basic (B) components. In co-crystal formation, there is a formation of a A-B composite in which no proton transfer occurs between the moieties, A and B. A salt forms when a proton (H$^+$) been transferred from an acid (A) to a base (B) and this depends on the pKa values of components. The pKa equalization principle states that the strength of the hydrogen bond increases with decreasing ΔpKa value, however it is important to note that the pKa value for a given substance depends on the solvent used. According to earlier studies, when the ΔpKa between a co-crystallising acid and base is greater than 2 or 3, salt formation is expected.[33] This is the so called 'pKa rule'. Nangia et al[34] suggested the extension of the pKa rule for co-crystals containing an acid-base pair. Several co-crystals and salts of carboxylic acids and pyridines were studied and they concluded a negative pKa difference between the co-crystallizing acid-base pairs will always yield co-crystals. Also, it has been stated that in the range of ΔpKa values between 0 and 3, the prediction of the formation of a co-crystal or a salt based on the pKa

values of the acid and the base is impossible.[34] Gilli et al[35] formulated the 'pKa slide rule' in the form of a bar chart which allows quick empirical predictions of the H-bond between a given donor and acceptor based on their pKa values. At this stage, the pKa equalization principle was more like a 'a rule of thumb' and it was not verified quantitatively until Cruz-Cabeza[36] analysed 6465 individual crystalline molecular complexes from the CSD. It was found that if the aqueous ΔpKa > 4, ionized species were found in the crystal structures almost exclusively. If the ΔpKa < -1 for a given acid-base pair, the compounds will stay neutral and form a co-crystal. The $-1 \leq \Delta$pKa ≤ 4 zone is the most interesting from the aspect of predicting the outcome of the crystallization. In this zone the probability of the occurrence of a salt increases linearly with the ΔpKa values while the probability of a formation of co-crystals is decreasing. This quantification of the pKa rule, hence the probability of the salt/co-crystal formations is very helpful for co-crystal design and salt selection strategies.

Typically co-crystals and salts are prepared by slow evaporation but also many other crystallization methods, such as a slurry, grinding or solvent-assisted grinding techniques can be used. Solvent drop grinding is a green and cost-effective method for preparation of new or existing co-crystals.[37]

1.9 Pharmaceutical co-crystals

Pharmaceutical co-crystals can be described as crystalline materials which contain an active pharmaceutical ingredient (API) in a neutral or zwitterionic state along with a neutral co-former (liquid or solid), which may be an excipient or another drug, held together with non-covalent, freely reversible interactions.[38] Pharmaceutical co-crystals are non-ionic supramolecular complexes. The co-crystal former should be non-toxic, and the GRAS (Generally Regarded as Safe) list provides one source of potential compounds for this purpose.[39] The API and the co-crystal former are quite likely to be solids under ambient conditions because this is the nature of the compounds most frequently applied as pharmaceuticals. Crystalline forms of APIs have traditionally been limited to salts, polymorphs, and solvates (including hydrates).[40]

The ability of an API to form a co-crystal may depend on many factors, such as the type of co-former, the co-former ratio, the applied solvents, the temperature, the pressure, the crystallization technique, etc. At the start of the preparation of a new pharmaceutical co-crystal, the API must be evaluated, including but not limited to, the number and arrangement of hydrogen bond donors and

acceptors, [41] salt forming ability (pKa's), [42] conformational flexibility, and solubility requirements.[43] Generally APIs that have (i) rigid and (ii) highly symmetrical molecular structures, (iii) low molecular weight and functional groups which are capable of strong non-bonded interactions, are promising candidates for co-crystallisation with co-formers or counter-ions.[44] Therefore the suitable co-formers are selected based on hydrogen bonding rules, probable molecular recognition events and toxicological profiles.

The number of books and journals describing crystal engineering and supramolecular synthesis of API-based co-crystals is broad and expected to grow.[45,46,47] Within the last decade, co-crystals found their place in pharmaceuticals due to their ability to control and alter physico-chemical properties without compromising the structural integrity of the API. Co-crystals may also play a role in drug development. The role of co-crystallisation in the pharmaceutical industry may be defined as to identify and develop new solid forms of already existing APIs. Pharmaceutical co-crystallization is a reliable method to increase dissolution, solubility, chemical and physical stability and bioavailabity of drugs without alternating their bioactivity. Acetaminophen,[48] aspirin,[49] ibuprofen,[50] and flurbiprophen[51] are examples of APIs which were combined with coformers and their pharmaceutical co-crystals are reported.

1.10 Solubility and melting point of crystalline materials

The solubility of a drug is responsible for its transport over biological membranes. The solubility of a drug in water and in ethanol provides a good indicator of the release, transport, and extent of absorption of pharmaceuticals into the human body.[52] The IUPAC definition of solubility is "the analytical composition of a saturated solution expressed as a proportion of a designated solute in a designated solvent".[53] The solubility of a substance depends on the solvent used, temperature and pressure. Solubility is commonly expressed as a concentration, either by mass (g of solute per kg of solvent, g per dL of solvent, molarity, molality, mole fraction) or other units of concentration. Solubility can also be expressed in terms of maximum volume or mass of a solvent. Generally, in the pharmaceutical field, the solubility of a compound is represented as $\log S$, where S is the concentration of the compound in mol.dm^{-3} for a saturated aqueous solution in equilibrium with a solid state.

There are different approaches available to measure the solubility of a given compound. Kinetic solubility is the concentration of a given compound in a solution when the precipitate appears. Typically it is measured with turbidimetry. [54] Intrinsic solubility represents the equilibrium solubility at thermodynamic equilibrium of the pure ionisable compound at a pH value where the compound is neutral. Measurements are typically taken at two temperatures namely at 4°C and 37°C to ensure physical and chemical stability for short-term storage and to support biopharmaceutical evaluation. A generally used method is the saturation shake-flask method when the compound is dissolved in a buffer and the analysis of the solution is carried out with instrumental analytical methods, such as chromatography or ultraviolet/ visible spectroscopy.[55] Equilibrium solubility is the concentration of a compound in an oversaturated solution when the solid is in equilibrium with the solution. The methods used to obtain the results are similar to the intrinsic technique, such as UV-Vis, chromatography and gravimetric/volumetric methods.[54]

Solubility is one of the main parameters to achieve concentration of a drug in systemic circulation. Unfortunately most of the drugs have poor aqueous solubility.[56] It is commonly accepted that a drug with low solubility will show low adsorption. Therefore the general aim is to elude poorly soluble compounds as drugs because they often require high doses in order to reach therapeutic plasma concentrations after oral administration. The major problem during formulation of a new API or a generic substance is low aqueous solubility. There are several methods to improve the solubility of poorly water soluble APIs, such as formation of nanoparticles, solid dispersions, cyclodextrin complexes, and the inclusion of additives (excipients), co-crystals and salts.[57] The formation of a co-crystal can improve the solubility of the API by 4-160 times and salt formation can alter the solubility by 100-1000 fold.[58] However in certain cases the formation of a co-crystal may lead to lowering the solubility of the API.[59] **Table 1.4** shows solubility terms given by the United States Pharmacopeia and National Formulary (volume 23).[61]

Table 1.4 Solubility terms given by the United States Pharmacopeia and National Formulary.[60]

Descriptive term	Parts of solvent required for 1 part of solute
Very soluble	≤ 1
Freely soluble	1 to 10
soluble	10 to 30
Sparingly soluble	30 to 100
Slightly soluble	100 to 1000
Very slightly soluble	1000 to 10000
Practically insoluble, or insoluble	≥ 10000

The melting point of a compound is a fundamental physical property determined by the temperature at which the solid phase is at equilibrium with the liquid phase. The prediction of the melting point of a compound remains a challenging process because it is influenced by the intermolecular forces, the molecular symmetry, the conformational freedom of the molecule and also its molecular motion in the crystal.[61] The prediction of the melting point of multicomponent crystals are more difficult because the different chemical entities have different properties and the combination of these compounds result in a new structural arrangement in the crystal. It is interesting to note that the melting point of a given drug has been shown to play a role in its aqueous solubility.[62] Also, a direct correlation between the melting point and solubility of some poorly soluble drugs has been drawn in the literature.[63] However, the solubility-melting point relationship of a co-crystal or salt is still an upcoming area of pharmaceutical and supramolecular research which is not fully understood.

1.11 The aspect of this research

The estimated cost of developing a new drug varies widely, however the estimated value is a staggering $ 1 billion. Also, the discovery and development of a new chemical entity takes at least ten years on average and the success rate is low (from a pool of ~10000 promising compounds only 1 compound will eventually become a marketed drug).[64]

Once the required active pharmaceutical ingredient (API) is fully developed it is not the end of the product development. Poor bioavailability, limited by the solubility of the final drug is a common problem occurs during drug development. Substantial amount of time and effort is spent on improving the solubility of the new chemical entity without tampering with its molecular structure or altering the biological activity.

Active pharmaceutical ingredients with poor physicochemical properties, such as solubility and stability, lead to the failure of many drug candidates. The design of a new solid form, (co-crystals or salts) of these compounds may improve the required physical chemical property.

The successful prediction of a new crystal structure has improved recently with the aid of high performance computing. However, the prediction of certain properties, such as solubility of the new solid form, is still desired. The common observation of no correlation between melting point

and solubility of co-crystals and salts raises the question of what the connection is between these properties (is there any?) and how we can analyze and measure it.

The aim of this research in the first part is to design and synthesize a series of model co-crystals where the API is replaced by a simple chemical unit with restricted secondary interaction possibilities and conformational motions, while the co-crystallising compound will be varied systematically. It is required that the type of possible intermolecular interactions are limited to make achievable the identification of the relevant differences in their strength, or their contribution to the overall changes observed during the subtle modification of the crystal. 4,4'-bipyridine (BIPY) and 1,2-bis(4-pyridyl)ethane (ETBIPY) were used to combine with a series of carboxylic acids as co-formers, such as p-toluic acid (PTA), rac-phenylbutyric acid (racPBA), racemic and S-phenylsuccinic acid (racPSA and S-PSA, respectively). These compounds were chosen to prepare the model co-crystals because of their ability to hydrogen bond via O-H⋯N interactions. The single crystal structures, powder diffraction patterns, thermal behaviour, solubility (measured in water and ethanol) of these crystals will be discussed.

In the second phase, more advanced co-crystals were investigated. Baclofen (BAC, (RS) 4-amino-3-(4-chlorophenyl)-butanoic acid) was used as an API. It is a slightly water and alcohol soluble drug, most widely used by patients with spasticity related problems, like cerebral palsy, dystonia and trigeminal neuralgia but it is also currently being investigated for the treatment of spinal cord injuries, binge eating and alcoholism.[65,66,67] Six new multicomponent crystals of baclofen were prepared with mono and dicarboxylic acids: two pharmaceutical co-crystals obtained with benzoic acid (BA) and p-toluic acid (PTA) and four pharmaceutical salts with 1-hydroxy-2-naphthoic acid (HNA), oxalic acid (OA), maleic acid (MA) and p-toluene sulfonic acid (PTSA). The single crystal structures will be analysed with the focus on the baclofen conformation. The powder diffraction patterns and the thermal behaviour of these crystals will also be discussed.

The molecular diagrams of the host compounds, 4,4'-bipyridine, 1,2-bis(4-pyridyl)ethane, baclofen and for all the co-former acids are shown in **Figure 1.7**.

HOST COMPOUNDS
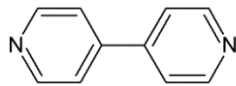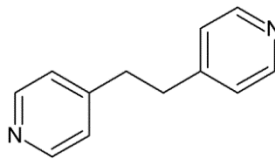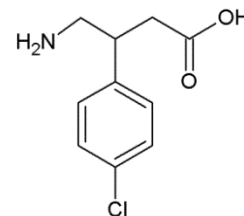
BIPY   ETBIPY   BAC

GUEST COMPOUNDS
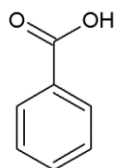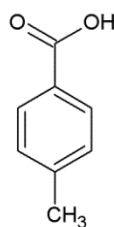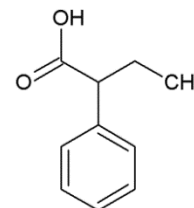
BA   PTA   (rac)PBA
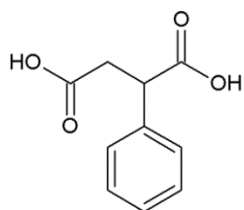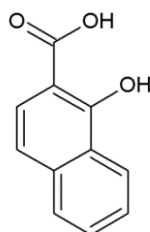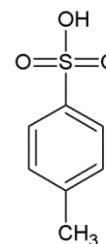
(rac)PSA   HNA   PTSA
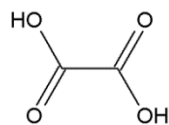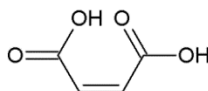
OA   MA

Figure 1.7 Structural line diagrams of host compound (4,4'-bipyridine: BIPY, 1,2-bis(4-pyridyl)ethane: ETBIPY, baclofen: BAC) and the coformers (benzoic acid: BA, p-toluic acid: PTA, rac-phenylbutyric acid: (rac)PBA, rac-phenylsuccinic acid: (rac)PSA, 1-hydroxy-2-naphthoic acid: HNA, p-toluene sulfonic acid: PTSA, oxalic acid: OA and maleic acid: MA).

References:

[1] Steed, J.W., Turner, D.R. & Wallace, K.J. 2007. *Core Concepts in Supramolecular Chemistry and Nanochemistry.* John Wiley & Sons.

[2] Steed, J.W. & Atwood, J.L. 2000. *Supramolecular Chemistry.* Singapore: John Wiley & Sons.

[3] Taylor, R. 2014. Which intermolecular interactions have a significant influence on crystal packing? *CrystEngComm*, DOI: 10,1039.

[4] Jeffrey, G.A. 1997. *An Introduction to Hydrogen Bonding*, Oxford University Press: Oxford.

[5] Arunan, E., Desiraju, G.R., Klein, R.A., Sadlej, J., Scheiner, S., Alkorta, I., Clary, D.C., Crabtree, R.H., Dannenberg, J.J., Hobza, P., Kjaergaard, H.G., Legon, A.C., Mennucci, B. & Nesbitt, D.J. 2011. *Pure Appl. Chem.*, 83: 1619-1636.

[6] Gale, P.A. & Steed, J.W. 2012. *Supramolecular Chemistry*. John Wiley & Sons.

[7] Desiraju, G.R. 2010. Crystal Engineering: a brief overview. *J. Chem. Sci*, 122(5): 667-675.

[8] Taylor, R. & Kennard, O. 2002. Hydrogen -bond in organic crystals. *Accounts of Chemical Research*, 17: 320-326.

[9] Shattock, T.R, Arora, K.K, Vishweshwar, P. & Zarworotko M.J. 2008. Crystal Engineering of Pharmaceutical Cocrystals. *Cryst.Growth Des.*, 8: 4533-4545.

[10] Barbour, J.L., Das, D., Jacobs, T., Lloyd, G.O. & Smith, V.J. 2012. *Concept and Nomenclature in Chemical Crystallography* in *Supramolecular Chemistry: From Molecules to Nanomaterials*. Ed. Jonathan W. Steed and Philip A. Gale, 2012, University of Cambridge, Cambridge, UK. John Wiley & Sons, Ltd.

[11] Desiraju, G.R. & Steiner, T. 2006. *The Weak Hydrogen Bond in Structural Chemistry and Biology*, Oxford University Press.

[12] Bernstein, J., Davis, R.E., Shimoni, L. & Chang, N.L. 1995. Patterns in Hydrogen Bonding: Functionality and Graph Set Analysis in Crystals. *Angew. Chem. Int. Ed*, 34: 1555-1573.

[13] Desiraju, G.R. 1995. Supramolecular synthons in crystal engineering- A new organic synthesis. *Angew. Chem. Int. Ed.* 34: 2311-2327.

[14] (a) Leiserowitz, L. 1976. Molecular Packing modes: Carboxylic acids. *Acta Crystallogr*, B32, 775-802. (b) Allen, F.H., Raithby, P.R., Shields, G.P. & Taylor, R. 1998. Probabilities of formation of bimolecular cyclic hydrogen-bonded motifs in organic crystal structures: a systematic database analysis. *Chem. Commun*, 9: 1043-1044. (c) Allen, F.H., Motherwell, W.D.S., Raithby, P.R., Shields, G.P. & Taylor, R. 1999. Systematic analysis of the probabilities of formation of bimolecular hydrogen-bonded ring motifs in organic crystal structures. *New. J. Chem*, 23(1): 25-34.

[15] Etter, M.C. 1990. Encoding and decoding hydrogen bond patterns of organic compounds. *Acc. Chem. Res.,* 23: 120-126.

[16] Von Hippel, A.R. 1962. Molecular designing of materials, *Science*, 138: 91-108.

[17] Schmidt, G.M.J. 1971. Photodimerization in the solid state. *Pure Appl. Chem.*, 27: 647-678.

[18] Lehn, J-M. 1995. *Supramolecular Chemistry : Concepts and Perspectives*. VCH:Weinheim.

[19] Schmidt, G.M.J. 1964. Topochemistry. Part III. The crystal chemistry of some trans-cinnamic acids. *J. Chem. Soc*. 2014-2021.

[20] Aakeröy, C.B. & Beatty, A.M. 2001. Review: Crystal Engineering of Hydrogen-Bonded Assemblies - A Progress Report, *Aust. J. Chem*. 54(7): 409-421.

[21] Zaworotko, M.J. 2001. Superstructural diversity in two dimensions: crystal engineering of laminated solids. *Chem.Comm.*, 1: 1-9.

[22] Desiraju, G.R. 2003. *Crystal Design: Structure and Function*; Ed; Wiley: New York

[23] Wöhler, F. 1844. Untersuchungen über das chinon. *Annalen.*, 51: 153

[24] Buck, J.S. & Ide, W.S. 1937. Mixed benzoins. VI. Further examples of reversibility. The formation of addition compounds. *J. Am. Chem. Soc.* 53: 2784-2787.

[25] Anderson, J.S. 1937. Structure of organic molecular compounds. *Nature*. 140: 583-584.

[26] Hall, B. & Devlin, J.P. 1967. 2:1 solid-state complex of hexamethylbenzene: tetracyanoethylene' *J. Phys. Chem*, 71: 465-466.

[27] Pekker, S., Kováts, É., Oszlányi, G., Bényei, G., Klupp, G., Bortel, G., Jalsovszky, I., Jakab, E., Borondics, F., Kamarás, K., Bokor, M., Kriza, G., Tompa, K., Faigel, G. 2005. Rotor-stator molecular crystals of fullerenes and cubane. *Nature Mat.*, 4: 764-767.

[28] Trask, A.V. 2007. An overview of pharmaceutical co-crystals as intellectual property. *Mol. Pharma.*, 4: 301-309.

[29] Aitipamula, S., Banerjee, R., Bansal, A.K., Biradha, K., Cheney, M.L., Choudhury, A.R., Desiraju, G.R., Dikundwar, A.G., Dubey, R., Duggirala, N., Ghogale, P.P., Gosh, S., Goswami, K.P, Goud, N.R., Jetti, R.R.K., Karpinski, P., Kaushik, P., Kumar, D., Kumar, V., Moulton, B., Mukherjee, A., Mukherjee, G., Myerson, A.S., Puri, V., Ramanan, A., Rajamannar, T., Reddy, C.M., Rodriguez-Hornedo, N., Rogers, R.D., Row, T.N.G., Sanphui, P.,

Shan, N., Shete, G., Singh, A., Sun, C.C., Swirft, J.A., Thaimattam, R., Thakur, T.S., Thaper, R.K., Thomas, S.P., Tothadi, S., Vangala, V.R., Variankaval, N., Vishweshwar, P., Weyna, D.R. & Zaworotko, M.J. 2012. Polymorphs, Salts, and Cocrystals: What's in a Name? *Cryst. Growth Des*, 2147-2152.

[30] Almarsson, Ö. & Zaworotko, M.J. 2004. Crystal engineering of the composition of pharmaceutical phases. Do pharmaceutical co-crystals represent a new path to improved medicines? *Chem. Commun*., 1889-1896.

[31] Childs, S.L., Sthaly, G.P. & Park, A. 2007. Salts and co-crystals of theophylline. *Mol. Pharma.*, 4: 323-338.

[32] Parkin, A., Seaton, C.C., Blagden, N. & Wilson, C.C. 2007. Designing hydrogen bonds with temperature-dependent proton disorder: the effect of crystal environment. *Cryst. Growth. Des*, 7: 531-534.

[33] Stahl, P.H. & Wermuth, C.G. 2002. *Handbook of Pharmaceutical Salts: Properties, Selection, and Use*. Wiley-vch.

[34] Bhogala, B.R, Basavoju, S. & Nangia, A. 2005. Three-component carboxylic acid-pyridine lattice inclusion host. Supramolecular synthesis of ternary cocrystals. *CrystEngComm*, 5: 1683-1686.

[35] Gilli, P., Pretto, L., Bertolasi, V. & Gastone, G. 2009. Predicting Hydrogen-Bond Strenghts from Acid-Base Molecular Properties. The pKa Slide Rule: Toward the Solution of a Long-Lasting Problem. *Acc. Chem. Res.*, 42(1): 33-44.

[36] Cruz-Cabeza, A.J. 2012. Acid-base crystalline complexes and the pKa rule. *CrystEngComm*, 14: 6362-6365.

[37] Weyna, D.R, Shattock, T., Vishweshwar, P. & Zaworotko, M.J. Synthesis and structural characterization of co-crystals and pharmaceutical co-crystals: Mechanochemistry vs slow evaporation from solution. *Cryst Growth Des,* 9: 1106-1123.

[38] Vishweshwar, P., McMahon, J.A. & Zarworotko, M.J. 2006. *Crystal Engineering of Pharmaceutical Co-crystals, in Frontiers in Crystal Engineering*, eds. E. R. T. Tiekink and J. J. Vittal, John Wiley & Sons, 25-49.

[39] Generally Recognized as Safe. http://www.fda.gov/food/ingredientspackaginglabeling/gras/default.htm.[January 2014]

[40] Haleblian, J.K. 1975. Characterization of habits and crystalline modification of solids and their pharmaceutical applications. *J. Pharm. Sci.,* 64: 1269-1288.

[41] Aakeroy, C.B. & Salmon, D.J. 2005. Building co-crystals with molecular sense and supramolecular sensibility. *CrystEngComm*, 7: 439-448.

[42] Kartum, G., Vogel, W. & Andrussov, K. 1961. *Dissociation Constants of Organic Acids in Aqueous Solutions*. Butterworth & Co. Publishers: London.

[43] (a) Chiarella, R.A., Davey, R.J., Petterson, M.L. 2007. Making co-crystals-The utility of ternary phases diagrams. *Cryst. Growth Des*, 7(7): 1223-1226. (b) Childs, S.L., Rodríguez-Hornedo, N., Reddy, L.S., Jayasankar, A., Maheshwari, C., McCausland, L., Shipplett, R., Stahly, B.C. 2008. Screening strategies based on solubility and solution composition generate pharmaceutically acceptable cocrystals of carbamazepine. *CrystEngComm*, 10: 856-864.

[44] Stahly, G.P. 2007. Diversity in single-and multiple-component crystals. The search for and prevalence of polymorphs and co-crystals. *Cryst. Growth Des*, 7: 1007-1026.

[45] Oswald, I.D.H, Allan, D.R, McGregor, P.A, Motherwell, W.D.S., Parsons, S. & Pulham, C.R. 2002. The formation of paracetamol (acetaminophen) adducts with hydrogen-bond acceptors. *Acta Crystallogr*. Sect. B 58, 1057-1066.

[46] Blagden, N., de Matas, M., Gavan, P.T & York, P. 2007. Crystal engineering of active pharmaceutical ingredients to improve solubility and dissolution rates. *Adv. Drug. Delivery Rev*. 59: 617-630.

[47] Stanton, M.K., Tufekcic, S., Morgan, C. & Bak, A. 2009. Drug substance and former structure property relationships in 15 diverse pharmaceutical co-crystals. *Cryst. Growth Des*, 9: 1344-1352.

[48] Rodriguez-Hornedo, N., Nehm, S.J., Jayasankar, A. 2007. *Cocrystals: design, properties and formation mechanisms*, In Encyclopedia of Pharmaceutical Technology, 3rd ed, Taylor & Francis, London.

[49] Vishweshwar, P., McMahon, J.A., Bis, J.A. & Zaworotko, M.J. 2006. Pharmaceutical co-crystals. *J. Pharm. Sci.;* 95: 499-516.

[50] Vishweshwar, P., McMahon, J.A., Peterson, M.L., Hickey, M.B., Shattock, T.R & Zawarotko, M.J. 2005. Crystal engineering of pharmaceutical co-crystal to improve oral bioavailability of a low solubility API. *Pharma Res*; 23: 1888-1897.

[51] Sarma, B., Reddy, L.S. & Nangia, A. 2008. Polymorphs and polymorphic cocrystals of temozolomide. *Chem Asian J.* 3: 1122-1133.

[52] Aulton, M. 2002. *Dissolution and solubility. Pharmaceutics: The Science of Dosage form Design*. 2nd edition. Churchill Livingstone.

[53] IUPAC gold book. http:// goldbook.iupac.org/S05740.html.

[54] Stuart, M. & Box, K. 2005. Chasing Equilibrium: Measuring the Intrinsic Solubility of Weak Acids and Bases. *Anal. Chem*. 77: 983-990.

[55] Connors, K.A. 1982. A Textbook of Pharmaceutical Analysis; John Wiley & Sons: New York.

[56] Sharma, D., Soni, M., Kumar, S. & Gupta, G.D. 2009. Solubility enhancement-eminent role in poorly soluble drugs. *Research Journal of Pharmacy and Technology*. 2(2): 220–224

[57] Darwish, M.K. & Foad, M.M. 2009. Enhancement of the dissolution profile of Tenoxicam by a solid dispersion technique and its analytical evaluation using HPLC. *Drug Discoveries Ther*. 3: 27-36.

[58] Aitipamula, S., Wong, A.B.H., Chow, P.S., Tan, R.B.H. 2012. Pharmaceutical cocrystals of ethenzamide: structural, solubility and dissolution studies. *CrystEngComm*, 14: 8515-8524.

[59] Bolla, G., Sanphui, P. & Nangia, A. 2013. Solubility advantage of Tenoxicam phenolic cocrystals compared to salts. *Cryst. Growth Des*, 13(5): 1988-2003.

[60] The United States Pharmacopeia and National Formulary. Vol. 23, 2007.

[61] Katritzky, A.R., Jain, R., Lomaka, A., Petrukhin, R., Maran, U. & Karelson, M. 2001. Perspective on the Relationship between Melting Points and Chemical Structure. *Cryst Growth Des*, 1(4): 261-265.

[62] Abramowitz, R., Yalkowsky, S. H. 1990. Melting point, Boiling point and Symmetry. *Pharm. Res*.7 (9): 942-947.

[63] Jain, N. & Yalkowsky, S.H. 2001. Estimation of the aqueous solubility, I: application to organic nonelectrolytes. *J. Pharm. Res*. 90: 234-252.

[64] Steven, M.P., Daniel, S.M., Christopher, T.D., Charles, C.P., Bernard, H.M., Stacy, R.L. & Aaron, L.S. 2010. How to improve R&D productivity: the pharmaceutical industry's grand challenge. *Nature Reviews Drug Discovery*.9:203-214.

[65] Koflen, M., Kronenberg, MF., Rifici, C., Saltuari, L. & Bauer, G. 1994. Epileptic seizures associated with intrathecal baclofen application. *Neurol*. 44: 25-28.

[66] Krach, L.E. 2001. Pharmacotherapy of spasticity: oral medications and intrathecal baclofen. *J. Child Neurol.* 16: 31-36.

[67] Price, G.W., Wilkin, G.P., Turnbull, M.J. & Bowery, M.G. 1984. Are baclofen sensitive $GABA_B$ receptors present on primary afferent terminals of the spinal cord? *Nature*, 307: 71-74.

Chapter 2

Experimental methods and materials

2.1 Experimental methods

2.1.1 Crystal Growth

Inclusion compounds were obtained by dissolving the host and guest compounds in a 1:1 stoichiometric ratio in excess solvent, heating to 60° C on a hot plate and stirring until the solution turned to clear. In case of the baclofen crystals the solutions were filtered and left to crystallize at room temperature. A series of solvents were selected with different polarity indices (P') and dielectric constants (ε), such as water, methanol, ethanol, isopropanol, dimethylsulfoxide, acetronitrile and acetone, see **Table 2.1** Some inclusion compounds were obtained by dissolving the host and the guest compounds separately in the same solvent in stoichiometric quantities and then mixing the solutions or by using grinding and then dissolution.

Table 2.1 Polarity index and dielectric constant of solvents.[1]

	Polarity Index (P')	Dielectric constants (ε)
Acetone	5.1	20.7
Acetronitrile	5.8	37.5
Dimethyl sulfoxide	7.2	46.7
Ethanol	5.2	24.5
Isopropanol	3.9	17.9
Methanol	5.1	32.7
Water	9.0	80.1

2.1.2 Thermal analysis

Thermogravimetry and Differential Scanning Calorimetry were performed on a Perkin-Elmer Pyris 6 instrument system under dry N_2 purge gas with a flow rate of 30 ml.min^{-1} with a constant scanning rate of 10 °C.min^{-1}. Crystals were removed from their mother liquor, carefully dried with a filter paper, crushed to a fine powder and placed in an open pan for TG analysis and vented pans were used for DSC analysis. The sample size was varied between 2 to 10 mg.[2]

2.1.2a Thermogravimetric analysis (TGA)

Thermogravimetric analysis (TGA) is the study of chemical changes in a material by measuring the sample weight as a function of temperature or time. A mass loss indicates that a degradation of the measured substance takes place. The sample is subjected to a temperature programme. The components of the TGA instrument are a thermobalance which is an analytical microbalance, furnace, temperature programmer, and sample holder, an enclosure for establishing the required atmosphere, and a recorder to display the data. A typical operating range for the furnace is from room temperature to 1000°C, with a heating rate up to 100°C/min. A thermocouple is placed close to the sample to indicate the sample temperature.

Thermogravimetric curves are referred to as mass loss curves. Thermogravimetric curves can be used to evaluate the temperatures ranges, the number of decomposition stages, and fractional weight loss of each stage.[3]

This technique is effective for quantitative analysis of thermal reactions that are accompanied by mass changes, such as evaporation, decomposition, gas absorption, desorption and dehydration.

In this project thermogravimetry was used to confirm that none of the co-crystals contained solvent as an inclusion with the exception of $(BAC^+)(PTSA^-) \cdot IPA$.

2.1.2b Differential scanning calorimetry (DSC)

DSC is one of the most sophisticated and advanced thermal analytical methods. This technique measures the differences in heat flow into a substance and a reference as a function of temperature.

DSC was employed to estimate the onset temperatures and the enthalpy change during the departure of a volatile guest from a host-guest system. These changes can be due to desolvation, phase transformation, melting and others thermal events. Two identical, crimped and vented aluminium pans with lids are used; one for the sample and the empty is the reference. The temperature of both pans is increased at a constant rate.[4]

The sample can undergo endothermic or exothermic processes which would result in a curve recorded against temperature. In DSC the endothermic peaks are plotted upwards ($\Delta H > 0$) and the

exothermic peaks are plotted downwards ($\Delta H < 0$). Temperature calibration is carried out by running standard materials (indium and zinc).

There are two major types of DSC:

- **Power compensated DSC:** Both the sample and reference crucibles have their own heating element and thermocouples. They are both heated and always controlled to have the same temperature with the aid of a temperature programmer. When a change in the sample happens (endothermic or exothermic process) heat will be needed to transfer to maintain the heating rate. The supplied power is plotted as a function of temperature or time.

- **Heat-flux DSC:** One heat source is used to heat the sample and the reference material and the temperature difference (ΔT) are measured. A calorimetric sensitivity which is governed by an instrumental constant K is needed to convert the difference in temperature to power difference (ΔP).

TGA and DSC results are influenced by the sample size; flow rate and heating rate of the N_2 gas.[3]

2.1.3   Single crystal X-ray diffraction

In 1895, X-rays were discovered by William Röentgen. In 1912, the exact nature of X-rays was established, the phenomenon of diffraction of X-rays by crystals was also discovered which provided a new method for investigating the fine structure of matter. In the same year, von Laue, Friedrich, and Knipping passed X-rays through crystal of zinc sulphide. They concluded that crystals cause distinct X-ray diffraction patterns due to their periodic arrays of atoms.[5]

X-rays are electromagnetic radiation with a very short wavelength ($\lambda = 10^{-10}$m $= 1$Å).[6] X-ray diffraction is generally a non-destructive analytical technique used to determine crystal structures and atomic spacing. Unit cell dimensions, bond-lengths, bond-angles, and details of site-ordering of crystalline materials can be obtained with the technique. Data obtained from X-ray analysis is refined and interpreted in order to solve crystal structures.[7]

X-ray diffraction studies of crystalline materials have four major steps: crystallization, data collection, structure solution and refinement.

Diffraction data for all compounds were collected on a Bruker APEX II diffractometer with a graphite-monochromated Mo $K_\alpha = 0.71073$ Å at 173 K using an Oxford Cryostream 700.[8]

Structures were solved using SHELXS-97[9] which was run under a graphical user interface, X-Seed[10]. The space groups were determined by using the collected intensities and pre-determined cell parameters as inputs to the program XPREP.[11] SHELXS-97[8] was used to solve all structures by direct methods and refinement was carried out with SHELXL-97[8] by employing full-matrix least-squares against F^2 for unique reflections:

$$\sum W\left(F_0^2 - kF_C^2\right)^2$$

The agreement between the observed structure factors (F_0) and the calculated structure factors (F_c) were monitored by assessing the residual index R. The residual index R_1 is the agreement between the observed and calculated structure factors based on F, while the residual index, R_2, is the agreement based on F^2.

$$R_1 = \frac{\sum \left\| F_0 \right| - \left| F_c \right\|}{\sum |F_0|} \qquad R_2 = \left[\frac{\sum w\left(F_0^2 - F_C^2\right)^2}{\sum w\left(F_0^2\right)^2} \right]^{1/2}$$

The weighing scheme w was used to yield a constant distribution in terms of a and b, and further refined in the final cycles of structure refinement.

$$w = \frac{1}{\sigma^2\left(F_0^2\right) + \left(aP\right)^2 + bP}$$

where
$$P = \frac{\max\left(0, F_0^2\right) + 2F_C^2}{3}$$

SHELXL-97[8] refines against F^2, which leads to greater deviations of the Goodness of Fit (S) from unity than the refinement against F. The Goodness of Fit expression is:

$$S = \left[\frac{\sum w \left(|F_0|^2 - |F_C|^2 \right)^2}{(N - n_p)} \right]^{1/2}$$

where N is the number of reflections and n_p is the total number of parameters refined.

The hydrogen atoms bound to carbon atoms were placed at idealized positions and refined as riding atoms with U_{iso} (H) = 1.2 U_{eq} (Ar-H, CH_2) or 1.5 U_{eq} (CH_3) of the atom to which the H is bound. H atoms bonded to the carboxylic acid, amine or amide groups were located in the difference electron density map and their coordinates refined freely but their isotropic displacement parameters were fixed (Uiso (H) = 1.2 Ueq(O) or Ueq(N)) if it was necessary.

X-ray powder patterns were calculated using LAZY PULVERIX[12] and compared to experimental powder patterns for characterization. All the crystal packing diagrams were generated with POV-Ray[13] .The program LAYER[14] was utilized to test systematic absences and space group symmetry. For verification of types of voids occupied by guest molecules, the program SECTION[15] was used to slice through cross sections of the unit cell. X-Seed were used as a graphical interface for the programs SHELXS-97, SHELXL-97, LAZY PULVERIX, Pov-Ray, LAYER and SECTION.

Others programs used in addition to X-Seed:

- Platon[16]
  - A multipurpose analytical tool for crystal structure analysis; calculates all molecular parameters for the structures.
- ConQuest[17]
  - Search engine using the Cambridge Structural Database (CSD) for informative and comparative structure details.

2.1.4 Powder X-ray diffraction (PXRD)

PXRD is a fundamental tool for the identification of compounds. It is used to monitor the phase changes of the reaction kinetics for solid crystalline materials. Samples are ground to a fine powder. Diffraction data for all compounds were collected on a Bruker D2 Phaser diffractometer with a graphite-monochromated Cu K$_\alpha$ radiation (λ = 1.5418 Å) at room temperature.[18]

A diffractogram was acquired under ambient conditions at a power setting of 40 kV and 20 mA in adsorption mode while the sample rotated perpendicular to the beam.

2.1.5 Solubility

Solubility of a substance can be defined as the amount of substance dissolved in a given amount of solvent. Solubility can be expressed in g (dissolved compound)/ g (solvent) or mg/g.

The following points should be addressed in all solubility determinations:

1. The solvent and the solute must be pure.
2. A saturated solution must be obtained before any solution is removed for analysis.
3. The method of separating a sample of saturated solution from undissolved solute must be satisfactory.
4. The temperature must be adequately controlled.

Solubility values were obtained by gravimetric method. A saturated solution was obtained by stirring known amount of excess powdered solute with known amount of solvent for six hours at ambient temperature. Some undissolved solid was present at the completion in order to ensure that the solution was saturated. The undissolved material was filtered off and its weight was recorded.

When we consider 1g of solute, this is said to be

- very soluble if it dissolves in less than 1g of solvent,
- freely soluble if it dissolves in 1g to 10 g of solvent, and
- very slightly soluble if it dissolves in 1000 to 10 000 g of solvent.[19]

2.1.6 Computing components

ConQuest: the primary program for searching and retrieving information from the Cambridge Structural Database (CSD).[15]

SADABS (Siemens Area Detector Absorption Corrections): an application in the APEX suite used to scale and correct data for absorption collected on a Bruker AXS area detector.[20] The

program is designed to exploit data redundancy, corrects for errors resulting from the variation in the volume of the crystal, absorption by the crystal support and crystal decay during the measurement.

XPREP: this program determines the space group, reads the raw data file (.raw) and the parameter file (.p4p) written by the diffractometer control program, also write the instruction file (.ins) and reflection data file (.hkl).[20]

X-Seed: Graphical User Interface for crystallography and graphical programs.[9]

Layer is a component of X-Seed. It displays simulated precession photographs of the reciprocal lattice levels using the intensity data.[13]

Lazy Pulverix: software which calculates the theoretical powder X-ray diffraction pattern from single crystal X-ray diffraction data.[11]

Pov-Ray: program which generates graphics.[12]

PovLabel: allows controlling the atom labels on an image rendered using Pov-Ray.[12]

Mercury: Analysis software which provides options to aid the investigation and analysis of crystal structures. It can import chemical bond types, 2D connection tables and present them in 3D illustration, generates packing diagrams, defines and visualises Miller planes, and take a slice through a crystal in any direction. Also, it displays space group symmetry elements, calculates voids based either on contact surface or solvent accessible surface and intermolecular potentials; also it performs basic gas phase calculation.[21]

Crystal Explorer[22]: A computer package that utilizes calculated Hirshfeld surfaces[23] of molecules within a crystal structure to determine the intermolecular interactions between particular molecules or for the crystal structure in its entirety. Hirshfeld surfaces are created by an extension of the weight function describing an atom in a molecule, to include the function of a molecule in a crystal.[24] The isosurfaces generated from these calculations, with a specified weight function w (r) = 0.5, surrounds the molecule and by partitioning the electron density of the molecular fragments, delineates the space occupied by a molecule in a crystal[25]. Hirshfeld surfaces can provide information about intermolecular interactions in the crystal as the surface is determined by both the enclosed molecule and its closest neighbours.[25] Fused sphere van der

Waals (or CPK), smoothed Connelly surfaces or other molecular surfaces can be used to visualise and quantify molecular geometries and designated only by the molecule itself. [25] The only prerequisite for quality data regarding intermolecular interactions to be extracted from Hirshfeld surfaces is that the crystal structures imported into the program are well-characterised with all hydrogen atoms located accurately. The equation used to define a Hirshfeld surface is w (r) = 0.5 where w (r) is the weight function[25] describe as

$$w(\text{r}) = \sum_{i \in molecule} \rho_i(r) / \sum_{i \in crystal} \rho_i(r)$$

where ρ_i(r) is a spherical atomic electron distribution located at the ith nucleus. The surfaces incorporated in this study are all calculated using the d_{norm} function so that the contact distance is normalised according to the formula

$$d_{norm} = \frac{d_i - r_i^{vdW}}{r_i^{vdW}} + \frac{d_e - r_e^{vdW}}{r_e^{vdW}},$$

d_i is the distance from the surface to the nearest atom interior to the surface; d_e is the distance from the surface to the nearest atom exterior to the surface. The sum of the two distances would give an approximate contact distance.

2.2 Materials

2.2.1 Host compounds

(*RS*)-4-Amino-3-(4-chlorophenyl)butanoic acid or baclofen (BAC), 4,4-bipyridine (BIPY), 1,2-bipyridine ethane (ETBIPY) are the host compounds used in this project. Their chemical structures are represented in Figure **2.1** and **Table 2.2** shows their molecular formulas.

a) (*RS*)-4-amino-3-(4-chlorophenyl)   b) 4,4'-bipyridine   c) 1,2-bis(4-pyridyl)ethane
    butanoic acid, Baclofen, BAC   BIPY   ETBIPY
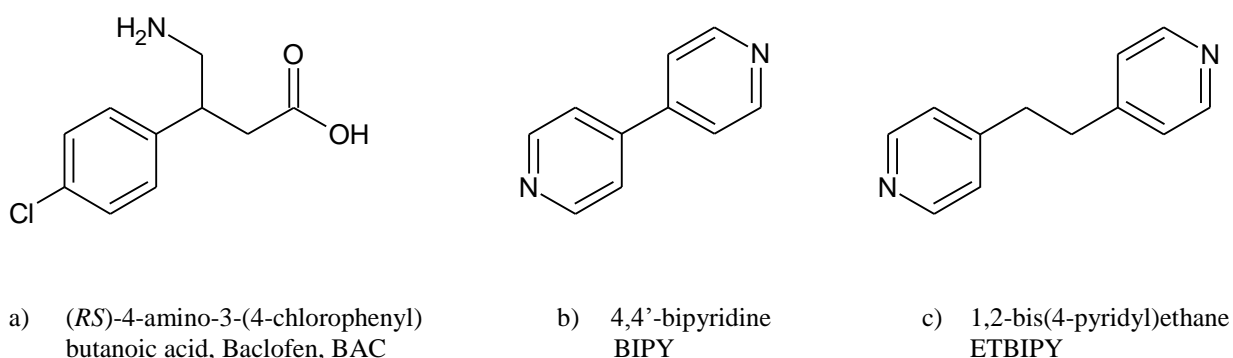
Figure 2.1 Chemical structures, systematic names, abbreviations and empirical formulas of host compounds.

Table 2.2 Physical properties and formulas of the host compounds used.

Host	Formula	Mr (g.mol⁻¹)	Mp (°C)
BAC (baclofen)	$C_{10}H_{12}ClNO_2$	213.66	206-208
BIPY (4,4'-bipyridine)	$C_{10}H_8N_2$	156.18	114
ETBIPY (1,2-bis(4-pyridyl)ethane)	$C_{12}H_{10}N_2$	184.24	110-112

2.2.2 Guest compounds

2-Phenylbutyric acid (racPBA), benzoic acid (BA), p-toluic acid (PTA),phenylsuccinic acid (PSA), oxalic acid (OA), maleic acid (MA), 1-hydroxy-2-naphthoic acid (HNA), p-toluene sulfonic acid (PTSA) were purchased from Sigma-Aldrich and Merck & Co. The physical properties of the mono- and dicarboxylic acid guest compounds with their chemical formulae and molecular weights are given in **Table 2.3** while their structures are illustrated in **Figure 2.2** (monocarboxylic acids) and **Figure 2.3** (dicarboxylic acids).

The mono- and the dicarboxylic acids were selected systematically. The applied compounds differ from each other in such a manner that it is possible to investigate their effect caused on the crystal packing. For example, comparison of benzoic acid and p-toluic acid cocrystals of baclofen may highlight the effect of the extra methyl group on the packing.

Table 2.3 Physical properties and formulas of the guest compounds.

Guests	Formula	Mr (g.mol^{-1})	Bp (°C)	Mp (°C)
BA (Benzoic acid)	$C_7H_6O_2$	122.12	249.2	122.4
PTA (p-Toluic acid)	$C_8H_8O_2$	136.15	274	180.5
PSA (Phenylsuccinic acid)	$C_{10}H_{10}O_4$	194.19	–	168
racPBA (2-Phenylbutyric acid)	$C_{10}H_{13}NO_2$	179.22	–	253
OA (Oxalic acid)	$C_2H_2O_4$	90.03	–	189-191
MA (Maleic acid)	$C_4H_4O_2$	116.07	–	135
PTSA (p-toluene sulfonic acid)	$C_7H_7SO_3H$	172.20	140	38
HNA (1-hydroxy-2-naphthoic acid)	$C_{11}H_8O_3$	188.18	–	195-200
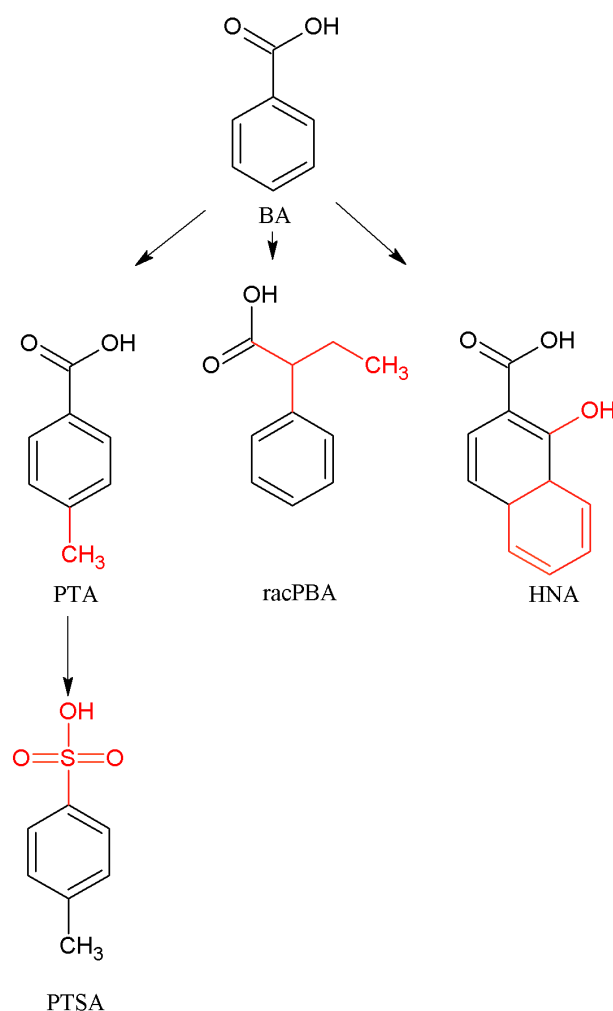
Figure 2.2 Chemical structures of monocarboxylic acid guest compounds. The systematic modification of the molecular structure is highlighted with red.
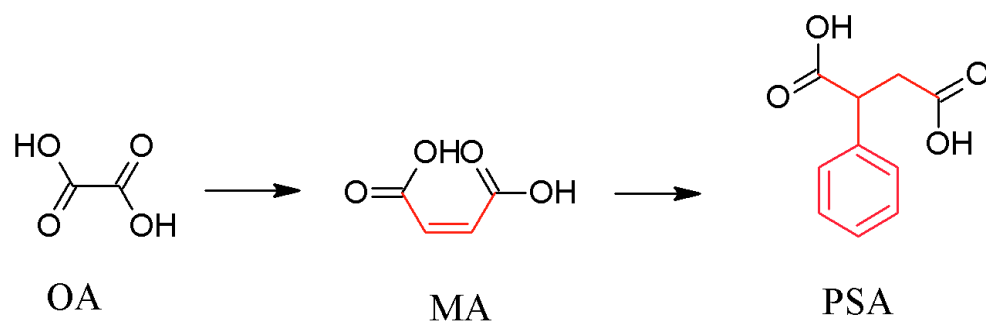
Figure 2.3 Chemical structure of dicarboxylic acid guest compounds and their systematic modification is highlighted with red.

References:

[1] Gordon, A.J. & Ford, R.A. 1972. *The Chemist's Companion: a Handbook of Practical Data, Techniques, and References.* John Wiley & Sons, New York, USA.

[2] Haines, P.J. 1995. *Thermal Methods and Analysis*. Blackie Academic & Professional, London.

[3] Brown, M.E. 1998. *Introduction to Thermal Analysis*. Chapman & Hall, London.

[4] Caira, M.R. & Nassimbeni, L.R. 1996. *Phase transformations in inclusion compounds, kinetics and thermodynamics of enclathration.* In Comprehensive Supramolecular Chemistry, MacNicol, D.D., Toda, F., Bishop, R., Eds; Pergamon: Oxford; Vol 6, Chapter 5.

[5] Stout, G.H. & Jensen, L.H. 1965. X-*ray Structure Determination: a practical guide*. The Macmillan Company, New York.

[6] Rissanen, K. 2014. X-Ray Crystallography. *Encyclopedia of Supramolecular Chemistry*, 2: 1586-1591.

[7] Brown, P.J. & Forsyth, J.B. 1973. *The crystal structure of solids*. Edward Arnold Limited, London.

[8] Bruker 2005. *APEX*2. Version 1.0-27. Bruker AXS Inc., Madison, Wisconsin, USA.

[9] Sheldrick, G.M. & Schneider, T.R. 1997. SHELXL: High resolution refinement. *Macromol. Crystallogr,* 277: 319-343.

[10] Barbour, L.J. 2003. X-Seed: Graphical interface for SHELX program. *J. Supramol. Chem*, 1: 189-191.

[11] XPREP, Data Preparation and Reciprocal Space Exploration, Version 5.1/NT ©1997, Bruker Analytical X-Ray Sytems.

[12] Yvon, K., Jeitschko, W. & Parthe, E.J. 1997. LAZY PULVERIX, a computer program, for calculating X-ray and neutron diffraction powder patterns. *J. Appl.Cryst.,* 10: 73-74.

[13] Pov-Ray for Windows, Version 3.1e.watcom.win32. The persistence of vision development team, ©1991-1999.

[14] Barbour, L.J. 1999. LAYER, A computer program for the graphic display of intensity data as simulated precession photographs. *J. Appl. Cryst.*, 32: 351.

[15] Barbour, L.J. 1999. Section, A computer program for the graphic display of cross sections through a unit cell. *J. Appl. Cryst.*, 32: 351.

[16] Spek, A.L. PLATON, A multipurpose crystallographic tool ,Version 10500 , © 1980-2000

[17] ConQuest, A program for the search of the CSD, version 1.7, © 2001.

[18] Bruker 2010. D2 PHASER.Version 3-07. Bruker AXS GmbH, Karlsruhe, Germany.

[19] Aulton, M.E. 2002. *Pharmaceutics: The Science of Dosage Form Design.* Second Edition, Churchill Livingstone.

[20] Sheldrick, G.M. 2002. University of Göttingen, Germany.

[21] Allen, F.H. & Lipscomb, K.J. 2004. The Cambridge Structural Database. *Encyclopaedia of Supramolecular Chemistry*, 1: 161-168.

[22] Wolff, S.K, Grimwood, D.J, McKinnon, J.J, Jayatilaka, D. & Spackman, M.A. 2007. Crystal Explorer 2.1. University of Western Australia, Perth.

[23] Hirshfeld, F.L. 1977. Bonded atom Fragments for Describing Molecular Charge Densities. *Theor. Chim. Acta,* 44: 129-138.

[24] Spackman, M.A. & Jayatilaka, D. 2009. Hirshfeld Surface Analysis *CrystEngComm*, 11: 19-32.

[25] The Crystal Explorer Manual. http://hirshfieldsurface.net/wiki/index.php/Surface_Properties. Accessed 15 February 2014.

Chapter 3

Analysis of model co-crystals

3.1 Co-crystals of 4,4'-bipyridine (BIPY)

The crystal structure, thermal analysis and powder X-ray analysis of the co-crystals formed between the host, 4,4'-bipyridine (BIPY) and the guest compounds, p-toluic acid (PTA), 2-phenylbutyric acid (racPBA) and racemic phenylsuccinic acid (racPSA) will be discussed. The line diagrams of the compounds are shown in **Figure 3.1.**

BIPY
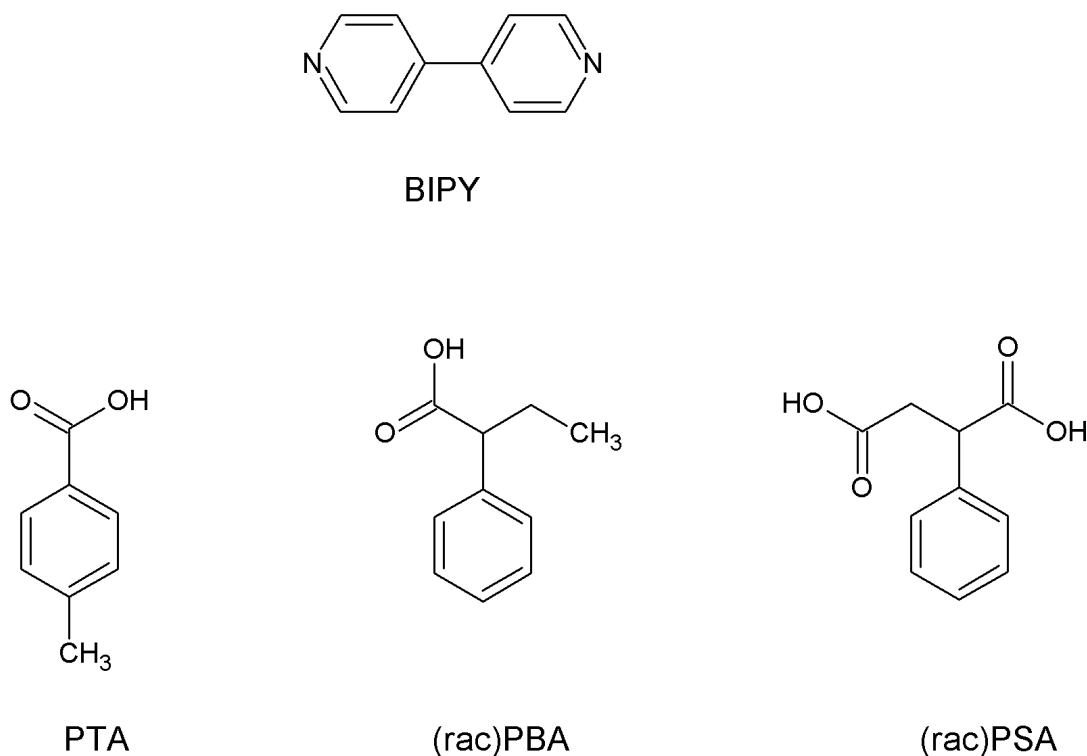
PTA   (rac)PBA   (rac)PSA

Figure 3.1 Structural line diagrams for 4,4'-bipyridine (BIPY) and the guest compounds, p-toluic acid (PTA), racemic 2-phenylbutyric acid (racPBA) and racemic phenylsuccinic acid (racPSA).

3.1.1 Co-crystal of 4,4'-bipyridine with p-toluic acid (BIPY•PTA)

The first results of the model co-crystals was the structure obtained from the phenylsuccinic acid (PSA) and BIPY co-crystallisation. These crystals contain 1:1 ratios of PSA and BIPY thus all other crystallisations were set up in this manner.

A 1:1 stoichiometric amount of the BIPY (59 mg, 0.38 mmol) and PTA (51 mg, 0.38 mmol) was added into a vial. The mixture was dissolved in a minimum amount of dimethyl sulfoxide (DMSO) until the solution became clear and left to evaporate at room temperature. Colourless block shape crystals were obtained after few weeks.

3.1.1a Crystal structure analysis of BIPY•PTA

A suitable crystal with dimensions 0.14×0.18×0.33 mm was selected for single crystal X-ray analysis. The compound crystallized in the monoclinic achiral space group $P2_1/c$ (No. 14) and its crystallographic asymmetric unit contains half a molecule of the BIPY and one molecule of p-toluic acid (PTA) with molecular formula of $C_{13}H_{12}NO_2$. The structure refined to $R_1=$ 0.0461 and $wR_2=$ 0.1298. The cell consists of four host molecules and two guest molecules (Z=4). The hydrogen atom (H18) on the carboxylic acid group was located in the electron density map and its coordinates refined freely. There is no proton transfer from the host to the guest compound; therefore this system is a co-crystal. The main building block of the crystal is represented in **Figure 3.2** which consists of one BIPY molecule connected to two carboxylic moieties on both sides. The BIPY lies on an inversion centre. The data collection and refinement details are summarized in **Table 3.1**.
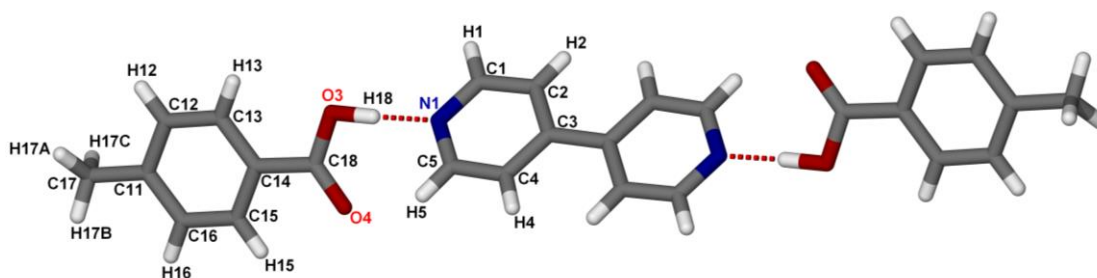
Figure 3.2 The structure of BIPY•PTA consists of hydrogen bonded molecular associates in the manner that one BIPY bonds to two PTA. The asymmetric unit is labelled**.**

In the crystal lattice of BIPY•PTA, the host molecule is hydrogen bonded to two PTA via the carboxylic acid group through O3-H18···N1 (2.67 Å, 178°) interactions. The two rings of the BIPY are coplanar while the angle between the planes formed by the BIPY and the carboxylic acid group is 46°. (**Figure 3.3**) Because of this conformational arrangement there is no hydrogen bond observed between the carbonyl moiety and the ortho position hydrogen of the BIPY. Also, weaker interactions such as C1-H1···O4 (3.24 Å, 157°) are present. The hydrogen bonds are given in **Table 3.2**. These hydrogen bonded units are packed into layers and generate zigzag chains sustained by -COOH···N_{arom} supramolecular heterosynthons. Two parallel motifs (blue and red) in the crystal packing are shown in **Figure 3.4.**
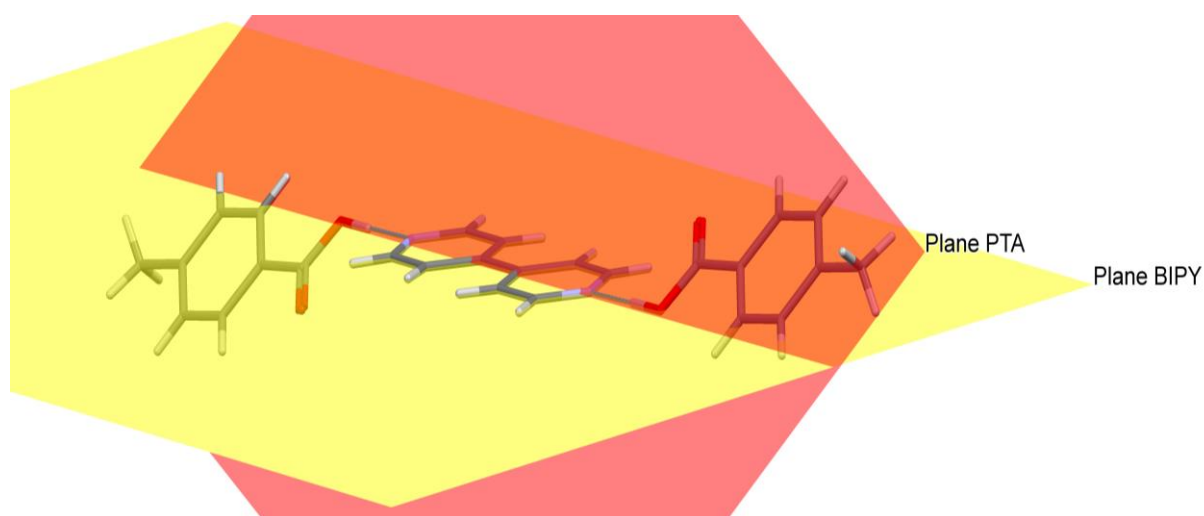
Figure 3.3 Molecular arrangement in the hydrogen bonded unit of BIPY•PTA. The enclosed angle of the plains (red-aromatic ring of PTA, yellow-aromatic ring of BIPY) is 46°.
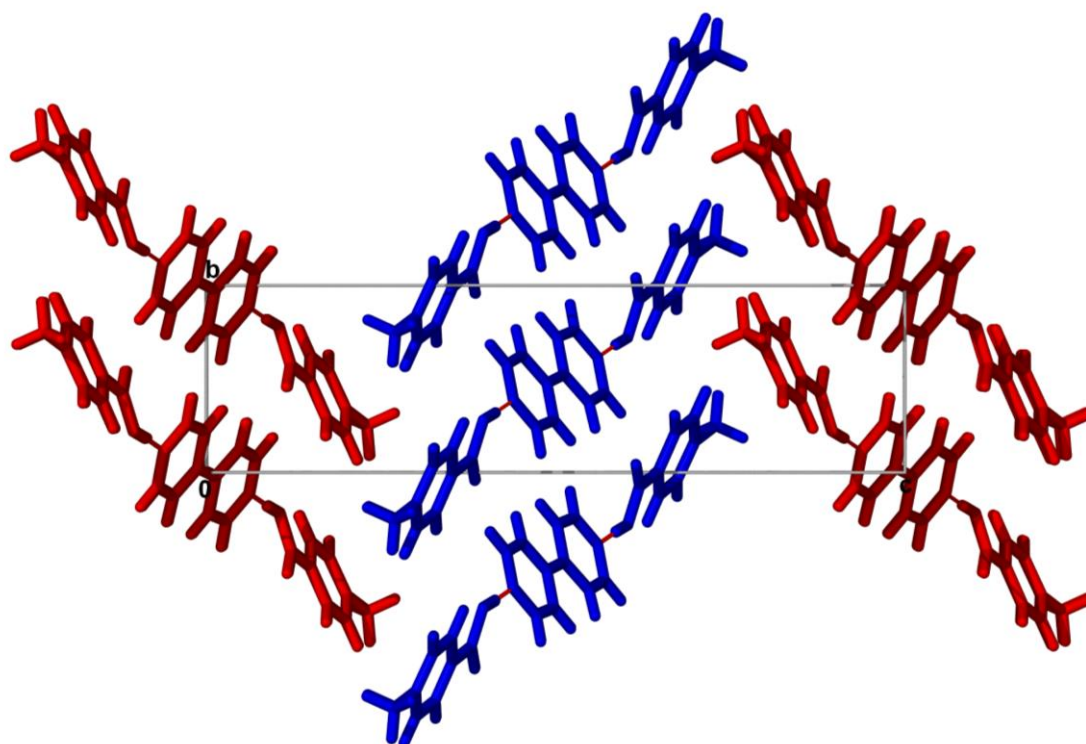
Figure 3.4 Packing diagram of BIPY•PTA down [100].

Table 3.1 Crystal data of BIPY•PTA, BIPY•(rac)PBA and BIPY•(rac)PSA

Crystal data			
Compounds	BIPY•PTA	BIPY•(rac)PBA	BIPY•(rac)PSA
Molecular formula	$C_{13}H_{12}NO_2$	$C_{15}H_{16}NO_2$	$C_{20}H_{18}N_2O_4$
Formula weight (g.mol^{-1})	214.24	242.29	350.36
Crystal system	monoclinic	monoclinic	monoclinic
Space group	P2$_1$/c (No.14)	P2$_1$/c(No.14)	P2$_1$/n(No.14)
a(Å)	7.8077(16)	5.695(11)	9.3729(19)
b(Å)	6.1034(12)	32.968(7)	18.545(4)
c(Å)	22.881(5)	7.224(14)	11.135(2)
α(°)	90.00	90.00	90.00
β(°)	91.67	109.74(3)	113.89(3)
γ(°)	90.00	90.00	90.00
V(Å)	1089.9(4)	1276.7(4)	1769.8(6)
Z	4	4	4
ρcalc / g.cm^{-3}	1.306	1.261	1.315
μ(MoKα)/ mm^{-1}	0.089	0.084	0.093
F(000)	452	516	736
Crystal size (mm)	0.14×0.18×0.33	0.11×0.42×0.48	0.18×0.23×0.32
Temperature (K)	173(2)	173(2)	173(2)
Radiation [Å]	MoKα, 0.71073	MoKα, 0.71073	MoKα, 0.71073
Theta min-max[°]	2.61, 28.29	2.47, 28.25	2.20, 28.37
Dataset	-8:10; -6:8; -30:18	-7:7; -43:43;-9:9	-12:12; -24:24; -6:14
Final R indices [I>2.0 (I)]	R$_1$=0.0461, wR$_2$=0.1163	R$_1$=0.0613, wR$_2$=0.1289	R$_1$=0.0411, wR$_2$=0.1006
R indices (all data)	R$_1$=0.0696, wR$_2$=0.1298	R$_1$=0.0762, wR$_2$=0.1350	R$_1$=0.0577, wR$_2$=0.1096
Tot., uniq.data, R(int)	5002, 1924, 0.0235	10554, 2470, 0.0297	12630, 3352, 0.0299
N$_{ref}$, N$_{par}$	1924, 148	3116, 166	3352, 238
S	1.038	1.087	1.040
Max. and av. Shift/error	0.00, 0.00	0.00, 0.00	0.082, 0.000
Min. and max. resd. dens	0.348, -0.179	0.483, -0.190	0.261, -0.190

Table 3.2 Hydrogen bonds of BIPY•PTA

D-H···A	d(D-H) (Å)	d(H···A) (Å)	d(D···A) (Å)	D-H···A (°)	Symmetry operator
O3-H18···N1	1.04	1.63	2.67	178	-1+x, y, z
C1-H1···O4	0.95	2.35	3.24	157	1+x, 1+y, z

3.1.1b Thermal analysis of BIPY•PTA

The DSC curve of BIPY•PTA shows one endotherm corresponding to the melting point of the crystal (T_{on}= 158.9°C, T_{peak}= 161.2°C). The melting point of the co-crystal is located between the melting points of the two starting material, BIPY (T_{on}= 108.6°C, T_{peak}= 111.2°C) and PTA (T_{on}= 178.0°C, T_{peak}= 181.8°C). BIPY hydrated during the sample preparation (grinding) for DSC measurement thus the first endotherm observed on the DSC curve is related to the loss of water of the BIPY•H_2O. (**Figure 3.5**)
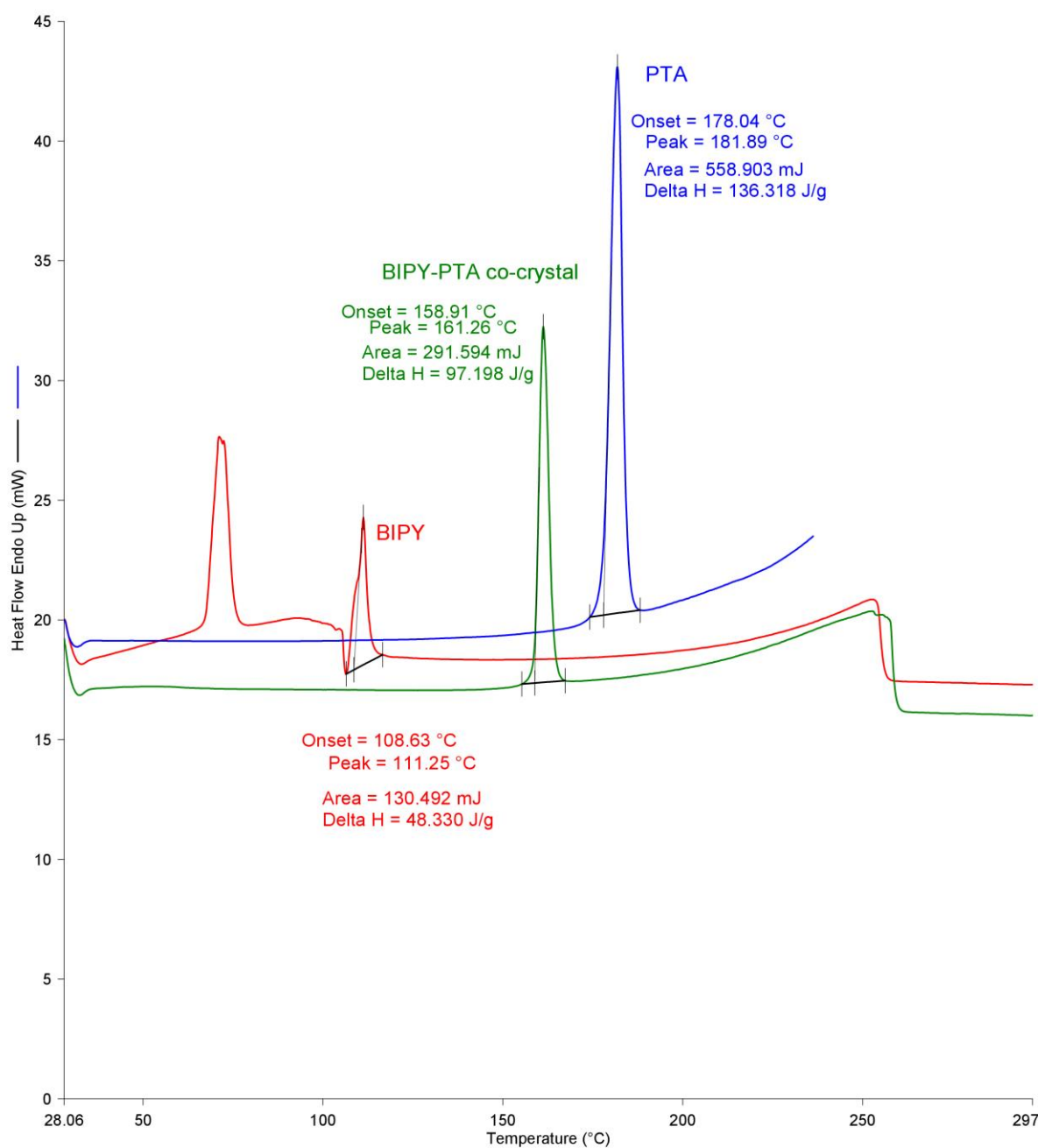
Figure 3.5 DSC curve of BIPY•PTA and the individual starting materials, BIPY and PTA.

3.1.1c Powder X-ray analysis of BIPY•PTA

Powder X-ray analysis was conducted to show that the structure detected by using one single crystal only (**Figure 3.6**, green-BIPY•PTA single crystal, calculated) is representative to the bulk material (**Figure 3.6**, red-BIPY•PTA bulk). Also PXRD analysis was used to show that the BIPY•PTA co-crystal can be prepared via a more environmental friendly method by using a minimal amount of solvent. Pure BIPY and PTA in a 1:1 ratio were ground with several drops of DMSO and after 30 mins the PXRD pattern was collected (**Figure 3.6**, blue-BIPY•PTA grinding) and was compared to the starting pattern of the pure BIPY and PTA (**Figure 3.6**, light blue-BIPY, purple-PTA). The patterns for the single crystal and the ground material are quite similar and clearly differ from the starting compounds. However, the match is not perfect and several peaks related to BIPY and PTA are still noticeable, therefore the reaction occurs only partially.
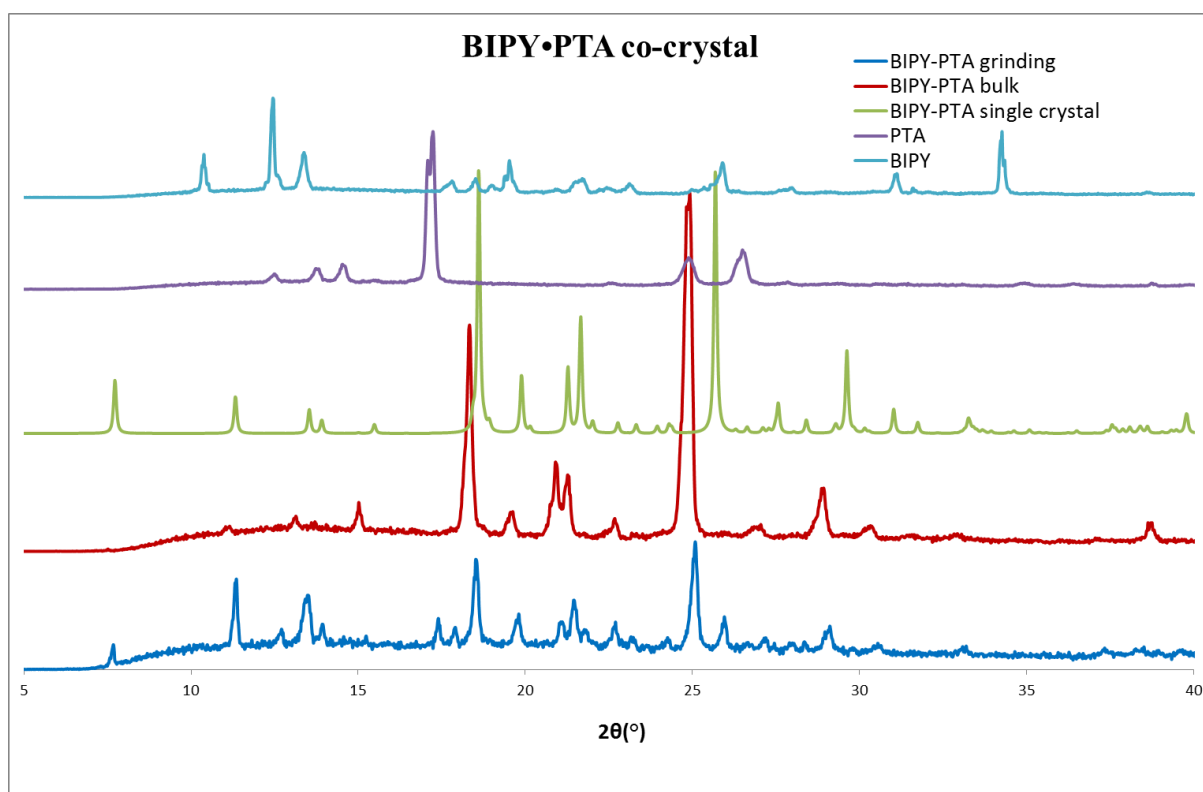
Figure 3.6 Comparison of PXRD patterns: pure BIPY(light blue), pure PTA (purple), the pattern generated from single crystal structure of BIPY•PTA (green), PXRD pattern of the bulk of the crystallisation (BIPY•PTA bulk -red) and the result of the solvent drop grinding (BIPY•PTA blue).

3.1.2 Co-crystal of 4, 4'-bipyridine with racemic 2-phenylbutyric acid, BIPY•(rac)PBA

Co-crystals of BIPY•(rac)PBA were prepared by dissolving 57 mg (0.36 mol) of BIPY and 60 mg (0.37 mol) of (rac)PBA in 3 ml methanol. The solution was stirred until it became clear and left to crystallise at room temperature. Block shape colourless crystals were obtained after two weeks.

3.1.2a Crystal structure analysis of BIPY•(rac)PBA

Data for a single crystal with dimensions of $0.11 \times 0.42 \times 0.48$ mm were collected and the structure of BIPY•(rac)PBA was solved in the monoclinic P2$_1$/c (No. 14) achiral space group. The structure was refined successfully to R$_1$=0.0613 with wR$_2$=0.1350 and the crystallographic data are summarized in **Table 3.1.** The asymmetric unit contains half a molecule of BIPY and one molecule of the PBA with the molecular formula of $C_{15}H_{16}NO_2$. The cell consists of four host molecules and two guest molecules (Z=4). The hydrogen atom (H15) on the carboxylic acid group was located in the electron density map and its coordinates refined freely. It is a co-crystal; no proton transfer was observed between the host and the guest. The main building block of the structure is presented in **Figure 3.7.** Both BIPY nitrogens hydrogen bonded to a PBA molecule via a O1-H15···N1 interaction (2.61Å, 164°). The two rings of the BIPY are coplanar (C2-C3-C3'-C4' torsion angle is 0°) while the angles between the planes formed by the BIPY and the carboxylic acid group of the PBA is 14°. Because of this conformational arrangement an extra hydrogen bond appears between the carbonyl moiety and the ortho position hydrogen of the BIPY (C5-H5···O2 3.34Å, 122°). The crystal structure contains both enantiomers of the racemic PBA. The BIPY molecule lies on a center of inversion, therefore it is hydrogen bonded to an S- and an R-PBA to form heterochiral dumbbell shape molecular associates. These units are bonded to their neighbour via the C4-H4···O2 and C5-H5···O2 bifurcated hydrogen bonds. This arrangement leads to the formation of tape like motifs in the crystal and eventually the tapes form a zigzag structure. This packing feature is illustrated in **Figure 3.8** where the tapes running parallel are drawn with different colours. The hydrogen bonds are summarized in **Table 3.3**.
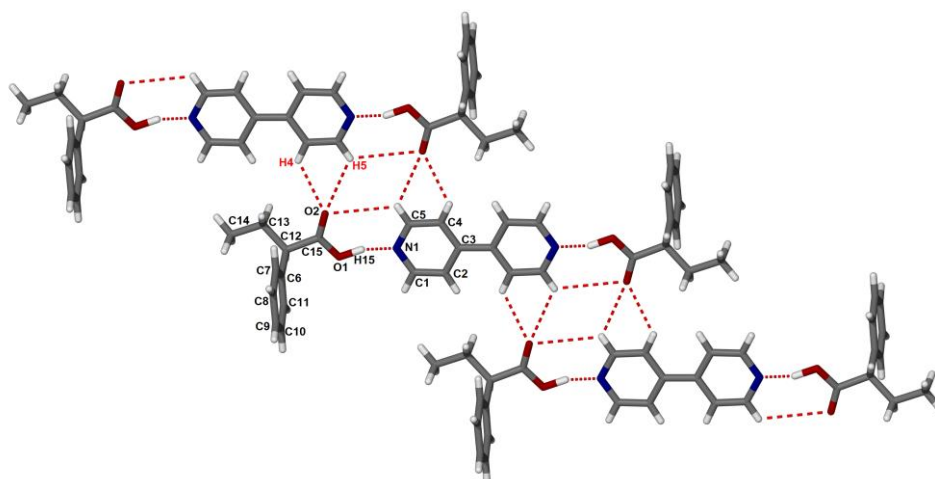
Figure 3.7 The dumbbell shape main building block of BIPY•(rac)PBA and the hydrogen bonding between the molecules. Only the atoms of the asymmetric unit are labelled. (Symmetry generated atom's labels are red.)
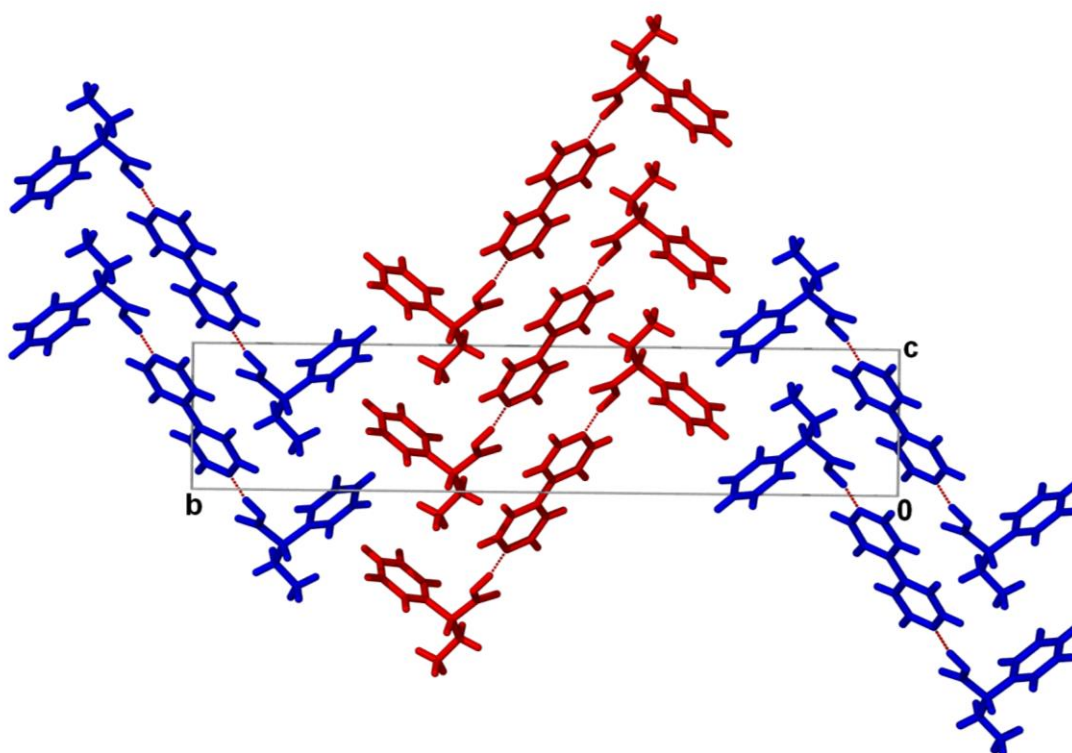
Figure 3.8 Packing diagram of BIPY•(rac)PBA view down [100]. The parallel tapes are coloured accordingly.

Table 3.3 Hydrogen bonds of BIPY•(rac)PBA

D-H···A	d(D-H) (Å)	d(H···A) (Å)	d(D···A) (Å)	D-H···A (°)	Symmetry operator
O1-H15···N1	1.06	1.63	2.61	164	x, y, -1+z
C5-H5···O2	0.95	2.74	3.34	122	1-x, -y, -z
C4-H4···O2	0.95	2.62	3.27	126	1-x, -y, -z

3.1.2b Thermal analysis of BIPY•(rac)PBA

The DSC curve of BIPY•(rac)PBA crystals shows one endotherm corresponding to the melting point of the crystal (T_{on}= 80.5°C, T_{peak}= 84.1°C). The melting point of the co-crystal is located between the melting points of the two starting material, BIPY (T_{on}= 108.6°C, T_{peak}= 111.3°C) and (rac)PBA (T_{on}= 39.9°C, T_{peak}= 43.7°C). The first endotherm observed on the DSC curve related to BIPY is related to the decomposition of the BIPY•H_2O that may form during sample preparation. (**Figure 3.9**)
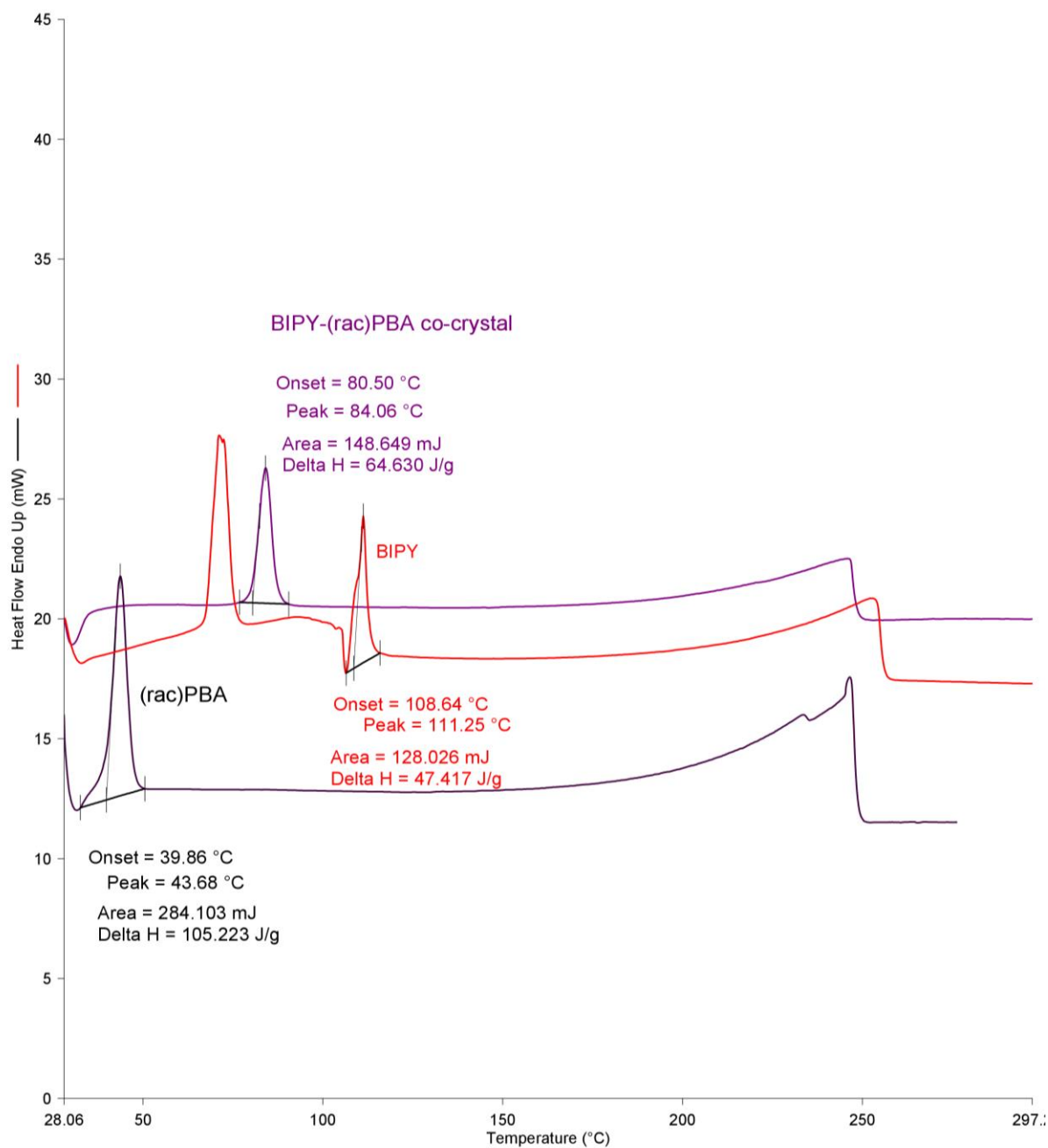
Figure 3.9 DSC curve of BIPY•(rac)PBA.

3.1.2c Powder X-ray analysis of BIPY•(rac)PBA

Powder X-ray analysis was carried out to show that the structure detected by using one single crystal only (**Figure 3.10** green-BIPY•(rac)PBA single crystal, calculated) is representative to the bulk material (**Figure 3.10** red-BIPY•(rac)PBA bulk). PXRD analysis was used to show that the BIPY•(rac)PBA co-crystal obtained via slow evaporation from methanol can be prepared via the environmentally friendly method, solvent drop grinding. Pure BIPY and (rac)PBA were ground with several drops of methanol in 1:1 ratio and after 10 mins the PXRD pattern was collected (**Figure 3.10** blue-BIPY•(rac)PBA grinding). This was compared to the starting pattern of the pure BIPY and (rac)PBA (**Figure 3.10** light blue-BIPY, purple-(rac)PBA). The patterns for the single crystal and the ground material are quite similar and clearly differ from the starting compounds. However, the match is not perfect and several peaks related to BIPY and PBA are still noticeable, therefore the reaction occurs only partially.
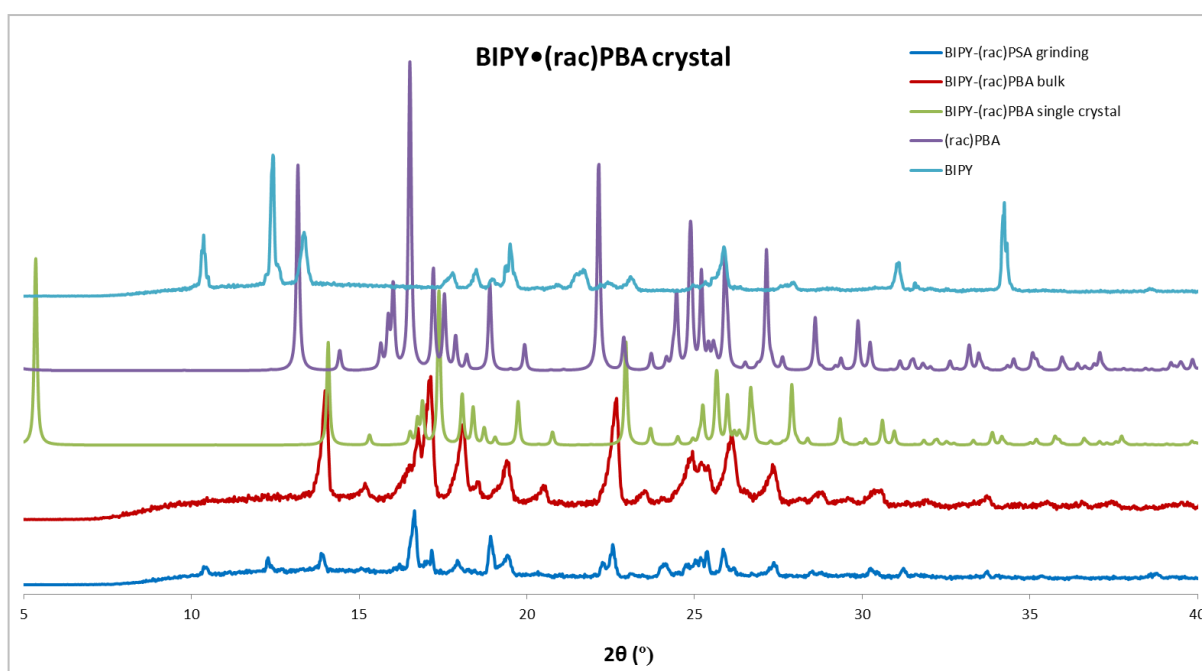
**Figure 3.10** Comparison of PXRD patterns: pure BIPY (light blue), pure (rac)PBA (purple), the pattern generated from single crystal structure of BIPY•(rac)PBA (green), PXRD pattern of the bulk of the crystallisation (BIPY•(rac)PBA bulk- red) and the result of the solvent drop grinding (BIPY•(rac)PBA blue).

3.1.3 Co-crystal of 4,4'-bipyridine with racemic phenylsuccinic acid, BIPY•(rac)PSA

The co-crystal of 4,4'-bipyridine (BIPY) and phenylsuccinic acid, (rac)PSA was prepared by dissolving 112 mg (0.72 mol) of BIPY and 140 mg (0.72 mol) of (rac)PSA in 2.8 ml of isopropanol until the solution became clear, and was left to crystallise at room temperature. Block shape yellow crystals were obtained after 1 week.

3.1.3a Crystal structure analysis of BIPY•(rac)PSA

A suitable crystal with dimensions 0.18×0.23×0.32 mm were selected and subjected to single crystal data collection. The structure of the BIPY•(rac)PSA co-crystal was solved in the monoclinic achiral space group P2$_1$/n (No. 14) with a molecular formula of $C_{20}H_{18}N_2O_4$. The structure refined to R$_1$= 0.0411 and wR$_2$=0.1096. The asymmetric unit consists of one BIPY and a hydrogen bonded PSA molecule. **Figure 3.11** shows the asymmetric unit with labelled atoms and the specified hydrogen bond. The related crystal data is summarized in **Table 3.1**. The unit cell consists of four host molecules and four guest molecules (Z=4). The hydrogen atom (H20) on the carboxylic acid group was located in the electron density map and its coordinates refined freely. There was no proton transfer observed from the host to the guest molecules, therefore this is a co-crystal.
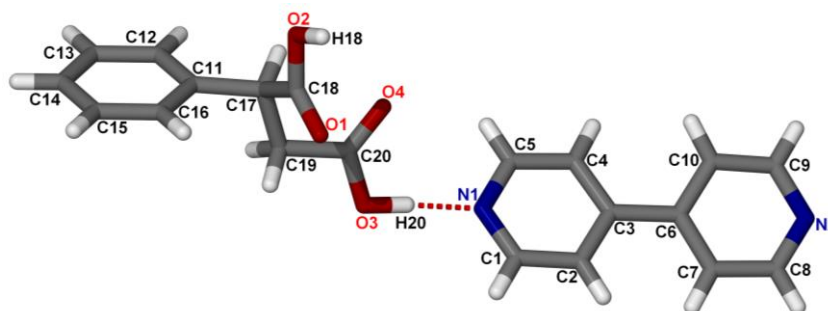
Figure 3.11 Asymmetric unit with numbered atoms with the hydrogen bond between BIPY and the PSA moiety.

In this case, the aromatic rings of the BIPY moiety are not coplanar; the torsion angle of C2-C3-C6-C7 is 15°. Both aromatic nitrogen atoms hydrogen bonded to a PSA moiety via their carboxylic acid group: O2-H18···N2 (2.66 Å, 168°) and O3-H20···N1 (2.65 Å, 176°). (**Table 3.4**) The molecules form a zigzag 1D chain along the b-axis [010] via these hydrogen bonds. (**Figure 3.12a**)

Analysis of the single crystal structure revealed that one BIPY hydrogen bonded to two molecules of PSA of the same chirality therefore the zigzag motif itself is homochiral. Also some additional hydrogen bonds can be formed between these homochiral chains of molecules: C1-H1···O4 (3.31Å, 167°), C8-H8···O2 (3.42Å, 153°C), C10-H10···O1 (3.35Å, 137°), C15-H15···O1 (3.46Å, 155°) and C17-H17···O3 (3.37Å, 158°). (**Figure 3.12b**)

Table 3.4 Hydrogen bonds of BIPY•(rac)PSA

D-H···A	d(D-H) (Å)	d(H···A) (Å)	d(D···A) (Å)	D-H···A (°)	Symmetry operator
O2-H18···N2	0.91	1.76	2.66	168	2-x, -y, 1-z
O3-H20···N1	0.96	1.70	2.65	176	½+x, ½-y, ½+z
C1-H1···O4	0.95	2.38	3.31	167	
C8-H8···O2	0.95	2.55	3.42	153	1+x, y, z
C10-H10···O1	0.95	2.60	3.35	137	x, y, 1-z
C15-H15···O1	0.95	2.57	3.46	155	1-x, -y, 2-z
C17-H17···O3	0.95	2.42	3.37	158	**- ½+x, ½-y, - ½+z**

(a)   **(b)**
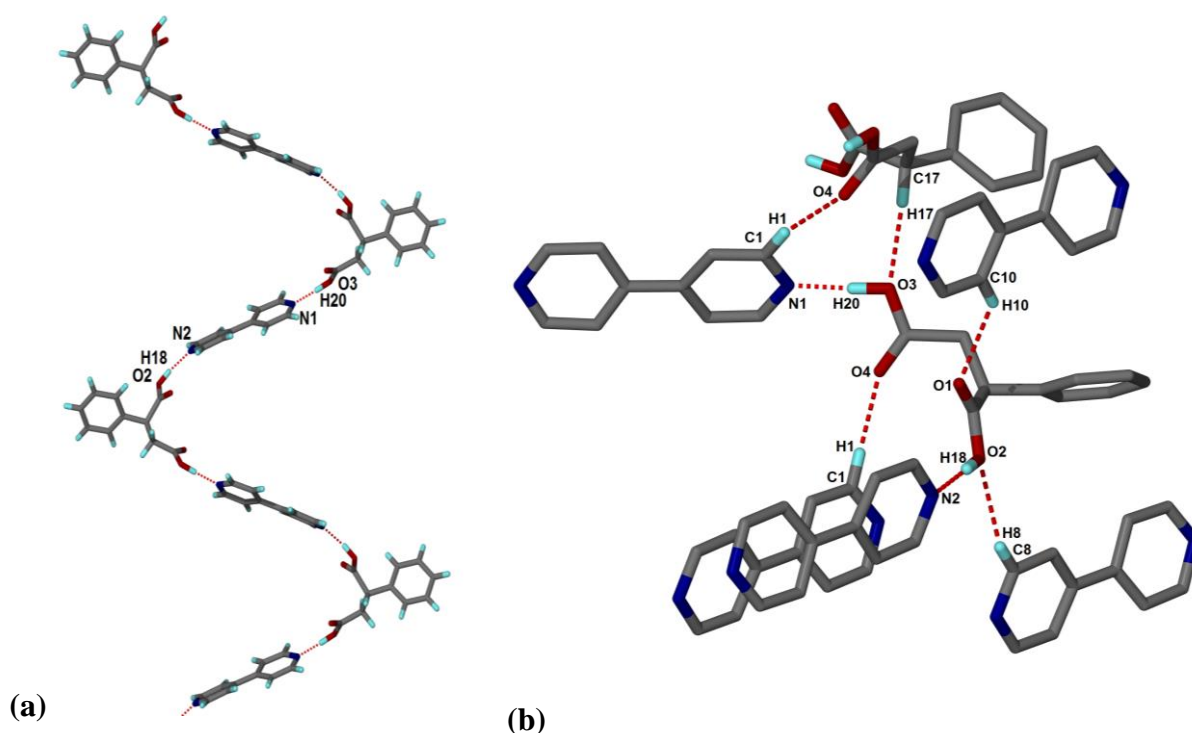
Figure 3.12 (a) Packing of BIPY•(rac)PSA view down [001] and the forming of the zigzag formation. (b) Extended hydrogen bond network in the co-crystal of BIPY•(rac)PSA.

These interactions assemble the 1D homochiral hydrogen bonded chains into homochiral layers. **Figure 3.13** shows the individual layers of molecules with the same chirality coloured with yellow (…S-PSA•BIPY•S-PSA…) and blue (…R-PSA•BIPY•R-PSA…) down [100] (a) and [001] (b) direction. The 3D structure formed by the alternating layers of opposite chirality.

(a)   **(b)**
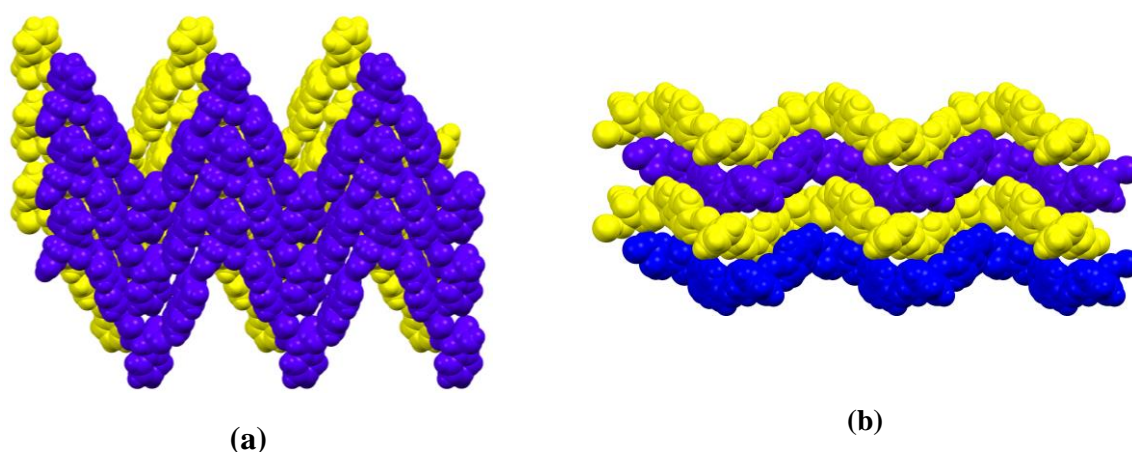
Figure 3.13 Individual layers of molecules with the same chirality coloured with yellow (…S-PSA•BIPY•S-PSA…) and blue (…R-PSA•BIPY•R-PSA…) down [100] (a) and [001] (b) direction.

3.1.3b Thermal analysis of BIPY•(rac)PSA

The DSC curve of BIPY•(rac)PSA crystals shows one endotherm corresponding to the melting point of the crystal (T_{on}= 148.4°C, T_{peak}= 150.4°C). The melting point of the co-crystal is located between the melting points of the two starting material, BIPY (T_{on}= 108.6°C, T_{peak}= 111.3°C) and (rac)PSA (T_{on}= 169.2°C, T_{peak}= 172.6°C). The first endotherm observed on the DSC curve related to BIPY is related to the decomposition of the BIPY.H_2O which formed during sample preparation. (**Figure 3.14**)

3.1.3c Powder X-ray analysis of BIPY•(rac)PSA

Powder X-ray analysis was carried out to show that the structure detected by using one single crystal only (**Figure 3.15**, green-BIPY•(rac)PSA single crystal, calculated) is representative to the bulk material (**Figure 3.15**, red-BIPY•(rac)PSA bulk). PXRD analysis was used to show

that the BIPY•(rac)PSA co-crystal obtained via slow evaporation from isopropanol can be prepared via the environmentally friendly method, solvent drop grinding. Pure BIPY and (rac)PSA were ground with several drops of isopropanol in 1:1 ratio and after 30 mins the PXRD pattern was collected (**Figure 3.15**, blue-BIPY•(rac)PSA grinding). This was compared to the starting pattern of the pure BIPY and (rac)PSA (**Figure 3.15**, light blue-BIPY, purple-(rac)PSA). The patterns for the single crystal and the ground material are quite similar and clearly differ from the starting compounds. However, the match is not perfect and several peaks related to BIPY and (rac)PSA are still noticeable, therefore the reaction occurs only partially.
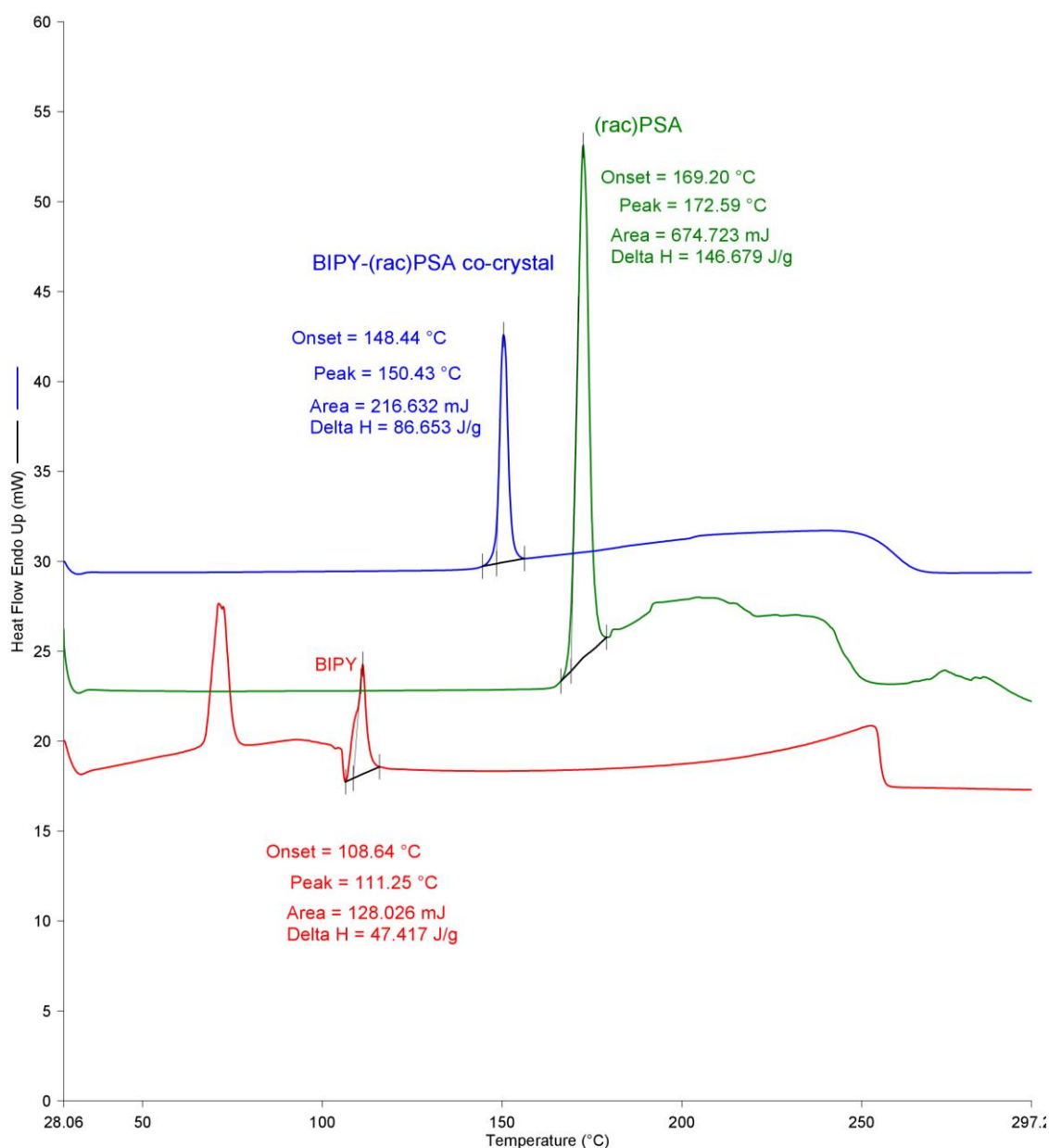
Figure 3.14 DSC curve of BIPY•(rac)PSA.
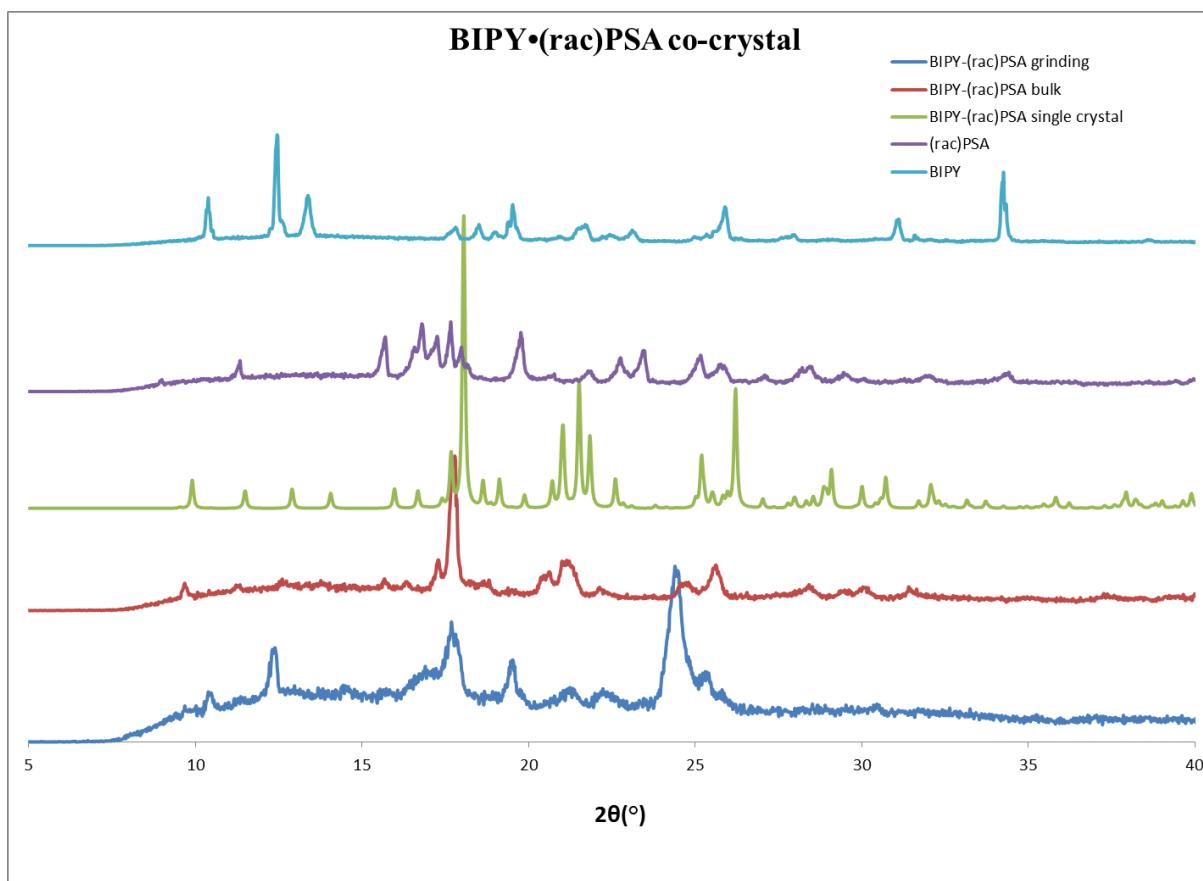
Figure 3.15 Comparison of PXRD patterns: pure BIPY(light blue), pure (rac)PSA (purple), the pattern generated from single crystal structure of BIPY•(rac)PSA (green), PXRD pattern of the bulk of the crystallisation (BIPY•(rac)PSA bulk- red) and the result of the solvent drop grinding (BIPY•(rac)PSA blue).

3.2 Co-crystals of 1,2-bis(4-pyridyl)ethane (ETBIPY)

The crystal struture, thermal analysis and powder X-ray analysis of the co-crystals formed between the host, 1,2-bis(4-pyridyl)ethane (ETBIPY) and the guest compounds: racemic phenylsuccinic acid (racPSA) and its chiral counterpart (S-PSA) will be presented. (**Figure 3.16**)
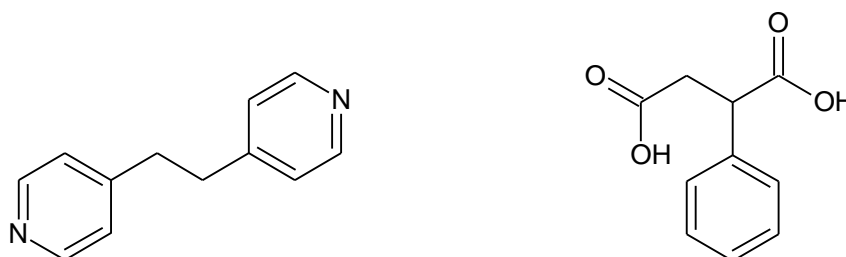
Figure 3.16 Structural line diagram of 1,2-bis(4-pyridyl)ethane (ETBIPY) and phenylsuccinic acid (PSA).

3.2.1   Preparation of the co-crystals of 1,2-bis(4-pyridyl)ethane (ETBIPY)

79 mg (0.43 mmol) of the 1,2-bis(4-pyridyl)ethane (ETBIPY) and 84 mg (0.43 mmol) of racemic phenylsuccinic acid (rac)PSA were dissolved in 1:1 mixture of propanol/water. Colourless crystals of ETBIPY•(rac)PSA were obtained within a few days via a slow evaporation method.

1,2-Bis(4-pyridyl)ethane (74 mg, 0.40 mmol) and (S)PSA (78 mg, 0.40 mmol) were dissolved in a minimal amount of DMSO. The solution was allowed to slowly evaporate at room temperature to yield colourless blocks crystals of ETBIPY•(S)PSA after 4 weeks.

3.2.1a Crystal structure analysis of ETBIPY•(rac)PSA and ETBIPY•(S)PSA

A suitable crystal of ETBIPY•(rac)PSA with dimensions of 0.09×0.12×0.24 mm were subjected to single crystal data collection. The compound crystallizes in the triclinic $P\bar{1}$ (No. 2) space group. The asymmetric unit contains two half ETBIPY moieties and one molecule of PSA with Z=2 and the molecular formula is $C_{22}H_{22}N_2O_4$. **Figure 3.17** shows the molecular arrangement in ETBIPY•(rac)PSA. The hydrogen atoms (H14 and H16) on the carboxylic acid groups were located in the electron density map and their coordinates refined freely. No proton has been transferred from the carboxyl-group of PSA to the nitrogen of the ETBIPY moiety therefore it is a co-crystal. Crystal data and refinement details are summarized in **Table 3.5**.
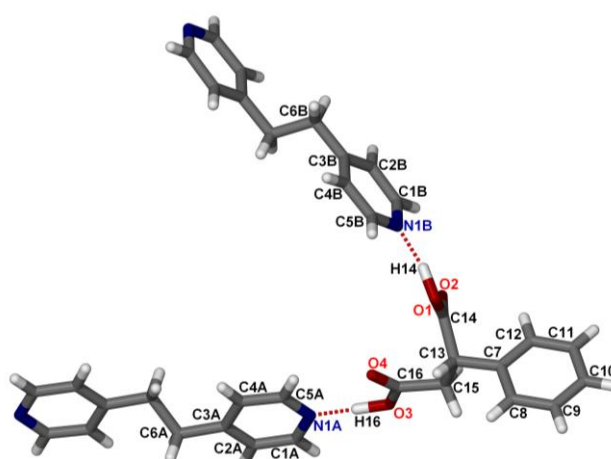
Figure 3.17 Molecular arrangement in ETBIPY•(rac)PSA. Only atoms of the asymmetric unit are labelled for clarity.

Table 3.5 Crystal data and refinement parameters of ETBIPY•(rac)PSA and ETBIPY•(S)PSA

Crystal data		
Compounds	**ETBIPY•(rac)PSA**	**ETBIPY•(S)PSA**
Molecular formula	$C_{22}H_{22}N_2O_4$	$C_{22}H_{22}N_2O_4$
Formula weight(g.mol^{-1})	378.42	378.42
Crystal system	Triclinic	Triclinic
Space group	$P\bar{1}$ (No. 2)	P1 (No. 1)
a(Å)	6.5593(13)	6.5705(13)
b(Å)	9.2837(19)	9.2493(18)
c(Å)	16.826(3)	17.129(3)
α(°)	82.39(3)	92.82(3)
β(°)	81.52(3)	99.52(3)
γ(°)	69.63(3)	110.25(3)
V(Å)	946.4(3)	956.8(3)
Z	2	2
ρcalc / g.cm^{-3}	1.328	1.314
μ(MoKα)/ mm^{-1}	0.092	0.091
F(000)	400	400
Crystal size (mm)	$0.09 \times 0.12 \times 0.24$	$0.10 \times 0.37 \times 0.40$
Temperature (K)	173(2)	173(2)
Radiation [Å]	MoKα, 0.71073	MoKα, 0.71073
Theta min-max[°]	2.35, 27.33	1.21, 28.29
Dataset	-8: 8; -11: 11; 0: 21	-8: 8; -12:12; -22: 22
Final R indices [I>2.0 (I)]	$R_1= 0.0771$, $wR_2= 0.1584$	$R_1= 0.0390$, $wR_2=0.0882$
R indices (all data)	$R_1= 0.1188$, $wR_2= 0.1749$	$R_1=0.0481$, $wR_2=0.0930$
Tot., uniq.data, R(int)	4116, 2868, 0.0494	9350, 8037, 0.0435
N_{ref}, N_{par}	2686, 256	8037, 510
S	1.058	1.040
Max. and av. Shift/error	0.00, 0.00	0.00, 0.00
Min. and max. resd. dens	0.346, -0.299	0.235, -0.171

The PSA is in a general position and the two half ETBIPY moieties are at different positions and lie in a centre of inversion. (Wyckoff position a and g) This makes the two molecules of ETBIPY crystallographically independent and indeed they display different conformations.

The ETBIPY has coordination freedom to rotate around the ethyl moiety and the crystal contains two slightly different conformations of this molecule. The ethyl bridge between the aromatic rings shows anti conformation in both molecules (C3A-C6A-C6A'-C3A' and C3B-C6B-C6B'-C3B') and their values are exactly the same (180° and -180° respectively). The two aromatic rings are parallel in both molecules but their distances differ significantly. Molecule A (coloured with yellow on **Figure 3.18**) has a more twisted conformation than B which may be described with the C4A-C3A-C6A-C6A' torsion angle (36°). The related torsion angle in molecule B (coloured blue) is 79°.
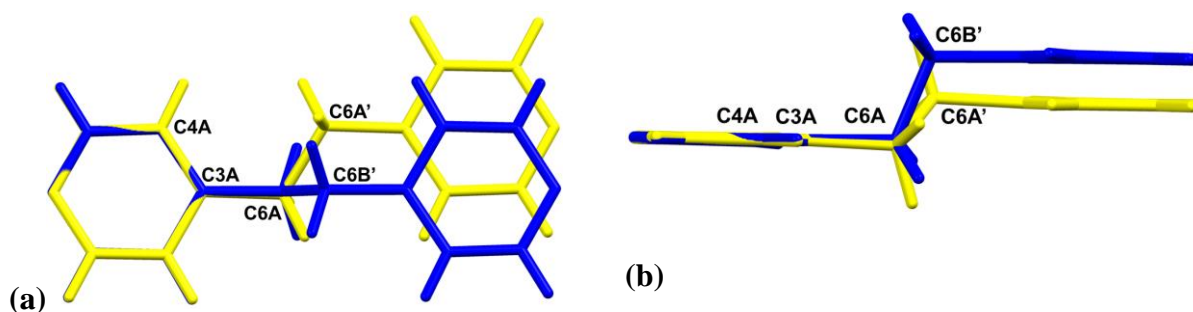
Figure 3.18 Overlap of the two different conformers of ETBIPY (molecule A- yellow, molecule B-blue) in ETBIPY•(rac)PSA from the top (a) and side view (b).

Both enantiomers of the racemic PSA are incorporated in the structure and form hydrogen bonds with the ETBIPY moieties via O1-H14···N1B (2.62Å, 159°) and O3-H16···N1A interactions (2.60Å, 178°). In the latter case an additional weak interaction can be defined between the ortho H of the pyridine ring and the carbonyl group of the acid (C5A-H5A···O4: 2.68 Å, 127°). This type of weaker interaction cannot be found at the other carboxylic acid functionality because of the lack of coplanarity between the functional groups. The main building block of the crystal is the wave-like arrangement of the ETBIPY and the PSA molecules via the previously discussed H-bonds. The motif contains both conformations of the ETBIPY and both enantiomers of the PSA in alternating nature. A ring style hydrogen bond motif can be described between the parallel waves via the already described –COOH···$N_{aromatic}$ hydrogen bond and an additional interaction between molecule B's ortho hydrogen and the carbonyl functionality: C5B-H5B···O1 (2.64Å, 141°). (**Figure 3.19a**) The result of these interactions is the zigzag layered structure of the crystal. (**Figure 3.19b**) Details of the hydrogen bonds and the relevant intermolecular interactions are summarized in **Table 3.6**.

A suitable crystal of ETBIPY•(S)PSA with dimensions of 0.10×0.37×0.40 mm was subjected to single crystal data collection. The compound crystallizes in triclinic P1 (No.1) chiral space group. The asymmetric unit contains two ETBIPY moieties and two molecules of PSA with an S conformation. (**Figure 3.20**) No proton has been transferred from the carboxylic group of PSA to the nitrogen of the ETBIPY moiety therefore it is a co-crystal. Crystal data and refinement details are summarized in **Table 3.5**.

(a)

(b)
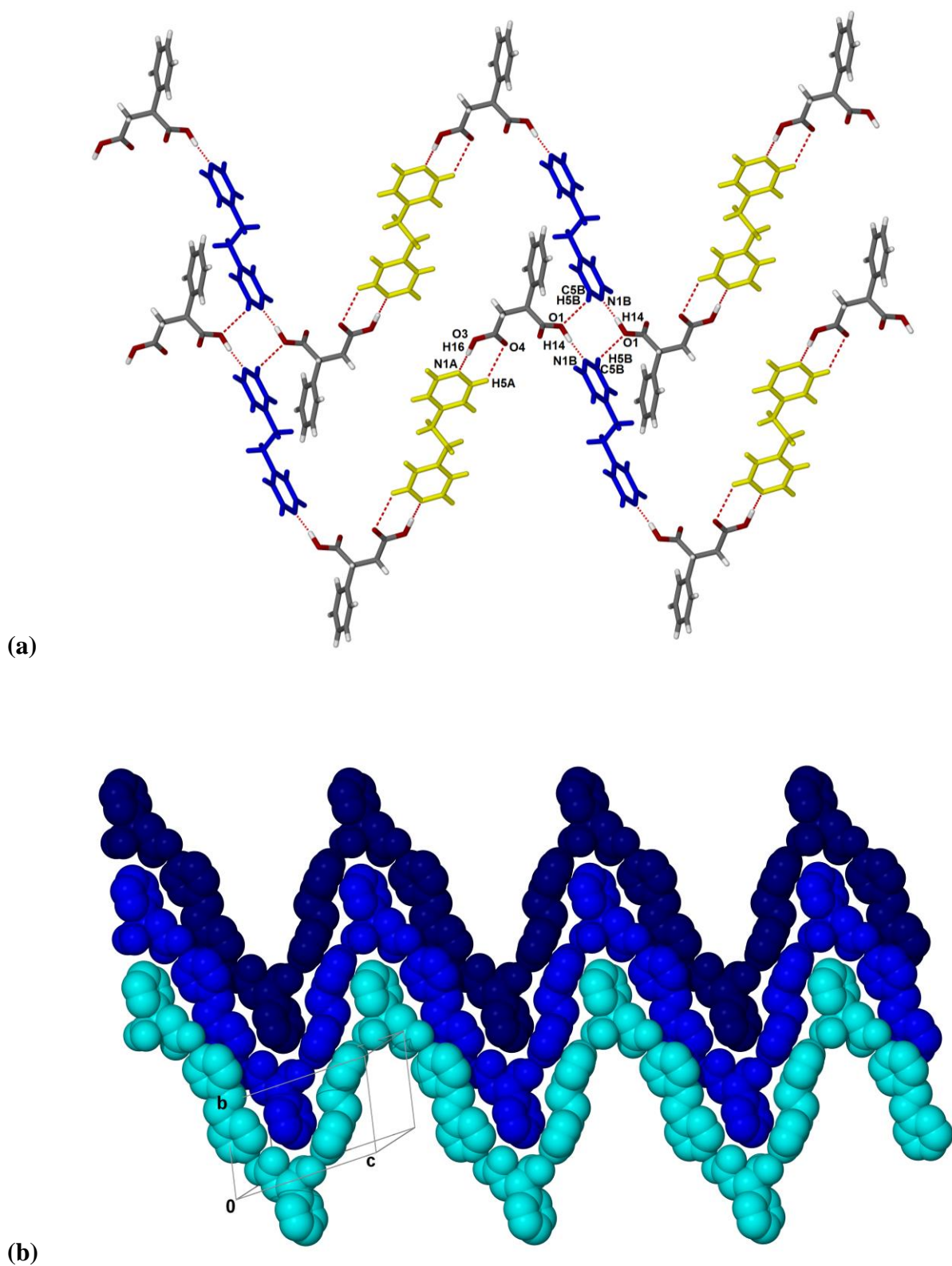
Figure 3.19 (a) Hydrogen bonding in the chains and between these motifs. The two different conformation of the ETBIPY moiety is coloured with yellow and blue. (b) Layers of zigzag motifs in ETBIPY•(rac)PSA.
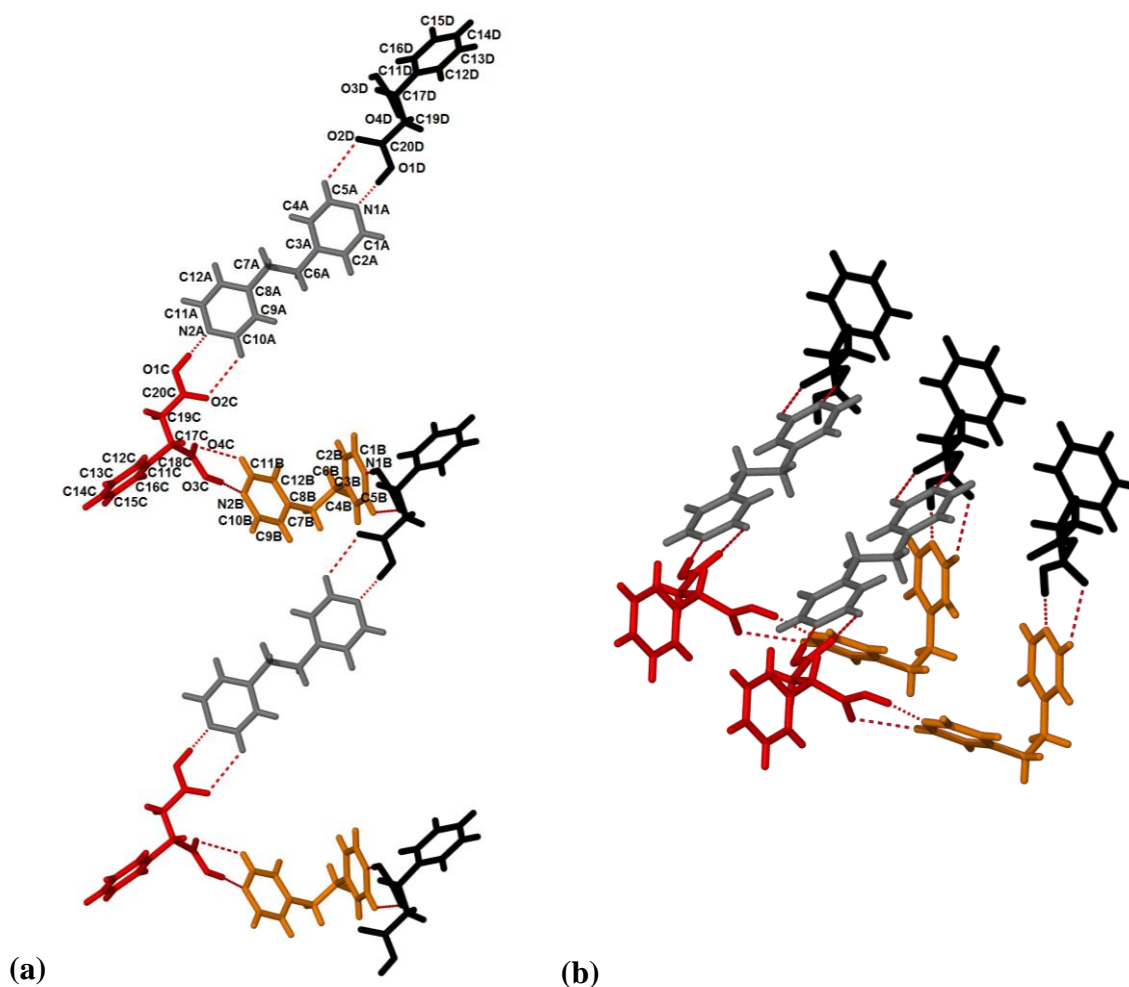
Figure 3.20 The hydrogen bonded helix (a- view down [100], b- view down [001]) is the main motif of the structure ETBIPY•(S)PSA. The atoms of the asymmetric unit are labelled. (Symmetry generated molecules coloured accordingly.)

Comparison of the two symmetrically independent (S)-PSA molecules revealed no significant conformational differences between them. (**Figure 3.21a**, molecule C- red, molecule D- black). However, the two ETBIPY moieties show remarkable differences. None of the ETBIPY moieties are sitting on a symmetry element, therefore there are multiple torsion angles needed to describe their conformation. Molecule A (**Figure 3.21b** and **c**, grey) has a similar anti conformation to molecule A of ETBIPY•(rac)PSA (**Figure 3.18**, yellow) and it may be described with the torsion angle of the ethyl moiety, C3A-C6A-C7A-C8A (-179°). The relative arrangement of the aromatic rings is defined with the C4A-C3A-C6A-C7A (-36°) and C9A-C8A-C7A-C6A (34°) torsion angles. Molecule B (**Figure 3.21b** and **c**, orange) adopted an eclipsed conformation and the torsion angle for the ethyl bridge, C8B-C7B-C6B-C3B is 59°. (**Table 3.6**)
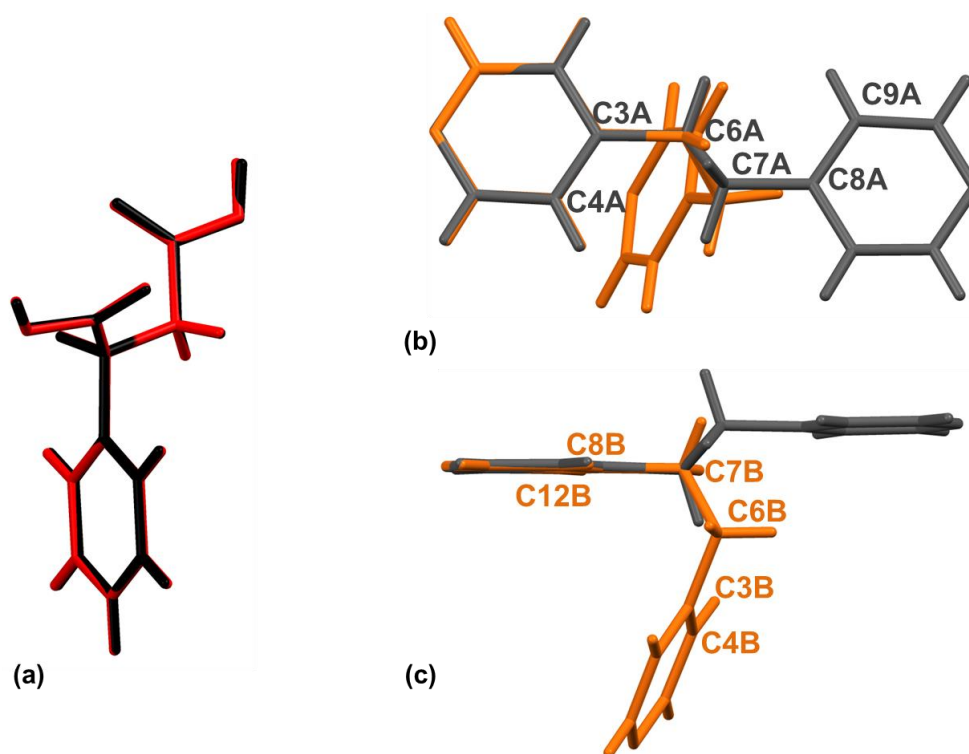
Figure 3.21. (a) The almost perfect overlap of the two symmetrically independent conformers of (S)-PSA (molecule C- red, molecule D- black) and the obvious difference between the two symmetrically independent ETBIPYs (molecule A- grey, molecule B- orange) in ETBIPY•(S)PSA from the top (b) and side view (c). Atoms used to describe torsional differences are labelled accordingly.

The two (S)PSA and the two ETBIPYs are hydrogen bonded in a manner that a helical arrangement forms. In this case, both (S)PSA form hydrogen bonds with the pyridine groups with all the four carboxylic acid moieties and in all cases an additional weak interaction can be defined between the ortho H of the pyridine ring and the carbonyl group of the acid. The main motif of the crystal is the resulted helical arrangement of the molecules via these H-bonds. Details of the hydrogen bonds and the relevant intermolecular interactions are summarized in **Table 3.6**. The motif contains both conformations of the ETBIPY and the two similar but symmetrically independent (S)PSA in an alternating nature. (**Figure 3.20a**) There is no significant hydrogen bonding between the helices. The packing of the crystal looks similar to the zigzag structure of ETBIPY•(rac)PSA (**Figure 3.20b**) however in this case the virtually 3-fold helices form a parallel net. (**Figure 3.22**)

Table 3.6 Hydrogen bonds of ETBIPY•(rac)PSA and ETBIPY•(S)PSA

D-H···A	d(D-H) (Å)	d(H···A) (Å)	d(D···A) (Å)	D-H···A (°C)	Symmetry operator
ETBIPY•(rac)PSA					
O1-H14···N1B	1.07	1.60	2.62	159	x, 1+y, z
O3-H16···N1A	1.08	1.53	2.60	178	1-x, 2-y, -z
C5A-H5A···O4	0.95	2.68	3.35	127	x, y, z
C5B-H5B···O1	0.95	2.64	3.44	141.7	1-x, -y, 1-z
ETBIPY•(S)PSA					
O1D-H20D···N1A	0.97	1.64	2.60	173	x+1, y+1, z
O1C-H20C···N2A	1.01	1.59	2.60	177	
O3D-H18D···N1B	1.03	1.59	2.63	178	x, y, z+1
O3C-H18C···N2B	0.97	1.66	2.63	172	x-1, y, z

Table 3.7 Torsion angles of ETBIPY•(rac)PSA and ETBIPY•(S)PSA

Torsion angles(°)	
ETBIPY•(rac)PSA	
C3A-C6A-C6A'-C3A'	180
C3B-C6B-C6B'-C3B'	-180
C4A-C3A-C6A-C6A'	36
C4A-C3A-C6A-C6B'	79
ETBIPY•(S)PSA	
C3A-C6A-C7A-C8A	-179
C4A-C3A-C6A-C7A	-36
C9A-C8A-C7A-C6A	34
C8B-C7B-C6B-C3B	59
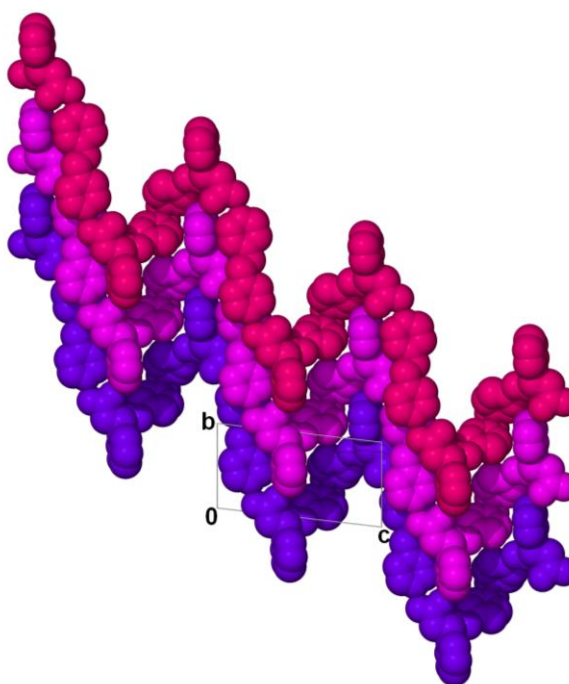
Figure 3.22 Space filling representation of the virtually 3-fold parallel net in ETBIPY•(S)PSA.

3.2.1b Thermal analysis of ETBIPY•(rac)PSA and ETBIPY•(S)PSA

The DSC curve of ETBIPY•(rac)PSA crystals shows one endotherm corresponding to the melting point of the crystal (T_{on}= 185.8°C, T_{peak}= 188.0°C). The melting point of the co-crystal is higher than the melting points of the two starting material, ETBIPY (T_{on}= 107.1°C, T_{peak}= 112.3°C) and (rac)PSA (T_{on}= 169.2°C, T_{peak}= 173.0°C). (**Figure 3.23**).
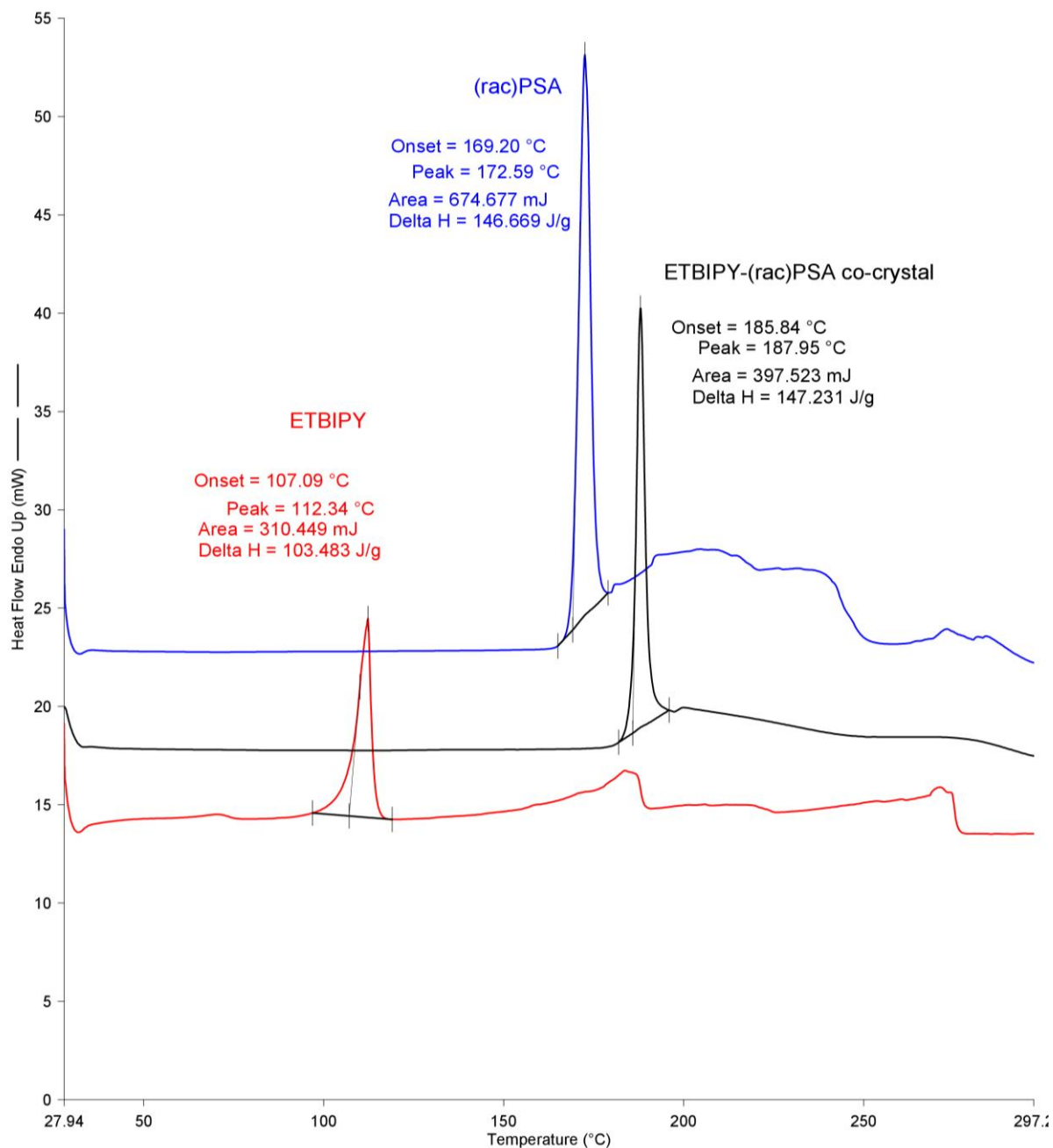
Figure 3.23 DSC curve of ETBIPY•(rac)PSA.

The DSC curve of ETBIPY•(S)PSA crystals shows a more complex melting process. The melting point of the co-crystal (T_{on}= 147.0°C, T_{peak}= 151.4°C) is between the melting points of the two starting material, ETBIPY (T_{on}= 107.1°C, T_{peak}= 112.3°C) and (S)-PSA (T_{on}= 178.2°C, T_{peak}= 182.5°C). (**Figure 3.24**).
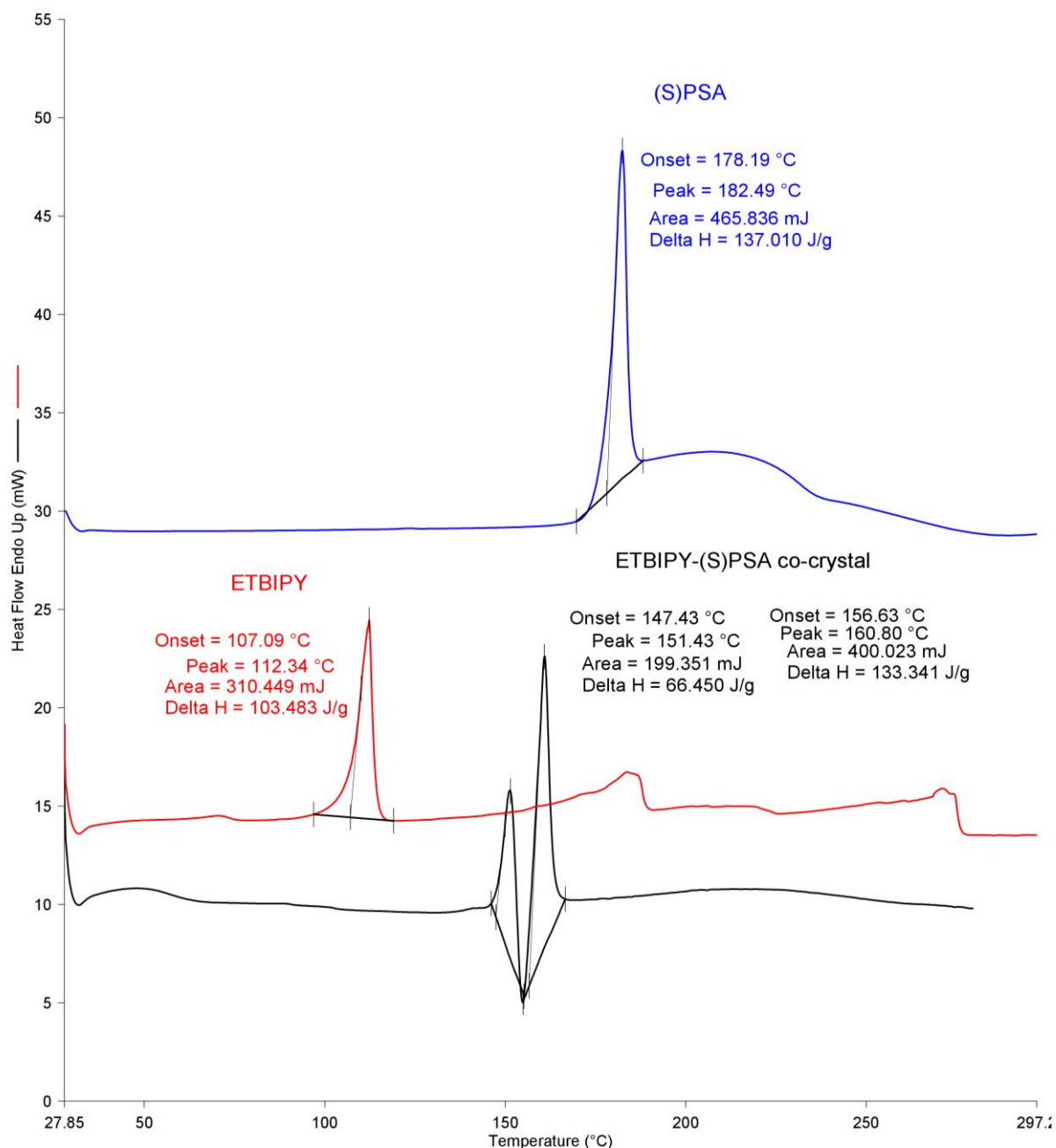
Figure 3.24 DSC curve of ETBIPY•(S)PSA.

3.2.1c Powder X-ray analysis of ETBIPY•(rac)PSA and ETBIPY•(S)PSA

Powder X-ray analysis was carried out to show that the structures of ETBIPY•(rac)PSA and ETBIPY•(S)PSA collected by using one single crystal in both cases only (**Figure 3.25** green-ETBIPY•(rac)PSA single crystal, **Figure 3.26** green-ETBIPY•(S)PSA single crystal, calculated) is representative to the bulk material (**Figure 3.25** red-ETBIPY•(rac)PSA bulk, **Figure 3.26** red-ETBIPY•(S)PSA bulk).

PXRD analysis was used to show that the co-crystals obtained via slow evaporation technique can be prepared via solvent drop grinding. Pure ETBIPY and (rac)PSA were ground with several drops of propanol/water 1:1 ratio and after 10 mins the PXRD pattern was collected (**Figure 3.25** blue-ETBIPY•(rac)PSA grinding). This was compared to the starting pattern of the pure ETBIPY and (rac)PSA (**Figure 3.25** light blue-ETBIPY, purple-(rac)PSA). The patterns for the single crystal and the ground material are not similar, thus the pattern analysis is inconclusive.
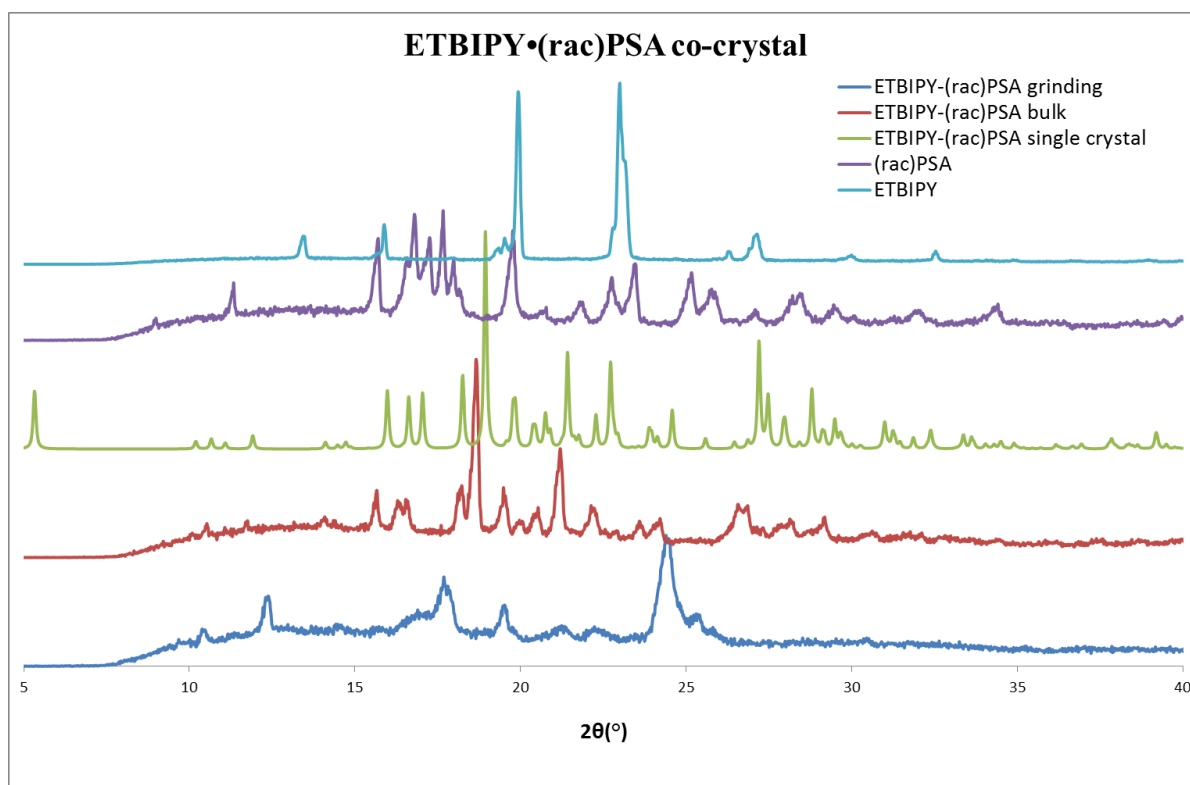
Figure 3.25 Comparison of PXRD patterns: pure ETBIPY (light blue), pure racPSA (purple), the pattern generated from single crystal structure of ETBIPY•racPSA (green), PXRD pattern of the bulk of the crystallisation (ETBIPY•racPSA bulk- red) and the result of the solvent drop grinding (ETBIPY•racPSA blue).

Pure ETBIPY and (S)PSA were ground with several drops of DMSO and after 10 mins the PXRD pattern was collected (**Figure 3.26** blue-ETBIPY•(S)PSA grinding). In similar manner, may be concluded that the patterns for the single crystal and the ground material are not similar, thus the pattern analysis is inconclusive.
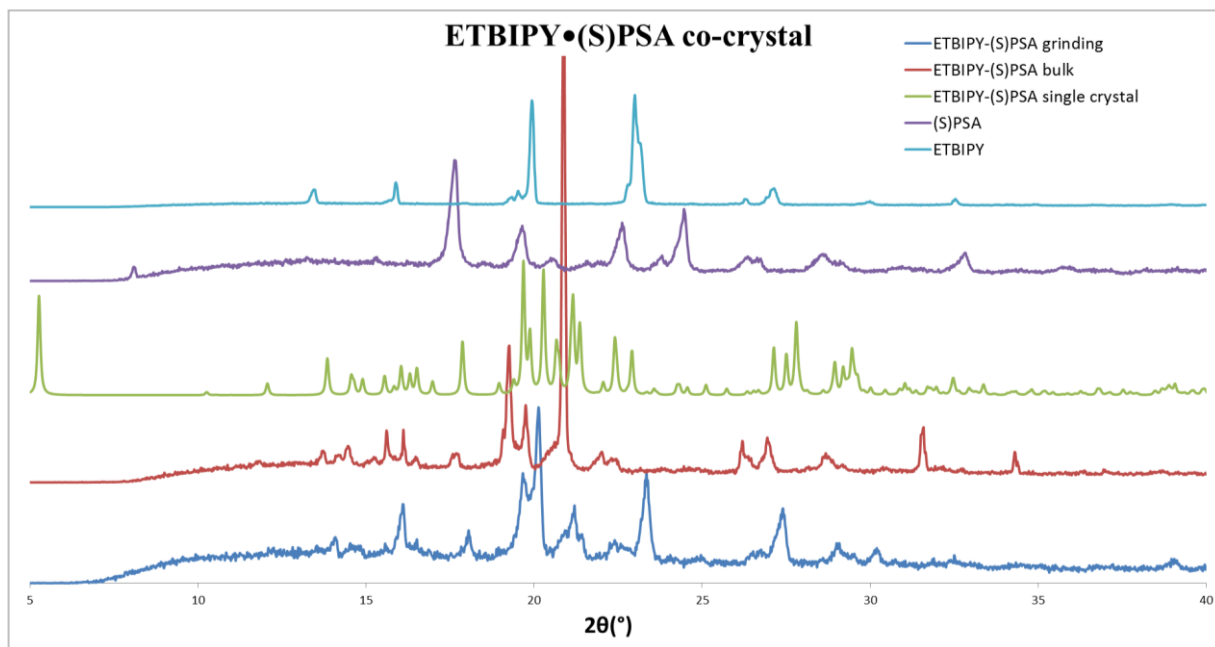
Figure 3.26 Comparison of PXRD patterns: pure ETBIPY (light blue), pure (S)PSA (purple), the pattern generated from single crystal structure of ETBIPY•(S)PSA (green), PXRD pattern of the bulk of the crystallisation (ETBIPY•(S)PSA bulk- red) and the result of the solvent drop grinding (ETBIPY•(S)PSA blue).

3.3. Solubility and melting point relation of model co-crystals

The solubility of a given compound mainly depends on the polarity of the system (applied solvent and the solute), however the crystal structure of the compound may have an effect on the process to a certain degree. The absorption of a drug can be affected by its aqueous solubility therefore water was selected primarily for the solubility measurements ($P'_w = 9.0$). Drugs taken orally may be soluble in water, soluble in alcohols or not soluble in either solvent. Therefore ethanol ($P'_e = 5.2$) was used as a secondary choice of solvent for the measurements. The melting points and the solubility of the model co-crystals and their starting materials were recorded in water and ethanol. (**Figure 3.27** and **3.28**) The melting points of the compounds are presented in the previous chapters and the details of the solubility measurements are shown in **Table 3.8** for BIPY co-crystals and in **Table 3.9** for ETBIPY co-crystals and their starting components.

The solubility of BIPY in water and ethanol differ significantly ($S_{w,BIPY}$= 32 mg/mL, $S_{e,BIPY}$= 73 mg/mL) and the melting points of BIPY co-crystals are decreasing in the following order: BIPY•PTA (159°C) > BIPY•(rac)PSA (148°C) > BIPY•(rac)PBA (80°C). (**Figure 3.27**) No correlation can be seen between the melting points and their solubility in ethanol for the analysed compounds. (**Figure 3.27** blue and green bars) The BIPY•(rac)PSA presents an extreme increase in solubility (532 mg/mL) when compared to BIPY•PTA (22 mg/mL) and BIPY•(rac)PBA (15 mg/mL). This very different behaviour may be explained with the homochiral layers in the crystal structure and the lack of strong interactions between these layers, however the effect of the looser packing should be seen as a lowering in the melting point of the compound (see **Figure 3.13**) Analysis of BIPY co-crystals revealed a reverse linear relationship between the change of their melting points and the aqueous solubility: BIPY•PTA (16 mg/mL) < BIPY•(rac)PSA (28 mg/mL) < BIPY•(rac)PBA (41 mg/mL). In general, we may conclude that the BIPY co-crystals have similar polarity therefore their interactions with the solvent are expected to be similar. Thus the change in solubility should be the result of the crystal packing only and eventually correlates with the melting point.

ETBIPY solubility values for water and ethanol are also different. (**Figure 3.28**, $S_{w,ETBIPY}$= 89 mg/mL, $S_{e,ETBIPY}$= 72 mg/mL) This difference resulted from the polarity difference between water and ethanol. The two co-crystals, ETBIPY•(rac)PSA and ETBIPY•(S)PSA have chemically the same building blocks; stereoisomers of PSA, therefore their polarity is the same. However, the solubility values show extreme differences. The values for ETBIPY•(rac)PSA are 7 mg/mL and 5 mg/mL while 245 mg/mL and 232 mg/mL for ETBIPY•(S)PSA in water and ethanol, respectively. Thus the difference observed between their solubility should be the result of the different crystal structures. The packing indices are almost identical ($PI_{ETBIPY•racPSA}$= 70.7, $PI_{ETBIPY•(S)PSA}$= 69.8), such are the calculated densities ($\rho_{ETBIPY•racPSA}$= 1.328 g.cm^{-3}, $\rho_{ETBIPY•(S)PSA}$= 1.314 g.cm^{-3}). Therefore the only difference which can be related to the observed change in the solubility is the packing feature. ETBIPY•(rac)PSA has zigzag chains of molecules and these chains bonded together via strong hydrogen bonds. (see **Figure 3.19a**) In case of ETBIPY•(S)PSA, the crystal builds up from virtually 3-folded helices without strong intermolecular interaction between these structures. (see **Figure 3.20**)
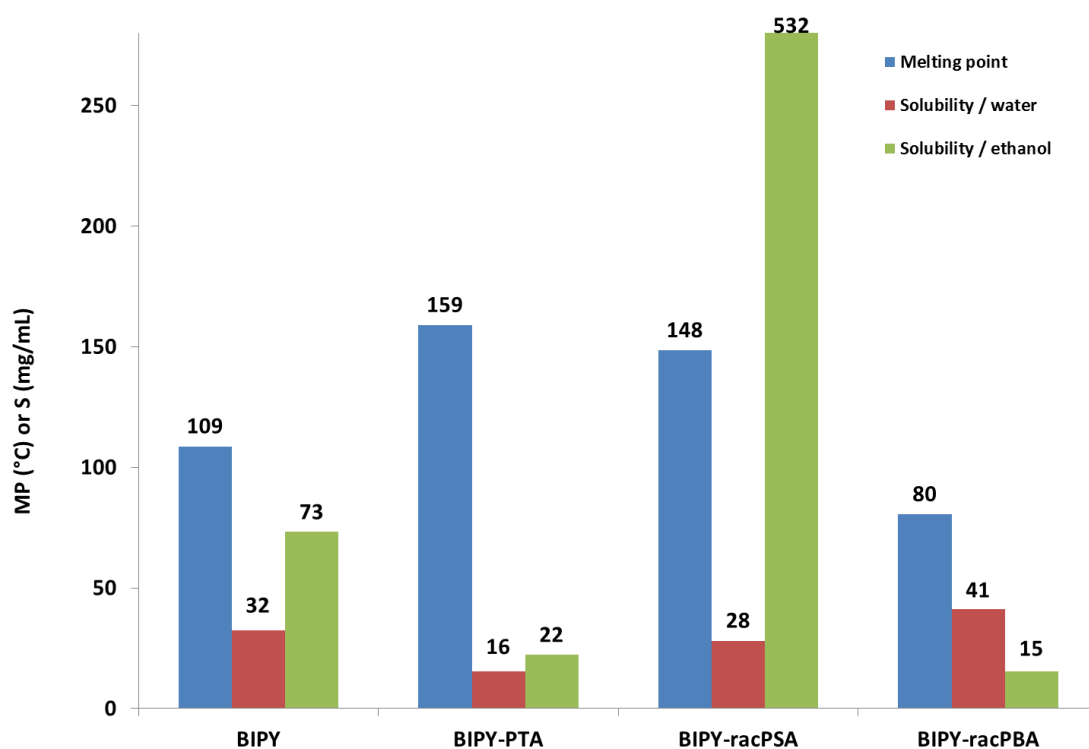
Figure 3.27 Melting points and solubility values measured in water and ethanol for BIPY and co-crystals of BIPY.
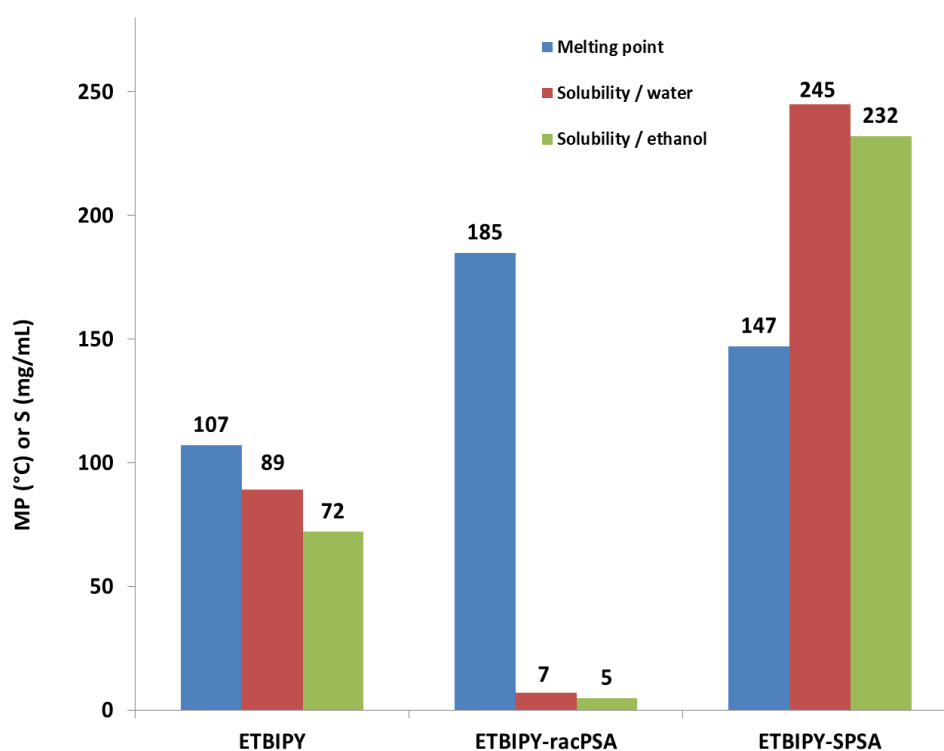
Figure 3.28 Melting points and solubility values measured in water and ethanol for ETBIPY and co-crystals of ETBIPY.

Table 3.8 Solubility values for BIPY, PTA, rac-PSA, rac-PBA and their co-crystals measured in water and ethanol.

	solvent	mass of vial	mass of vial+ solvent	mass of vial+ solvent+ compound	mass of compound	mass of solvent	mass of paper	mass of paper+ undissolved compound	mass of undissolved	mass of dissolved	volume of solvent	solubility	solubility	average solubility
unit		(g)	(g)	(g)	(g)	(g)	(g)	(g)	(g)	(g)	(mL)	(g/g)	(mg/mL)	(mg/mL)
BIPY	ethanol	150.1820	159.2330	160.8580	1.6250	9.0510	3.179	3.544	0.3650	1.2600	11.4715	0.1392	excluded	
		154.0390	158.1430	159.3060	1.1630	4.1040	3.218	4.025	0.8070	0.3560	5.2015	0.0867	68.44	
		151.9580	157.0250	158.1420	1.1170	5.0670	3.181	3.796	0.6150	0.5020	6.4221	0.0991	78.17	73.30
	water	151.7790	167.6150	168.6020	0.9870	15.8360	3.193	3.716	0.5230	0.4640	15.8360	0.0293	29.30	
		151.8670	167.4590	168.3040	0.8450	15.5920	3.238	3.530	0.2920	0.5530	15.5920	0.0355	35.47	
		154.2250	168.6620	169.5210	0.8590	14.4370	3.214	3.664	0.4500	0.4090	14.4370	0.0283	28.33	31.03
PTA	ethanol	143.3110	150.9000	153.1050	2.2050	7.5890	3.257	4.882	1.6250	0.5800	9.6185	0.0764	60.30	
		139.0110	149.9200	151.5340	1.6140	10.9090	3.187	3.836	0.6490	0.9650	13.8264	0.0885	69.79	
		143.2600	151.8740	153.2960	1.4220	8.6140	3.212	4.288	1.0760	0.3460	10.9176	0.0402	excluded	65.05
	water	118.5850	132.0510	152.7300	20.6790	13.4660	3.198	4.569	1.3710	19.3080	13.4660	1.4338	1433.83	
		122.5150	133.7230	154.5640	20.8410	11.2080	3.205	4.505	1.3000	19.5410	11.2080	1.7435	1743.49	
		122.9810	134.2790	154.8110	20.5320	11.2980	3.157	4.429	1.2720	19.2600	11.2980	1.7047	1704.73	1627.35
PSA	ethanol	141.1650	151.4940	152.1750	0.6810	10.3290	3.233	3.512	0.2790	0.4020	13.0913	0.0389	30.71	
		141.3680	151.1360	151.6620	0.5260	9.7680	3.208	3.472	0.2640	0.2620	12.3802	0.0268	21.16	
		142.6380	149.3060	150.3710	1.0650	6.6680	3.203	3.935	0.7320	0.3330	8.4512	0.0499	39.40	30.42
	water	141.8750	149.1490	149.6430	0.4940	7.2740	3.17	3.58	0.4100	0.0840	7.2740	0.0115	11.55	
		140.8270	154.3690	154.8560	0.4870	13.5420	3.179	3.525	0.3460	0.1410	13.5420	0.0104	10.41	
		140.6640	154.1940	154.6910	0.4970	13.5300	3.203	3.552	0.3490	0.1480	13.5300	0.0109	10.94	10.97
PBA	ethanol	141.9430	148.3940	149.5920	1.1980	6.4510	3.123	3.671	0.5480	0.6500	8.1762	0.1008	79.50	
		134.1450	142.1640	143.1880	1.0240	8.0190	3.121	3.583	0.4620	0.5620	10.1635	0.0701	55.30	
		136.0300	139.6160	140.6030	0.9870	3.5860	3.152	4.061	0.9090	0.0780	4.5450	0.0218	excluded	67.40
	water	142.2340	147.4650	147.8060	0.3410	5.2310	3.128	3.21	0.0820	0.2590	5.2310	0.0495	49.51	
		133.4820	145.7280	146.7480	1.0200	12.2460	3.151	3.389	0.2380	0.7820	12.2460	0.0639	63.86	
		131.0030	139.8190	140.1490	0.3300	8.8160	3.186	3.303	0.1170	0.2130	8.8160	0.0242	excluded	56.69

	solvent	mass of vial	mass of vial+ solvent	mass of vial+ solvent+ compound	mass of compound	mass of solvent	mass of paper	mass of paper+ undissolved compound	mass of undissolved	mass of dissolved	volume of solvent	solubility	solubility	average solubility
unit		(g)	(g)	(g)	(g)	(g)	(g)	(g)	(g)	(g)	(mL)	(g/g)	(mg/mL)	(mg/mL)
BIPY-PTA	ethanol	148.5160	156.6860	157.0040	0.3180	8.1700	3.3	3.413	0.1130	0.2050	10.3549	0.0251	**19.80**	
		151.2420	159.9360	159.6360	-0.3000	8.6940	3.296	3.384	0.0880	-0.3880	11.0190	-0.0446	**excluded**	
		124.7620	131.8630	132.2700	0.4070	7.1010	3.304	3.49	0.1860	0.2210	9.0000	0.0311	**24.56**	**22.18**
	water	149.1460	161.0560	161.3800	0.3240	11.9100	3.298	3.413	0.1150	0.2090	11.9100	0.0175	**17.55**	
		145.0740	152.8070	153.0370	0.2300	7.7330	3.3	3.503	0.2030	0.0270	7.7330	0.0035	**excluded**	
		151.3320	163.7690	164.0830	0.3140	12.4370	3.218	3.364	0.1460	0.1680	12.4370	0.0135	**13.51**	**15.53**
BIPY-PSA	ethanol	138.8950	141.8950	148.0860	6.1910	3.0000	3.213	3.298	0.0850	6.1060	3.8023	2.0353	**excluded**	
		138.7890	141.7190	144.1040	2.3850	2.9300	3.2	3.314	0.1140	2.2710	3.7136	0.7751	**611.54**	
		143.2000	145.5400	147.0000	1.4600	2.3400	3.189	3.303	0.1140	1.3460	2.9658	0.5752	**453.84**	**532.69**
	water	142.1710	150.9450	151.1260	0.1810	8.7740	3.13	3.161	0.0310	0.1500	8.7740	0.0171	**excluded**	
		136.7560	142.8800	143.1080	0.2280	6.1240	3.168	3.229	0.0610	0.1670	6.1240	0.0273	**27.27**	
		140.3770	145.9140	146.2200	0.3060	5.5370	3.183	3.329	0.1460	0.1600	5.5370	0.0289	**28.90**	**28.08**
BIPY-PBA	ethanol	123.1610	130.3240	130.6900	0.3660	7.1630	3.2	3.431	0.2310	0.1350	9.0786	0.0188	**14.87**	
		121.4670	130.8170	131.2520	0.4350	9.3500	3.19	3.402	0.2120	0.2230	11.8504	0.0239	**18.82**	
		123.7870	129.8680	130.1550	0.2870	6.0810	3.22	3.41	0.1900	0.0970	7.7072	0.0160	**12.59**	**15.42**
	water	123.3280	134.0040	134.2410	0.2370	10.6760	3.247	3.491	0.2440	-0.0070	10.6760	-0.0007	**excluded**	
		122.0850	128.4750	128.8580	0.3830	6.3900	3.127	3.313	0.1860	0.1970	6.3900	0.0308	**30.83**	
		123.0450	130.0760	130.6380	0.5620	7.0310	3.224	3.422	0.1980	0.3640	7.0310	0.0518	**51.77**	**41.30**

Table 3.9 Solubility values for ETBIPY, rac-PSA, S-PSA and its co-crystals measured in water and ethanol.

	solvent	mass of vial	mass of vial+ solvent	mass of vial+ solvent+ compound	mass of compound	mass of solvent	mass of paper	mass of paper+ undissolved compound	mass of undissolved	mass of dissolved	volume of solvent	solubility	solubility	average solubility
unit		(g)	(g)	(g)	(g)	(g)	(g)	(g)	(g)	(g)	(mL)	(g/g)	(mg/mL)	(mg/mL)
ETBIPY	ethanol	148.7450	153.0880	154.7400	1.6520	4.3430	3.1870	4.3650	1.1780	0.4740	5.5044	0.1091	86.11	
		150.9410	157.7070	159.1010	1.3940	6.7660	3.2140	4.1150	0.9010	0.4930	8.5754	0.0729	57.49	
		152.5810	158.1060	159.6620	1.5560	5.5250	3.1750	3.6720	0.4970	1.0590	7.0025	0.1917	excluded	71.80
	water	147.7390	154.6590	155.0120	0.3530	6.9200	3.2430	3.2940	0.0510	0.3020	6.9200	0.0436	43.64	
		151.0000	158.1060	159.1190	1.0130	7.1060	3.2160	3.2700	0.0540	0.9590	7.1060	0.1350	134.96	
		152.7480	161.2160	169.5210	8.3050	8.4680	3.1860	3.2500	0.0640	8.2410	8.4680	0.9732	973.19	89.30
PSA	ethanol	141.1650	151.4940	152.1750	0.6810	10.3290	3.2330	3.5120	0.2790	0.4020	13.0913	0.0389	30.71	
		141.3680	151.1360	151.6620	0.5260	9.7680	3.2080	3.4720	0.2640	0.2620	12.3802	0.0268	21.16	
		142.6380	149.3060	150.3710	1.0650	6.6680	3.2320	3.9350	0.7030	0.3620	8.4512	0.0543	42.83	31.57
	water	141.8750	149.1400	149.6430	0.5030	7.2650	3.1700	3.5800	0.4100	0.0930	7.2650	0.0128	12.80	
		140.8270	154.3690	154.8560	0.4870	13.5420	3.1790	3.5250	0.3460	0.1410	13.5420	0.0104	10.41	
		140.6640	154.1940	154.6910	0.4970	13.5300	3.2030	3.5520	0.3490	0.1480	13.5300	0.0109	10.94	11.38
(S)PSA	ethanol	139.7880	147.4790	147.9160	0.4370	7.6910	3.2430	3.5600	0.3170	0.1200	9.7478	0.0156	12.31	
		143.3180	151.7210	152.1020	0.3810	8.4030	3.2100	3.5100	0.3000	0.0810	10.6502	0.0096	7.61	
		141.1490	148.8810	149.1100	0.2290	7.7320	3.2300	3.4560	0.2260	0.0030	9.7997	0.0004	excluded	9.96
	water	140.4880	151.9270	152.3110	0.3840	11.4390	3.1380	3.2000	0.0620	0.3220	11.4390	0.0281	28.15	
		142.0700	151.0830	151.7050	0.6220	9.0130	3.1700	3.2200	0.0500	0.5720	9.0130	0.0635	excluded	
		141.7590	151.3080	151.6760	0.3680	9.5490	3.2400	3.2800	0.0400	0.3280	9.5490	0.0343	34.35	31.25
ETBIPY-racPSA	ethanol	139.2280	143.1900	143.2740	0.0840	3.9620	3.1860	3.2440	0.0580	0.0260	5.0215	0.0066	5.18	
		142.7850	145.1370	145.2090	0.0720	2.3520	3.2170	3.2540	0.0370	0.0350	2.9810	0.0149	excluded	
		137.3360	141.6100	141.7040	0.0940	4.2740	3.1800	3.2510	0.0710	0.0230	5.4170	0.0054	4.25	4.71
	water	139.3790	145.0620	145.1650	0.1030	5.6830	3.2480	3.3340	0.0860	0.0170	5.6830	0.0030	excluded	
		137.9110	144.3020	144.3740	0.0720	6.3910	3.1960	3.2280	0.0320	0.0400	6.3910	0.0063	6.26	
		141.7170	148.2480	148.3390	0.0910	6.5310	3.2340	3.2760	0.0420	0.0490	6.5310	0.0075	7.50	6.88

	solvent	mass of vial	mass of vial+ solvent	mass of vial+ solvent+ compound	mass of compound	mass of solvent	mass of paper	mass of paper+ undissolved compound	mass of undissolved	mass of dissolved	volume of solvent	solubility	solubility	average solubility
unit		(g)	(g)	(g)	(g)	(g)	(g)	(g)	(g)	(g)	(mL)	(g/g)	(mg/mL)	(mg/mL)
ETBIPY-(S)PSA	ethanol	142.3110	147.4700	149.3990	1.9290	5.1590	3.2020	3.3850	0.1830	1.7460	6.5387	0.3384	267.03	
		133.1220	138.3680	139.8500	1.4820	5.2460	3.1880	3.3500	0.1620	1.3200	6.6489	0.2516	198.53	
		139.7020	147.5380	148.2440	0.7060	7.8360	3.1730	3.2710	0.0980	0.6080	9.9316	0.0776	excluded	232.78
	water	134.0770	141.3890	142.9540	1.5650	7.3120	3.1980	3.2230	0.0250	1.5400	7.3120	0.2106	210.61	
		142.2150	149.5630	151.6610	2.0980	7.3480	3.2660	3.3110	0.0450	2.0530	7.3480	0.2794	279.40	
		136.3670	144.7000	145.6310	0.9310	8.3330	3.1900	3.2180	0.0280	0.9030	8.3330	0.1084	excluded	245.00

Chapter 4

Multicomponent crystals of baclofen

4. Multicomponent crystals of baclofen (BAC)

Baclofen, (*RS*)-4-amino-3-(4-chlorophenyl)butanoic acid is a slightly water soluble drug and primarily used in the treatment of spiral spasticity. The crystal structure, thermal analysis and powder X-ray analysis of the multicomponent crystals formed between baclofen (host) and several guest compounds such as monocarboxylic acids (benzoic acid, p-toluic acid and 1-hydroxy-2-naphthoic acid), dicarboxylic acids (oxalic acid and maleic acid) and p-toluene sulfonic acid will be discussed in this chapter. A structural diagram of baclofen (BAC) and the guest compounds are shown in **Figure 4.**
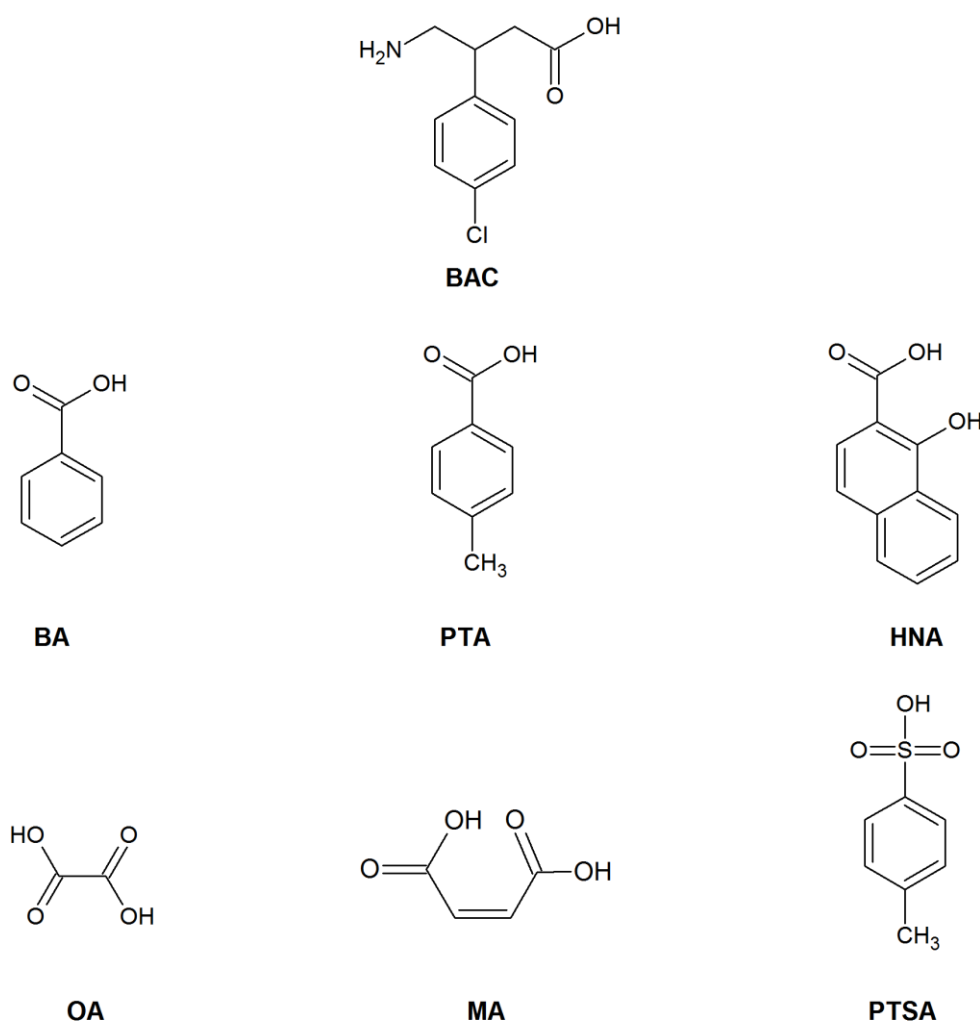
Figure 4 Structural diagram of baclofen (BAC) and the guest compounds: benzoic acid (BA), p-toluic acid (PTA), 1-hydroxy-2-naphthoic acid (HNA), oxalic acid (OA), maleic acid (MA) and p-toluene sulfonic acid (PTSA).

The pKa of the amino group is 9.79 and for the carboxylic acid 3.89 in baclofen (ΔpKa= 5.90). Therefore, baclofen is likely to be in the Zwitterionic form in this range of the pH scale. Comparison of the pKa values of the used compounds suggests co-crystal formation between BAC and BA, PTA and HNA because the ΔpKa values are between -1 and 4, however in case of PTSA (ΔpKa= 6.57) salt formation was expected. Applying the pKa rule for the formation of the BAC-OX (ΔpKa= 2.53) and BAC-MA (ΔpKa= 2.02) crystals, we were not able to predict the salt vs. co-crystal formation. The pKa values for all the compounds used in this chapter are summarized in **Table 4**.

Table 4 Calculated pKa values for baclofen (BAC) and the guest compounds: benzoic acid (BA), p-toluic acid (PTA), 1-hydroxy-2-naphthoic acid (HNA), oxalic acid (OA), maleic acid (MA) and p-toluene sulfonic acid (PTSA)[1]

compound	pKa$_1$(COOH)	pKa$_2$(NH$_2$)	pKa$_2$(COOH)	pKa(SO$_3$H)
Baclofen (BAC)	3.89	9.79		
Benzoic acid (BA)	4.08			
p-toluic acid (PTA)	4.26			
1-hydroxy-2-naphthoic acid (HNA)	2.70			
p-toluene sulfonic acid (PTSA)				-2.14
oxalic acid (OA)	1.36		4.11	
maleic acid (MA)	3.05		5.91	

4.1. Preparation of multicomponent crystals of baclofen with monocarboxylic acids: benzoic acid, p-toluic acid and 1-hydroxy-2-naphthoic acid

Single crystals of baclofen with benzoic acid were obtained by slow evaporation of 1:1 methanol/water solution containing 50 mg baclofen (0.23 mmol) and 30 mg benzoic acid (0.25 mmol). Colourless crystals were obtained after 4 weeks.

Baclofen (33 mg, 0.15 mmol) and p-toluic acid (34 mg, 0.25 mmol) were dissolved in a minimum amount of 1:1 ethanol/water and colourless crystals of BAC•PTA were obtained by slow evaporation of the solvent after 4 weeks.

Baclofen (20 mg, 0.10 mmol) and 1-hydroxy-2-naphthoic acid (20mg, 0.10 mmol) were mixed together and dissolved in 1:1 of ethanol/water. The solution was allowed to slowly evaporate at room temperature to yield brown block shaped crystals after 4 weeks.

4.1.1 Crystal structure analysis of the co-crystal of baclofen with benzoic acid (BAC•BA)

A suitable crystal with dimensions 0.05×0.23×0.30 mm was selected for single crystal X-ray analysis. This compound crystallizes in the monoclinic achiral space group $P2_1/c$ (No. 14) with two molecules of baclofen (BAC) and three molecules of benzoic acid (BA) in the asymmetric unit and the molecular formula of $C_{41}H_{42}Cl_2N_2O_{10}$. (**Figure 4.1**) The structure refined to $R_1 = 0.0430$ and $wR_2 = 0.0966$. The data collection and refinement details are summarized in **Table 4.1**. The hydrogen atoms on the carboxylic acid groups and on the amine moieties were located in the electron density map and their coordinates refined freely. There was no proton transferred from the BA to the BAC therefore this system is a co-crystal.
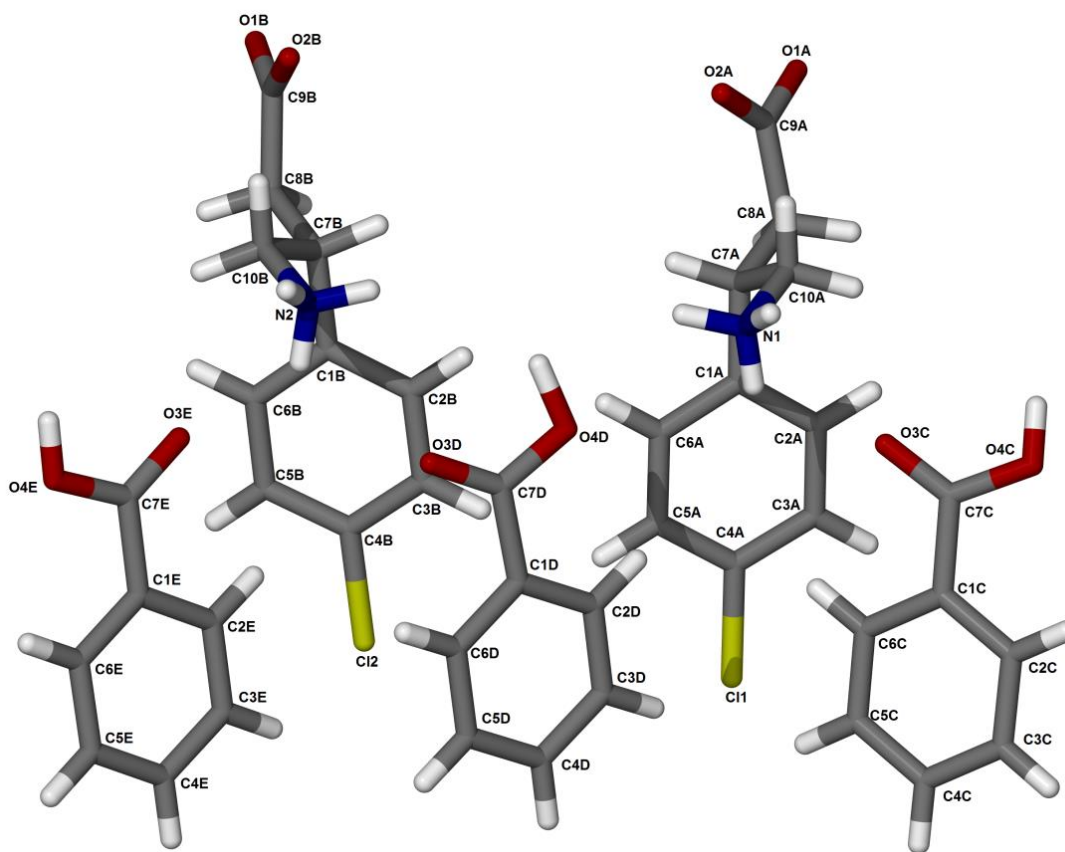
Figure 4.1 The asymmetric unit of BAC•BA co-crystal with labelled non-hydrogen atoms. (Labels of hydrogen atoms are omitted for clarity.)

**Table 4.1** Crystallographic data and structure refinement parameters for BAC•BA, BAC•PTA and (BAC$^+$)(HNA$^-$)

Crystal data			
Compounds	**BAC•BA**	**BAC•PTA**	**(BAC$^+$)(HNA$^-$)**
Molecular formula	$C_{41}H_{42}Cl_2N_2O_{10}$	$C_{18}H_{20}ClNO_4$	$C_{21}H_{20}ClNO_5$
Formula weight(g.mol^{-1})	793.67	349.80	401.83
Crystal system	monoclinic	triclinic	monoclinic
Space group	P2$_1$/c (No.14)	P-1 (No.2)	P2$_1$/c (No. 14)
a(Å)	14.910(3)	6.1768(12)	6.6251(13)
b(Å)	35.478(7)	7.5101(15)	34.490(7)
c(Å)	7.4293(15)	19.092(4)	8.4698(17)
α(°)	90.00	79.43(3)	90.00
β(°)	99.21(3)	82.90(3)	95.75(3)
γ(°)	90.00	84.25(3)	90.00
V(Å)	3879.3(14)	861.2(3)	1925.6(7)
Z	4	2	4
ρcalc/ g.cm^{-3}	1.359	1.349	1.386
µ(MoKα)/mm^{-1}	0.229	0.243	0.231
F(000)	1664	368	840
Crystal size (mm)	0.05 ×0.23 ×0.30	0.02×0.07 ×0.80	0.11×0.16×0.45
Temperature (K)	173(2)	173(2)	173(2)
Radiation [Å]	MoKα, 0.71073	MoKα, 0.71073	MoKα, 0.71073
Theta min-max[°]	1.80, 26.38	2.18, 27.94	2.36, 27.12
Dataset	-18:18; -44: 0; 0: 9	-8: 8; -9:9; -25: 25	-6:8;-44:44;-10:10
Final R indices [I>2.0 (I)]	R$_1$= 0.0430, wR$_2$= 0.0966	R$_1$= 0.0385, wR$_2$=0.0985	R$_1$= 0.0424, wR2=0.0955
R indices (all data)	R$_1$= 0.0610, wR$_2$= 0.1068	R$_1$=0.0484, wR$_2$=0.1045	R$_1$= 0.0655, wR2=0.1065
Tot., uniq.data, R(int)	7879, 6254, 0.0243	4103, 3392, 0.0304	4260, 3098, 0.0343
N$_{ref}$, N$_{par}$	7879, 533	4103, 223	4260,274
S	1.029	1.044	1.022
Max. and av. Shift/error	0.00, 0.00	0.00, 0.00	0.00, 0.00
Min. and max. res. dens.	0.550, -0.383	0.275, -0.285	0.296, -0.450

Because of the Zwitterionic nature of the baclofen molecule, it's amino and carboxylate functionality is likely to be involved in strong hydrogen bonding. Indeed, all hydrogen atoms of the amino groups and all hydroxyl and carbonyl groups are hydrogen bonded in the structure and form an extended hydrogen bonded network. (**Figure 4.2**) Graph set notation[2] was used to describe the network in detail and the main motifs are highlighted with green on **Figure 4.2**. We have used a limited number of motifs to describe this difficult hydrogen bond system for clarity. Therefore, the network may be described with three ring motifs. The biggest ring R_3^3(18) is formed via N2-H11E···O1A (2.99 Å, 175°), N1-H11B···O3C (2.70 Å, 120°) and O4C-H7C···O1B (2.60 Å, 176°) hydrogen bonds. The R_2^2(14) motif is built by N1-H11A···O2A (2.72 Å, 154°) and its symmetry

generated counterpart. The smallest ring, $R_4^4(12)$ is constructed by N1-H11A···O2A (2.72 Å, 154°), its symmetry generated counterpart and N1-H11C···O1A (2.77 Å, 171°) hydrogen bonds. Hydrogen bonds which are not involved in the previously mentioned ring motifs are summarized in **Table 4.2**.
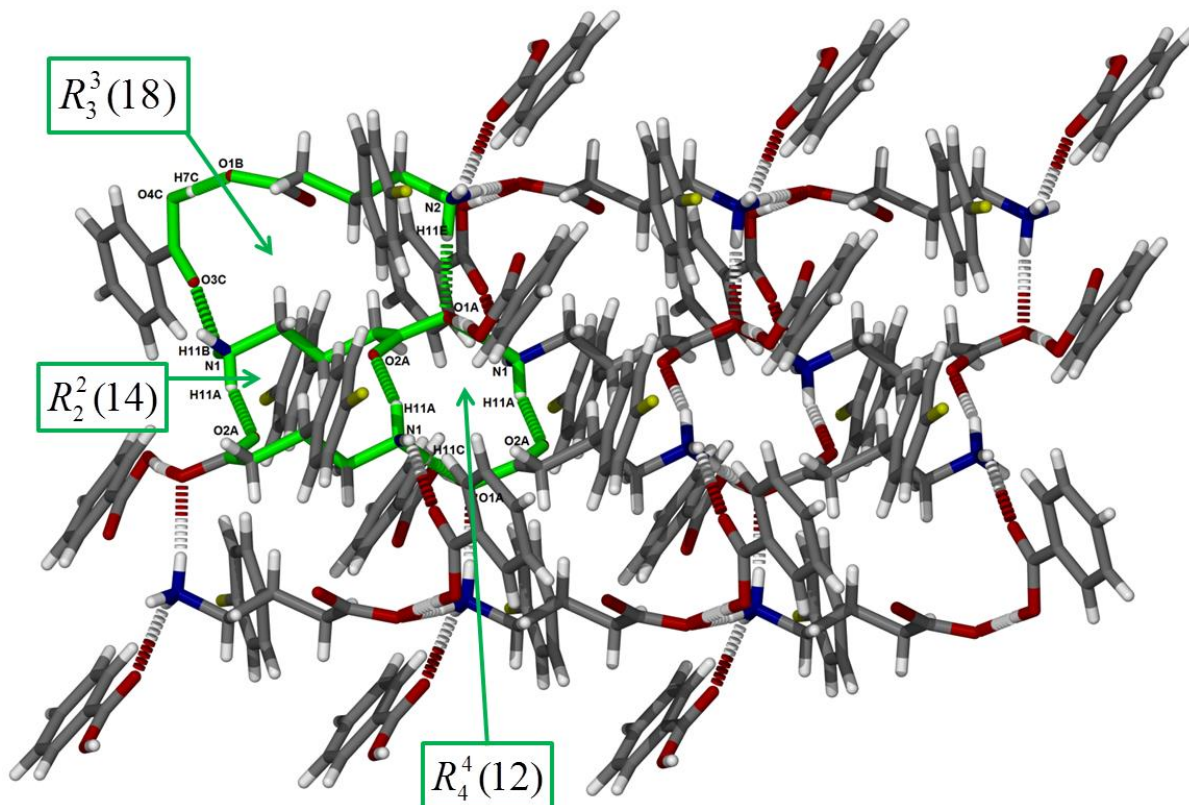

Figure 4.2 Hydrogen bonding motifs along the [001] direction in BAC•BA.

Table 4.2 Hydrogen bonds of BAC•BA

D-H···A	d(D-H) (Å)	d(H···A) (Å)	d(D···A) (Å)	D-H···A (°)	Symmetry operator
O4C-H7C···O1B	0.88	1.72	2.60	176	1-x, -y, 2-z
O4D-H7D···O1A	1.05	1.59	2.63	172	1-x, -y,1- z
N1-H11A···O2A	0.93	1.85	2.72	154	1-x, -y,- z
N1-H11B···O3C	0.88	2.15	2.70	120	x, y,-1+ z
N1-H11C···O1A	1.00	1.78	2.77	171	x, y,-1+ z
N2-H11D···O3D	0.89	2.57	3.03	113	
N2-H11D···O3E	0.89	2.12	2.76	128	
N2-H11E···O1A	0.91	2.08	2.99	175	1-x, -y,1- z
N2-H11F···O1B	0.91	1.79	2.73	170	x, y,-1+ z
C5C-H5C···Cl1	0.95	2.76	3.52	137	x, ½-y, ½+z
C10A-H10A···O2B	0.99	2.53	3.46	157	1-x, -y,1- z
C10A-H10B···O2A	0.99	2.44	3.05	120	
C10B-H10C···O2B	0.99	2.35	3.01	124	

The main feature of the crystal is the alternation of the previously described hydrogen bonded layers and the aromatic layers without strong interactions. **Figure 4.3** shows the crystal packing don the [001] direction. The molecules are coloured according to their symmetry equivalents and the symmetry independent molecules are presented with different colours (BAC molecule A: light yellow, BAC molecule B: yellow, BA molecule C: dark purple, BA molecule D: purple and BA molecule E: blue). Down the [100] direction the crystal packing presents an interesting optical effect, the so called Zöllner illusion. The packing of the molecules looks antiparallel; however they are indeed parallel, hence the space group is monoclinic. (**Figure 4.4**)
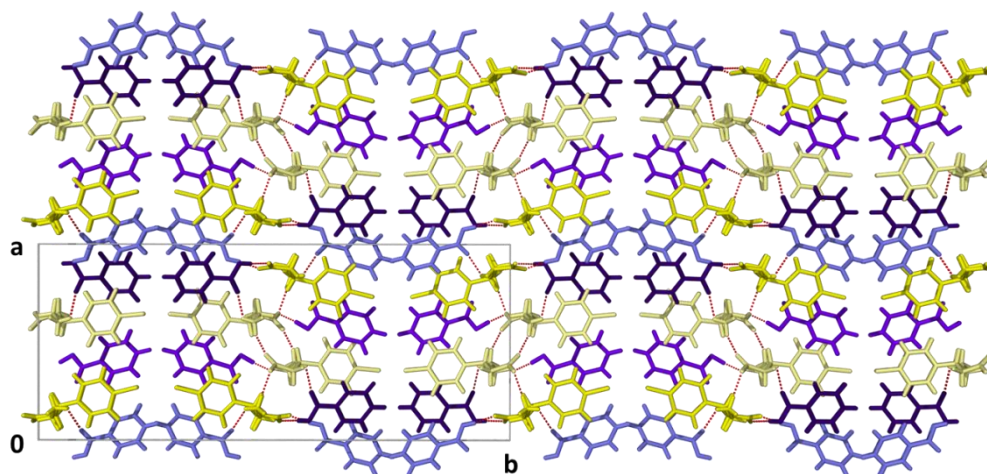
Figure 4.3 Crystal packing of BAC•BA down [001]. The symmetry independent baclofen molecules are coloured with light yellow and yellow and the symmetry independent benzoic acids are coloured with three shades of blue.

(a)   (b)
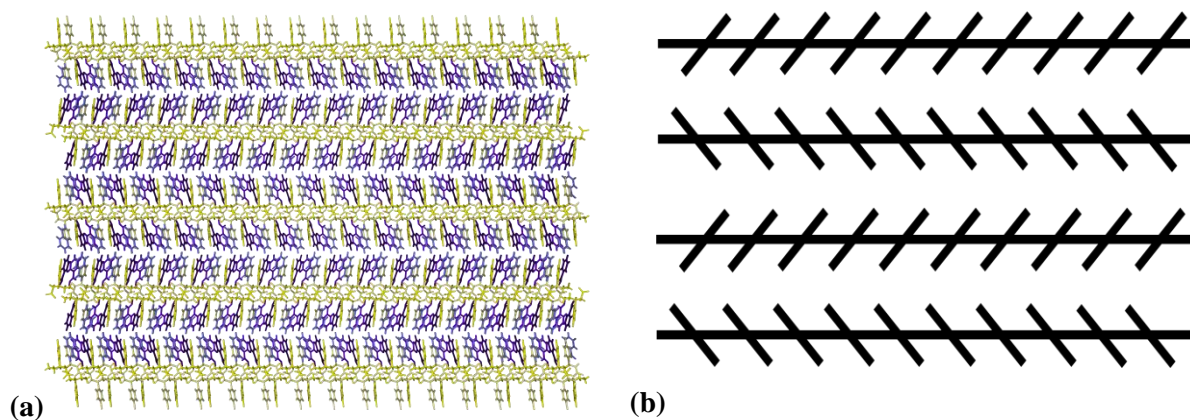
Figure 4.4 Zöllner illusion in BAC•BA in the [001] direction (a) and its graphical representation with seemingly antiparallel lines (b).

4.1.2 Crystal structure analysis of co-crystal of baclofen with p-toluic acid (BAC•PTA)

A suitable crystal of BAC•PTA with dimensions of 0.02×0.07×0.80 mm were subjected to single crystal data collection. The structure was solved in the triclinic $P\bar{1}$ (No. 2) space group and the molecular formula is $C_{18}H_{20}ClNO_4$. The asymmetric unit contains one molecule of baclofen and one p-toluic acid. **Figure 4.5** shows the asymmetric unit with labelled atoms and the specified hydrogen bond. The unit cell consists of two host molecules and two guest molecules, therefore Z=2. The structure refined to R_1= 0.0385 and wR_2=0.0985. The related crystal data is summarized in **Table 4.1.** The hydrogen atoms on the carboxylic acid group and on the amine moiety were located in the electron density map and their coordinates were refined freely. The BAC is in the Zwitterionic form; there was no proton transfer observed from the carboxylic acid group of the PTA to BAC thus it is a co-crystal.
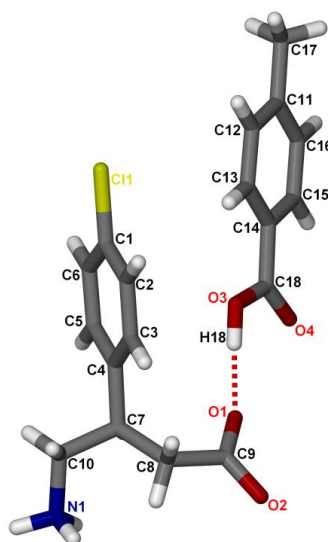
Figure 4.5 Asymmetric unit with labelled heavy atoms and the hydrogen bond between BAC and PTA**.** (Labels of hydrogen atoms are omitted for clarity.)

Similar to the BAC•BA structure an extended hydrogen bonding network may be described with graph set notation and these motifs are highlighted with green on **Figure 4.6**. The network may be described with three ring motifs. The biggest ring $R_2^2(14)$ is formed via N1-H11A···O1 (2.81 Å, 169°) and its symmetry generated counterpart. The $R_4^4(12)$ motif is built by N1-H11A···O1 (2.81 Å, 169°) and N1-H11C···O2 (2.77 Å, 169°) and their symmetry generated counterparts in an alternating manner. The smallest ring $R_4^4(8)$ is constructed by N1-H11B···O2 (2.77 Å, 163°) and

N1-H11C⋯O2 (2.77 Å, 169°) and their symmetry generated counterparts in a similar alternating manner. Weaker hydrogen bonds which are not involved in the previously mentioned ring motifs are cited in **Table 4.3**. The main feature of the crystal is the alternation of the hydrogen bonded layers and the aromatic layers without strong interactions. In this manner, the BAC•PTA crystal structure shows remarkable similarities to in BAC•BA. **Figure 4.7** shows the crystal packing down [100] direction.
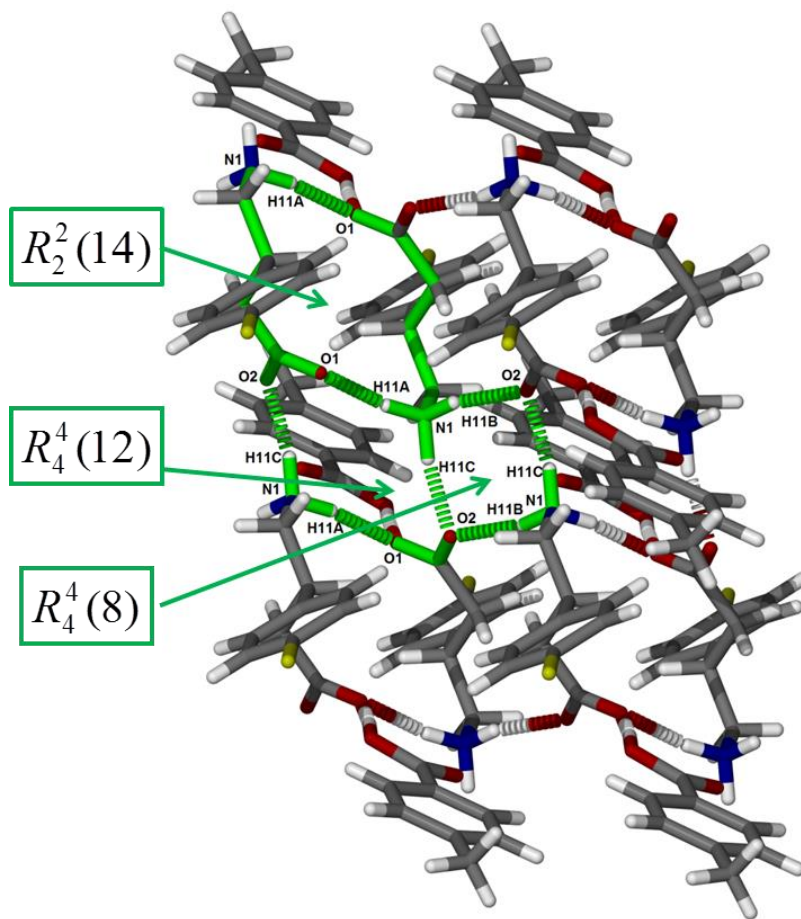
Figure 4.6 Hydrogen bonding motifs along the [100] direction in BAC•PTA.

Table 4.3 Hydrogen bonds of BAC•PTA

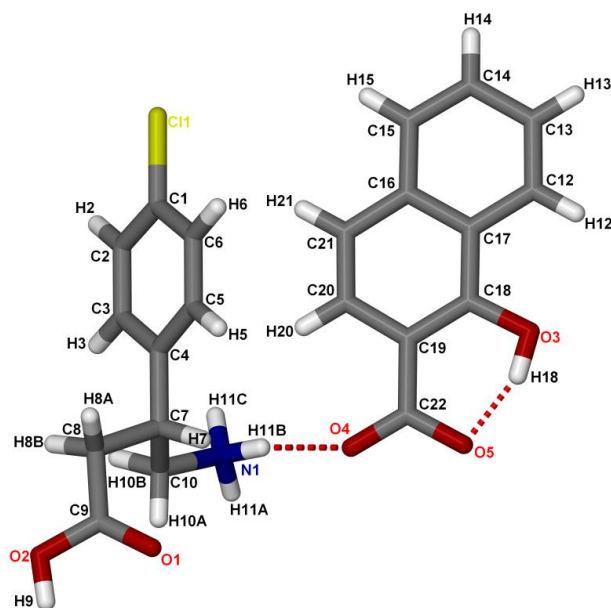| D-H⋯A	d(D-H) (Å)	d(H⋯A) (Å)	d(D⋯A) (Å)	D-H⋯A (°)	Symmetry operator
N1-H11A⋯O1	0.94	1.88	2.81	169	-x, -y, 1-z
N1-H11B⋯O2	0.92	1.88	2.77	163	1-x, -y,1- z
N1-H11C⋯O2	0.95	1.83	2.77	169	x, 1+y, z
O3-H18⋯O1	0.91	1.73	2.64	175	1+x, 1+y, z
C7-H7⋯O2	1.00	2.55	3.49	156	-x, -y,1- z
C8-H8B⋯N1	0.99	2.48	2.98	111	
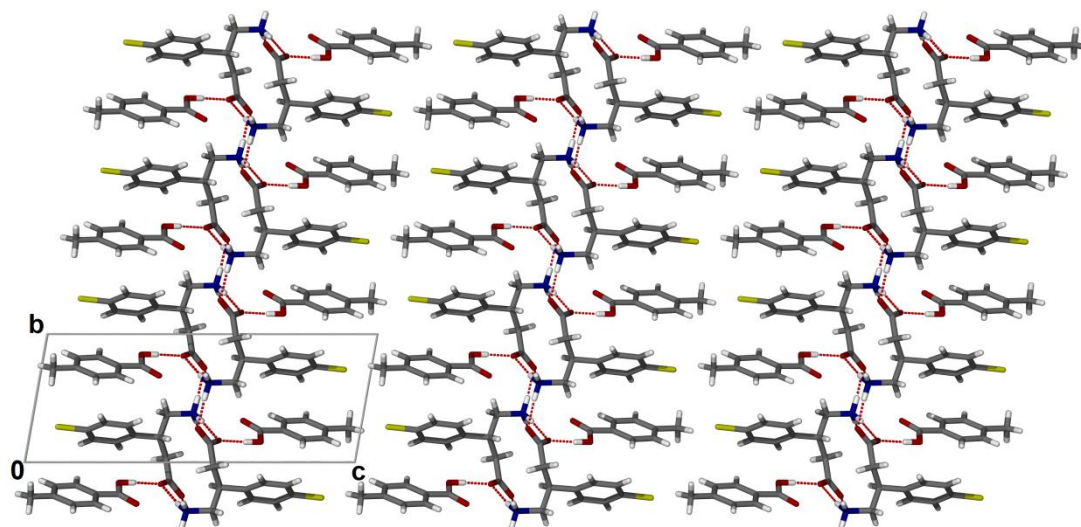
**Figure 4.7** Crystal packing of **BAC•PTA** down [100]

4.1.3 Crystal structure analysis of salt of baclofen with 1-hydroxy-2-naphthoic acid, (BAC$^+$)(HNA$^-$)

A suitable crystal of (BAC$^+$)(HNA$^-$) with dimensions of 0.11×0.16×0.45 mm was selected for single crystal X-ray analysis. The structure was solved in the monoclinic achiral space group P2$_1$/c (No.14). The structure refined to R$_1$= 0.0424 and wR$_2$=0.0955 and the crystallographic parameters are summarized in **Table 4.1**. The asymmetric unit consists of one molecule of BAC and one molecule of HNA with molecular formula of C$_{21}$H$_{20}$ClNO$_5$. The unit cell consists of four host molecules and four guest molecules (Z=4). The single crystal X-ray analysis revealed that the carboxylic proton of the HNA was transferred to the BAC, therefore the crystal is a salt. This is a very interesting result because the probability of the formation of a co-crystal or a salt is almost identical with this ΔpKa value (1.19). The hydrogen atoms on the carboxylic acid group and on the amine moiety were located in the electron density map and their coordinates refined freely. The asymmetric unit of the structure and the intramolecular hydrogen bond of the (HNA$^-$) anion (O3-H18⋯O5, 2.54 Å, 157°) are presented in **Figure 4.8.** The hydrogen bonding may be described with two ring motifs. The $R_4^4(12)$ is formed via N1-H11A⋯O5 (2.93 Å, 172°) and N1-H11B⋯O4 (2.85 Å, 169°) and their symmetry generated counterparts in an alternating manner. The $R_2^2(8)$ motif is constructed via N1-H11A⋯O5 (2.93 Å, 172°) and N1-H11C⋯O5 (2.89 Å, 162°) and theirs symmetry generated counterparts.

The carboxylic acid group of (BAC$^+$) is also involved in hydrogen bonding (O2-H9···O4, 2.61 Å, 173°). The weaker hydrogen bonds which are not involved in the previously mentioned ring motifs are presented in **Table 4.4**. Similarly to the previously discussed BAC co-crystals (BAC•BA and BAC•PTA), the main feature of the crystal is the alternation of the hydrogen bonded layers and the aromatic layers. **Figure 4.10** shows the crystal packing down [100] direction.

Figure 4.8 Asymmetric unit with labelled atoms and the hydrogen bond between BAC and HNA.
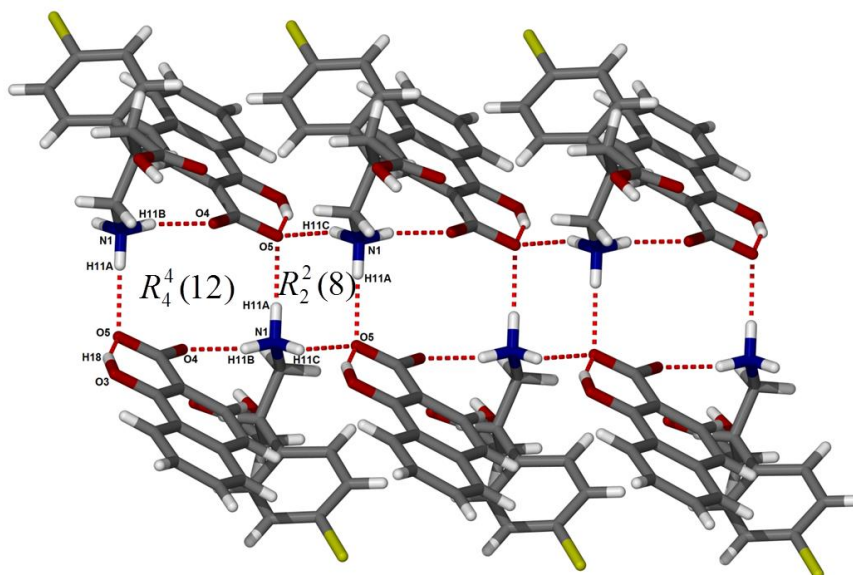

Figure 4.9 Hydrogen bonding motifs along the [100] direction in (BAC$^+$)(HNA$^-$).

Table 4.4 Hydrogen bonds of (BAC$^+$)(HNA$^-$)

D-H···A	d(D-H) (Å)	d(H···A) (Å)	d(D···A) (Å)	D-H···A (°)	Symmetry operator
O2-H9···O4	0.93	1.69	2.61	173	1-x, -y, 2-z
N1-H11A···O5	0.95	1.99	2.93	172	1-x, -y,1-z
N1-H11B···O4	0.92	1.94	2.85	169	1+x, y, z
N1-H11C···O5	0.92	2.00	2.89	162	
O3-H18···O5	0.89	1.70	2.54	157	
C8-H8B···O3	0.99	2.54	3.18	122	x, y,1+z
C10-H10A···O1	0.99	2.32	2.99	124	2-x, -y, 2-z
C10-H10B···O2	0.99	2.54	3.17	121	1-x, -y,2-z
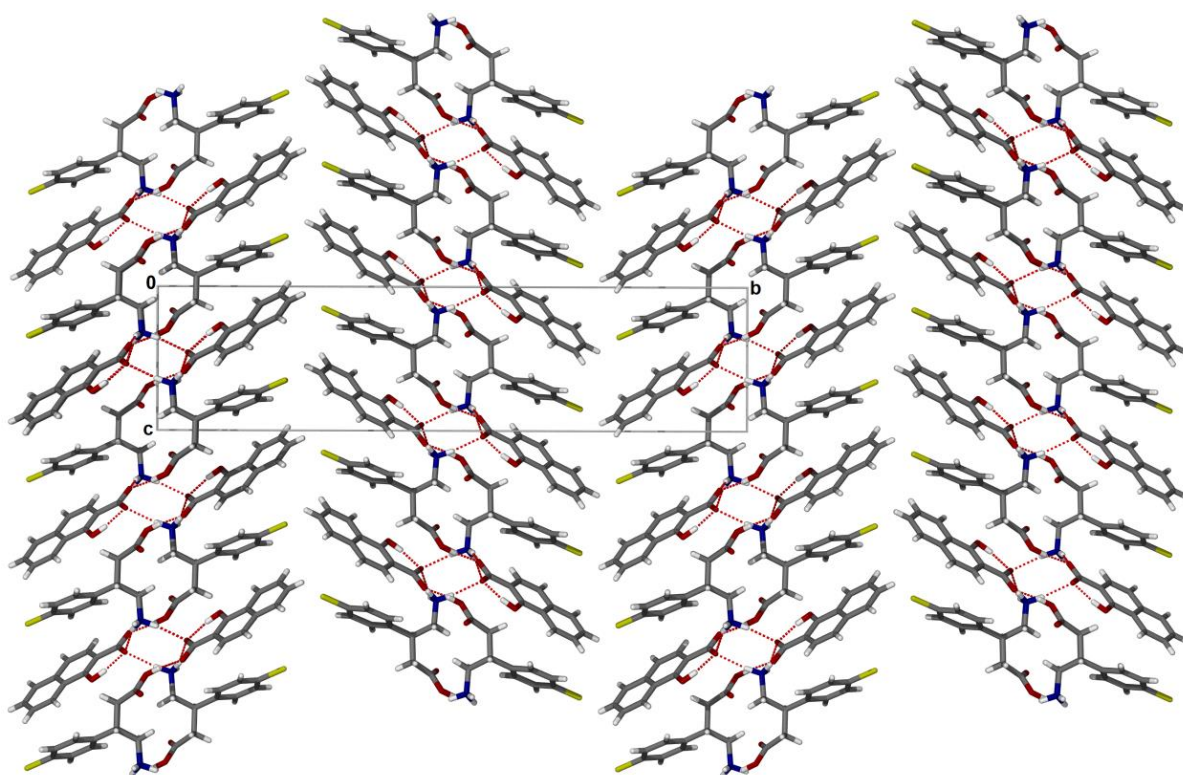
Figure 4.10 Crystal packing of (BAC$^+$)(HNA$^-$) down [100]

4.1.4 Thermal analysis of BAC•BA, BAC•PTA and (BAC⁺)(HNA⁻) crystals

The DSC curve of BAC•BA crystals (**Figure 4.11**) is inconclusive. A possible explanation of the thermal events is that the minor endotherm correspons to the melting point of the crystal (T_{1on}= 98.1°C, T_{1peak}= 98.7°C). Thus the melting point of the co-crystal is lower than the melting points of the two starting material, BAC (T_{on}= 205.5°C, T_{peak}= 210.4°C) and BA (T_{on}= 121.6°C, T_{peak}= 125.5°C). The other two endotherms between ca. 150 and 160°C are likely to be associated with the unreacted starting material.
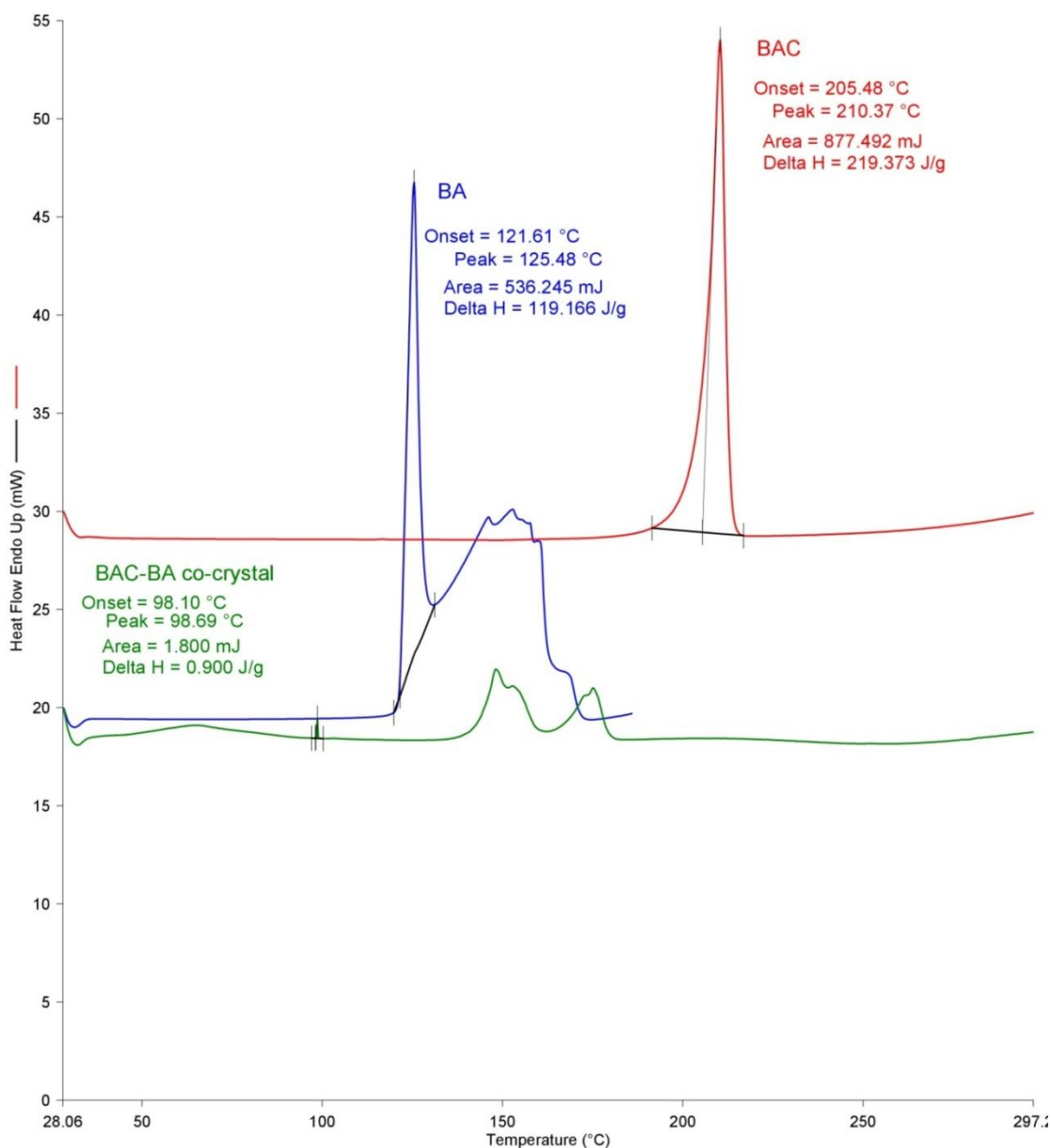
Figure 4.11 DSC curve of BAC•BA.

The DSC curve of BAC•PTA crystal (**Figure 4.12**) shows one endotherm corresponding to the melting of the co-crystal (T_{on}= 166.7°C, T_{peak}= 171.4°C). The melting point of the co-crystal is lower than the melting points of the two starting materials, BAC (T_{on}= 205.5°C, T_{peak}= 210.4°C) and PTA (T_{on}= 178.0°C, T_{peak}= 181.9°C).
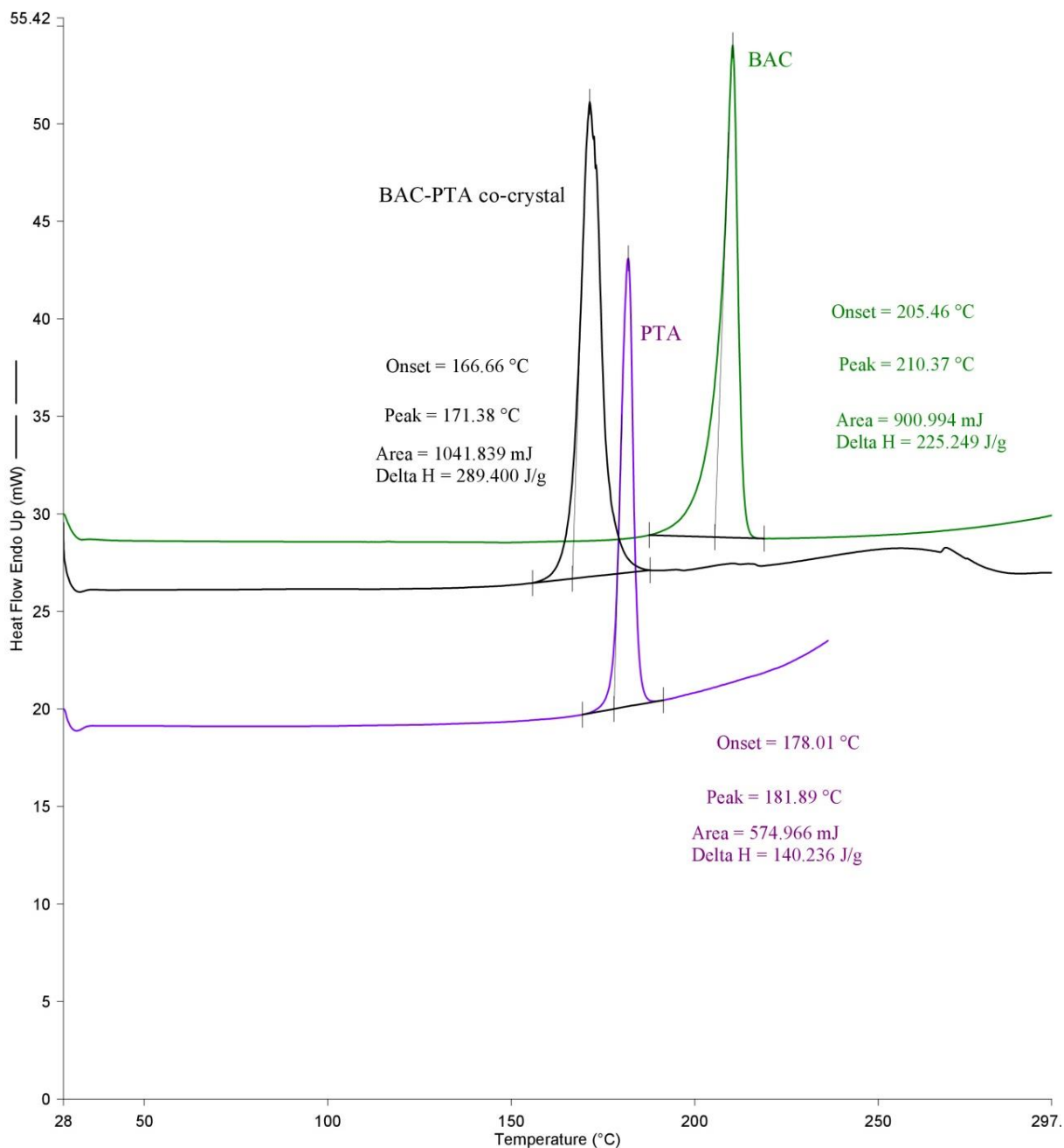
Figure 4.12 DSC curve of BAC•PTA.

The DSC curve of (BAC$^+$)(HNA$^-$) crystals (**Figure 4.13**) shows one endotherm corresponding to the melting point of the crystal (T$_{on}$= 166.4°C, T$_{peak}$= 170.3°C). The melting point of the salt is lower than the melting points of the two starting material, BAC (T$_{on}$= 205.5°C, T$_{peak}$= 210.4°C) and HNA (T$_{on}$= 195.6°C, T$_{peak}$= 200.8°C).
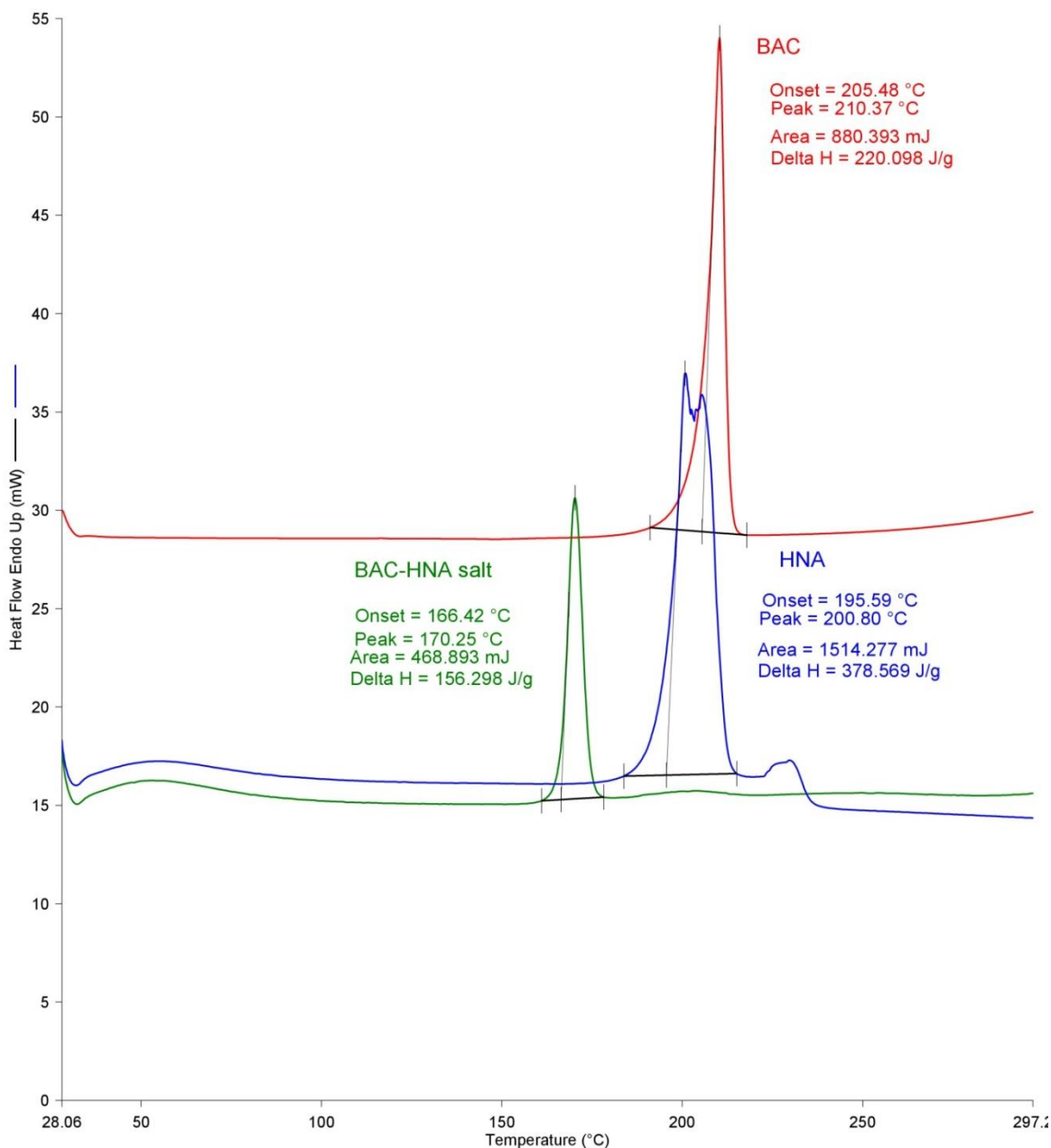
Figure 4.13 DSC curve of (BAC$^+$)(HNA$^-$)

4.1.5 Powder X-ray analysis of BAC•BA, BAC•PTA and (BAC⁺)(HNA⁻) crystals

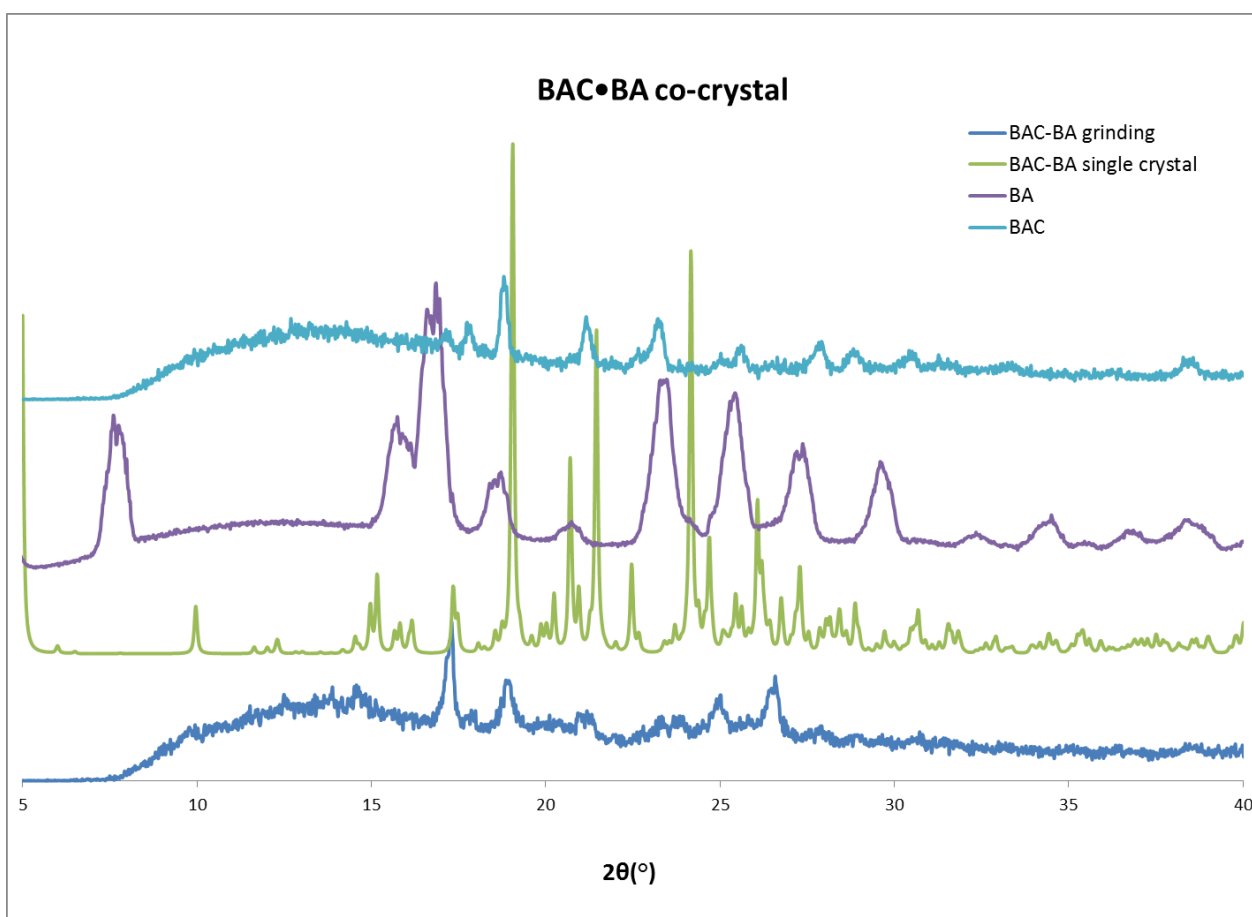PXRD analysis was used to follow the grinding experiment carried out with 1:1 ratio of BAC and BA with the addition of several drops of 1:1 methanol/water. After 60 minutes the PXRD pattern was collected (**Figure 4.14**, blue-BAC•BA grinding) and compared to the single crystal structure of BAC•BA (**Figure 4.14**, green-BAC•BA single crystal, calculated). The obtained pattern from the ground material did not show good agreement with the generated pattern of the single crystal data. The 60 mins grinding resulted in a physical mixture of BA (**Figure 4.14**, purple-BA) and BAC (**Figure 4.14**, light blue-BAC). It may be concluded that the grinding experiment was unsuccessful. The crystallisation from solution yielded very few crystals thus the PXRD pattern of the bulk material was not recorded. Several attempts were made to reproduce more co-crystals but these were unsuccessful because of the time limit of the project.

Figure 4.14 PXRD pattern of BAC (light blue), BA (purple), BAC•BA single crystal (green), BAC•BA grinding (blue).

PXRD analysis was used to track the grinding experiment carried out with 1:1 ratio of BAC and PTA with the addition of several drops of 1:1 ethanol/water. After 60 minutes the PXRD pattern was collected (**Figure 4.15**, blue-BAC•PTA grinding) and compared to the single crystal structure of BAC•PTA (**Figure 4.15**, green-BAC•PTA single crystal, calculated). The 60 mins grinding resulted in a physical mixture of PTA (**Figure 4.15**, purple-PTA) and BAC (**Figure 4.15**, light blue-BAC). It may be concluded that the more environmental friendly method, the solvent drop grinding was not successful in case of BAC and PTA. The crystallisation from solution yielded very few crystals thus the PXRD pattern of the bulk material were not recorded. Several attempts were made to reproduce more co-crystals but these were unsuccessful because of the time limit of the project.
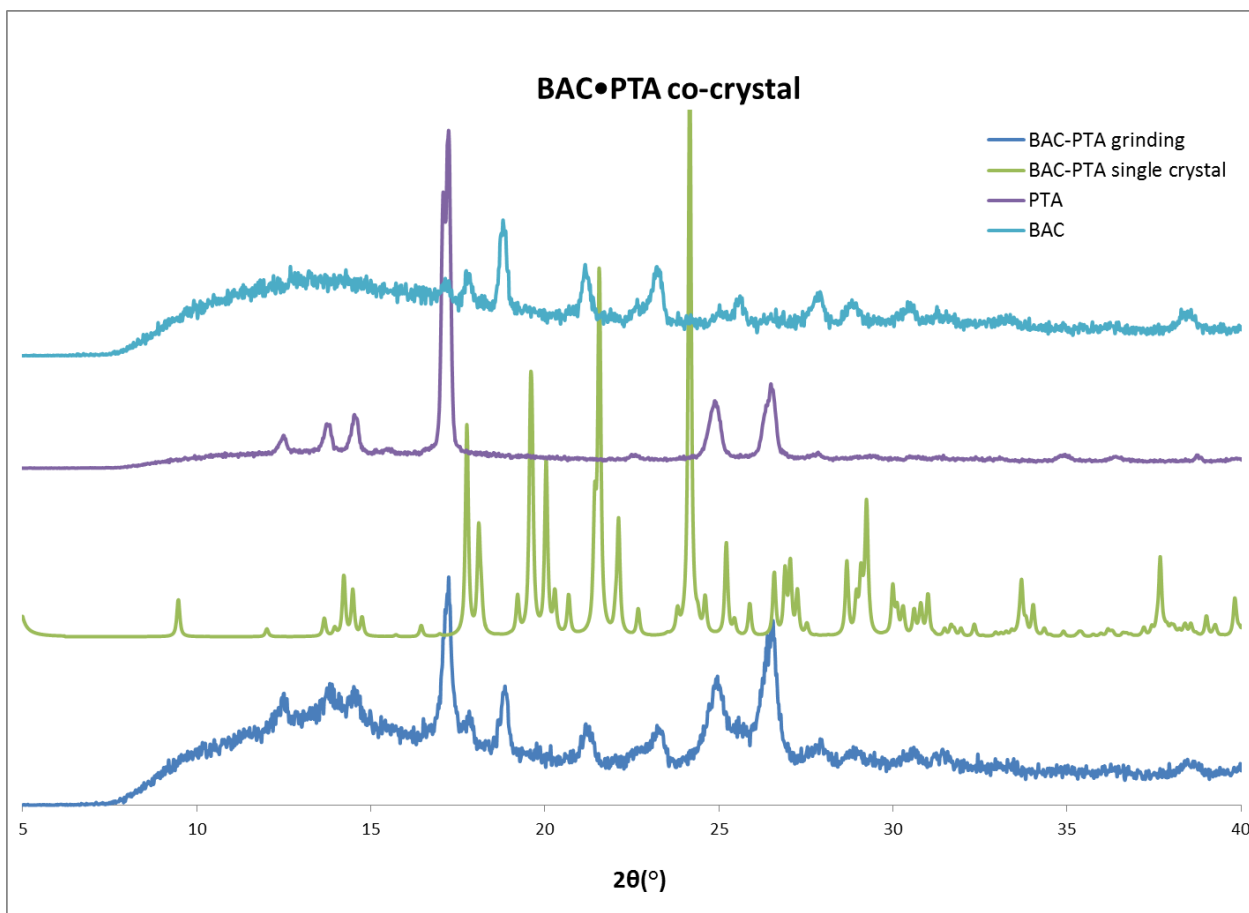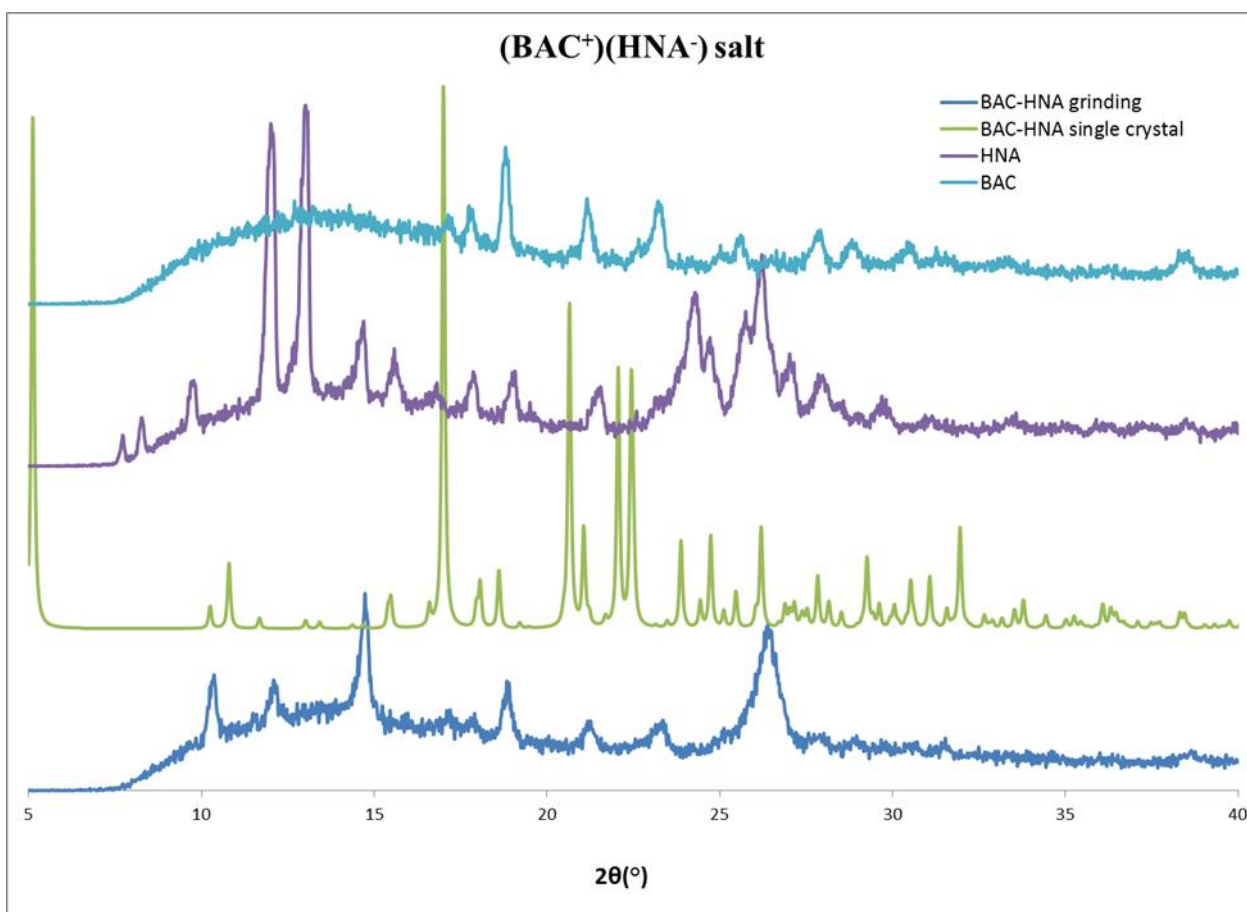

Figure 4.15 PXRD pattern of BAC (light blue), PTA (purple), BAC•PTA single crystal (green), BAC•PTA grinding (blue).

PXRD analysis was used to track the grinding experiment carried out with 1:1 ratio of BAC and HNA with the addition of several drops of 1:1 ethanol/water. After 60 minutes the PXRD pattern was collected (**Figure 4.16**, blue-(BAC$^+$)(HNA$^-$) grinding) and compared to the single crystal structure of (BAC$^+$)(HNA$^-$) (**Figure 4.16**, green-(BAC$^+$)(HNA$^-$) single crystal, calculated). During the 60 mins grinding a pattern emerged that shows similarities with the pattern derived from the single crystal structure. However, several peaks appear on the pattern which may be related to residual of BAC in the ground material. Thus it may be concluded that solvent drop grinding is a promising method to form a salt pair of BAC and HNA but clearly not an efficient way because 60 mins grinding did not result in a good conversion of the starting materials. The crystallisation from solution yielded very few crystals thus the PXRD pattern of the bulk material were not recorded. Several attempts were made to reproduce more co-crystals but these were unsuccessful because of the time limit of the project.

Figure 4.16 PXRD pattern of BAC (light blue), HNA (purple), (BAC$^+$)(HNA$^-$) single crystal (green), (BAC$^+$)(HNA$^-$) grinding (blue).

4.2 Multicomponent crystals of baclofen with dicarboxylic acids: oxalic and maleic acid

Crystals of baclofen (BAC) and oxalic acid (OA) were prepared by dissolving 49 mg (0.23 mmol) of BAC and 20 mg (0.22 mmol) of OA in a minimal amount of methanol. The solution was stirred until it became clear and left to crystallize at room temperature. Colourless blocked shape crystals were obtained after 4 weeks.

Crystals of baclofen (BAC) and maleic acid (MA) were prepared by dissolving 35 mg (0.17 mmol) of BAC with 20 mg (0.17 mmol) of MA in 1:1 ethanol/water. The solution was stirred until it became clear and left to crystallize at room temperature. Colourless blocked shape crystals were obtained after several weeks.

The ΔpKa values for the combination of BAC with OA and MA (2.53 and 2.02, respectively, Table 4) predict 40% probability for co-crystal and 60% probability for salt formation. In case of both dicarboxylic acids the crystallisation resulted in multicomponent salts.

4.2.1 Crystal structure analysis of the multicomponent crystal of baclofen with oxalic acid $2(BAC^+)(OA^{2-})$

A suitable crystal of $2(BAC^+)(OA^{2-})$ with dimensions of 0.09×0.17×0.24 mm was selected for single crystal X-ray analysis. The structure was solved in the monoclinic achiral space group P2$_1$/c (No.14) and the asymmetric unit contains one molecule of BAC and half molecule of OA with molecular formula $C_{11}H_{13}ClNO_4$. (**Figure 4.17**) The unit cell consists of four host molecules and two guest molecule (Z=4). The structure refined to R$_1$=0.0353, wR$_2$=0.0886 and the crystallographic data are summarized in **Table 4.5**. The hydrogen atoms on the carboxylic acid group and on the amine moiety were located in the electron density map and their coordinates refined freely. Both of the carboxylic protons from the OA were transferred to two BAC molecules, therefore the crystal is a salt. The main packing motif in the crystal is the hydrogen bonded tape of molecules shown in **Figure 4.18**. This structure may be described by the two ring formations of the hydrogen bonds. The bigger ring $R_4^4(22)$ is formed via N1-H11B···O4 (2.85 Å, 157°) and O2-H9···O3 (2.50 Å, 179°) and their symmetry generated counterparts. The smaller $R_3^3(11)$ ring is formed via N1-H11B···O4 (2.85 Å, 157°), N1-H11A···O1 (2.88 Å, 175°) and O2-H9···O3 (2.50 Å, 179°) interactions. The intermolecular interactions of $2(BAC^+)(OA^{2-})$ are summarized in **Table 4.6**.
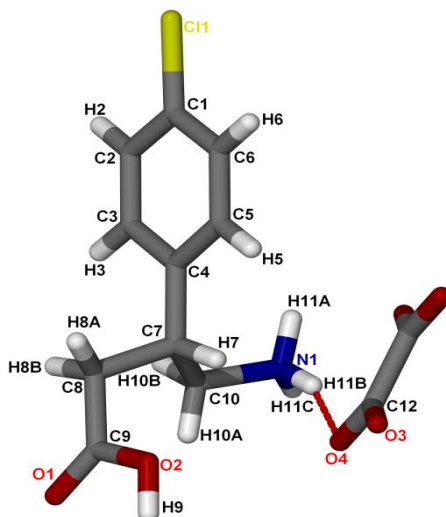
Figure 4.17 Asymmetric unit with labelled atoms and the hydrogen bond between BAC^+ and OA^{2-}.

Table 4.5 Crystallographic data and structure refinement parameters of $2(BAC^+)(OA^{2-})$ and $(BAC^+)(MA^-)$

| Crystal data		
Compounds	$2(BAC^+)(OA^{2-})$	$(BAC^+)(MA^-)$
Molecular formula	$C_{11}H_{13}ClNO_4$	$C_{14}H_{16}ClNO_6$
Formula weight(g.mol^{-1})	258.67	329.73
Crystal system	Monoclinic	Monoclinic
Space group	$P2_1/c$ (No. 14)	$P2_1$ (No. 4)
a(Å)	15.035(3)	5.7206(11)
b(Å)	7.2113(14)	13.677(3)
c(Å)	11.025(2)	9.6377(19)
α(°)	90.00	90.00
β(°)	106.86(3)	106.78(3)
γ(°)	90.00	90.00
V(Å)	1143.9(4)	722.00(2)
Z	4	2
ρcalc / g.cm^{-3}	1.502	1.517
μ(MoKα)/ mm^{-1}	0.336	0.295
F(000)	540	344
Crystal size (mm)	0.09×0.17×0.24	0.16×0.18×0.28
Temperature (K)	173(2)	173(2)
Radiation [Å]	MoKα, 0.71073	MoKα, 0.71073
Theta min-max[°]	2.83, 27.48	2.21,28.37
Dataset	-19:19; -9:9; -14:14	-7:7;-18:18;-8:12
Final R indices [I>2.0 (I)]	R_1=0.0353, wR_2=0.0886	R1=0.0330, wR2=0.0783
R indices (all data)	R_1=0.0508, wR_2=0.0979	R1=0.0369, wR2=0.0807
Tot., uniq.data, R(int)	2618, 2054, 0.0161	3605, 3345, 0.0210
N$_{ref}$, N$_{par}$	2618,171	3605,220
S	1.046	1.047
Max. and av. Shift/error	0.00, 0.00	0.00, 0.00
Min. and max. res. dens.	0.214, -0.279	0.218, -0.179

The hydrogen bonded tapes form hydrogen bonded layers in the [010] direction via N1-H11C···O2 (2.54 Å, 133°) and N1-H11C···O4 (2.47 Å, 113°) bifurcated hydrogen bonds (**Figure 4.19**) and these layers interact via an aromatic layer.
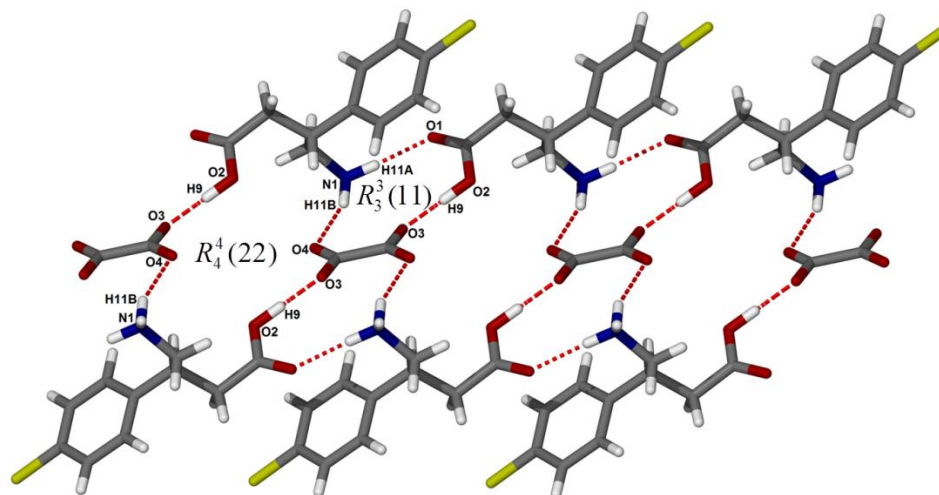
Figure 4.18 Hydrogen bonding motifs along the [001] direction in 2(BAC$^+$)(OA^{2-}).

Table 4.6 Hydrogen bonds of 2(BAC$^+$)(OA^{2-}).

D-H···A	d(D-H) (Å)	d(H···A) (Å)	d(D···A) (Å)	D-H···A (°C)	Symmetry operator
O2-H9···O3	0.97	1.53	2.50	179	x, 3/2-y, ½+z
N1-H11A···O1	0.94	1.95	2.88	175	x, -1+y, z
N1-H11B···O4	0.89	2.01	2.85	157	-x, 1/2+y, ½-z
N1-H11B···O3	0.89	2.26	2.82	120	x, ½-y,1/2+z
N1-H11C···O4	0.90	2.47	2.94	113	
N1-H11C···O2	0.90	2.54	3.22	133	x, 3/2-y, -1/2+z
C7-H7···O2	1.00	2.53	2.92	103	
C7-H7···O4	1.00	2.59	3.37	134	-x, ½+y, ½-z
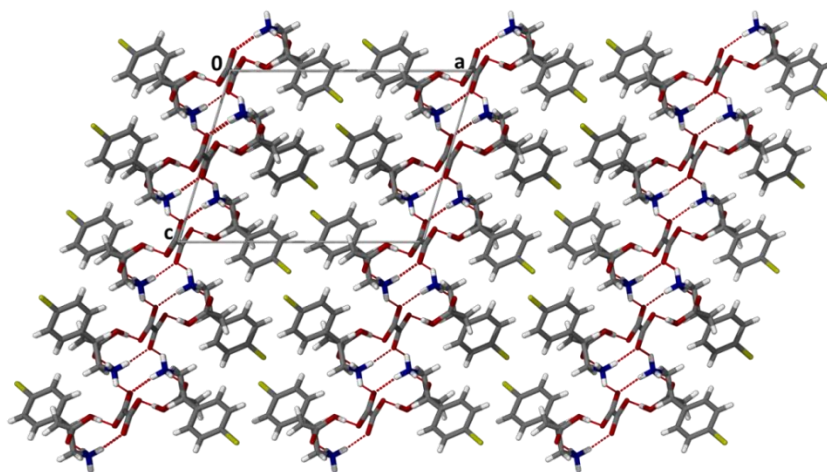
Figure 4.19 Crystal packing of 2(BAC$^+$)(OA^{2-}) view down [010].

4.2.2 Crystal structure analysis of the multicomponent crystal of baclofen with maleic acid (BAC⁺)(MA⁻)

A suitable crystal of (BAC⁺)(MA⁻) with dimensions of 0.16×0.18×0.28 mm was selected for single crystal X-ray data collection. **Table 4.5** summarizes the data collection and refinement details. The structure was solved in the monoclinic chiral space group P2₁ (No. 4) and the asymmetric unit contains one molecule of BAC and one molecule of MA with molecular formula $C_{14}H_{16}ClNO_6$. (**Figure 4.20a**) The structure was solved for the S enantiomer of BAC with Flack parameter -0.03(5) therefore the absolute structure given by the structure refinement is likely correct. The unit cell consists of two host molecules and two guest molecule (Z=2). The structure refined to R_1=0.0330 and wR_2=0.0783 and the crystallographic data are summarized in **Table 4.5.** The hydrogen atoms on the carboxylic acid group and on the amine moiety were located in the electron density map and their coordinates refined freely. One of the carboxylic protons were transferred from the MA moiety to the BAC, therefore the crystal is a salt. The H14 hydroxyl proton of the MA forms an intramolecular hydrogen bond and it is positioned at an equal distance from O5 and O6 atoms. This can bee seen on the difference Fourier map on **Figure 4.20b**. The O···O- distance in maleate anion (O5···O6 2.41Å) is not unusual. Neutron studies have shown that it ranges from 2.393(3)Å to 2.445(2)Å.[3]

(a)   **(b)**
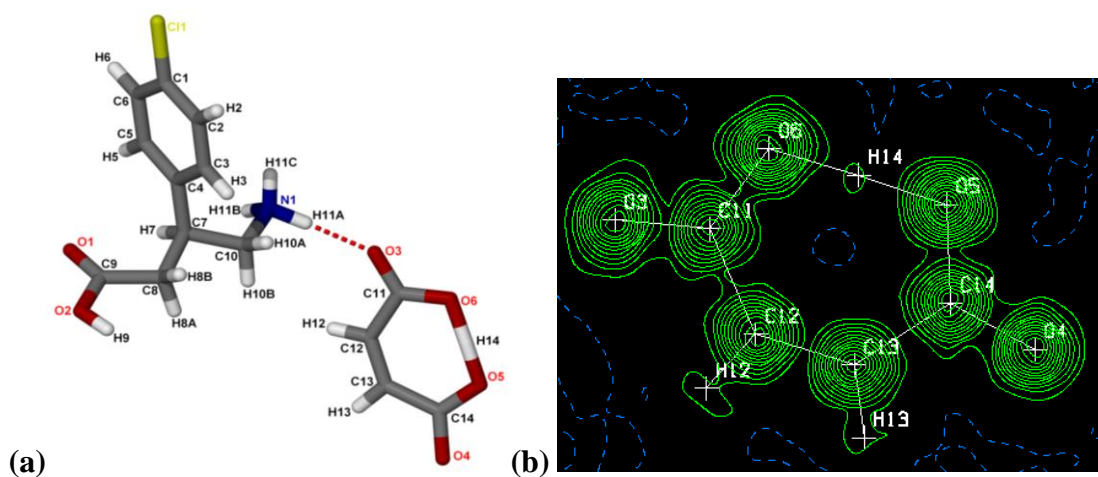
Figure 4.20 (a) Asymmetric unit with labelled atoms and the hydrogen bond between BAC and MA moieties. (b) Difference Fourier map of MA moiety (plane fitted to O5, O6, C12 and C13 atoms).

The main packing motif in the crystal is the hydrogen bonded 2D net of molecules shown in **Figure 4.21a**. The main feature of this structure is the $R_5^6(32)$ ring formed via N1-H11A···O3 (2.82 Å, 155°), N1-H11C···O4 (2.86 Å, 149°), O2-H9···O4 (2.65 Å, 170°) and their symmetry equivalents. These off-set brick type 2D structures bonded together via bifurcated hydrogen bonds, N1-H11B···O3 (2.56 Å, 160°) and N1-H11B···O6 (2.28 Å, 126°). (**Figure 4.21b**) The intermolecular interactions of (BAC$^+$)(MA$^-$) are summarized in **Table 4.7**.
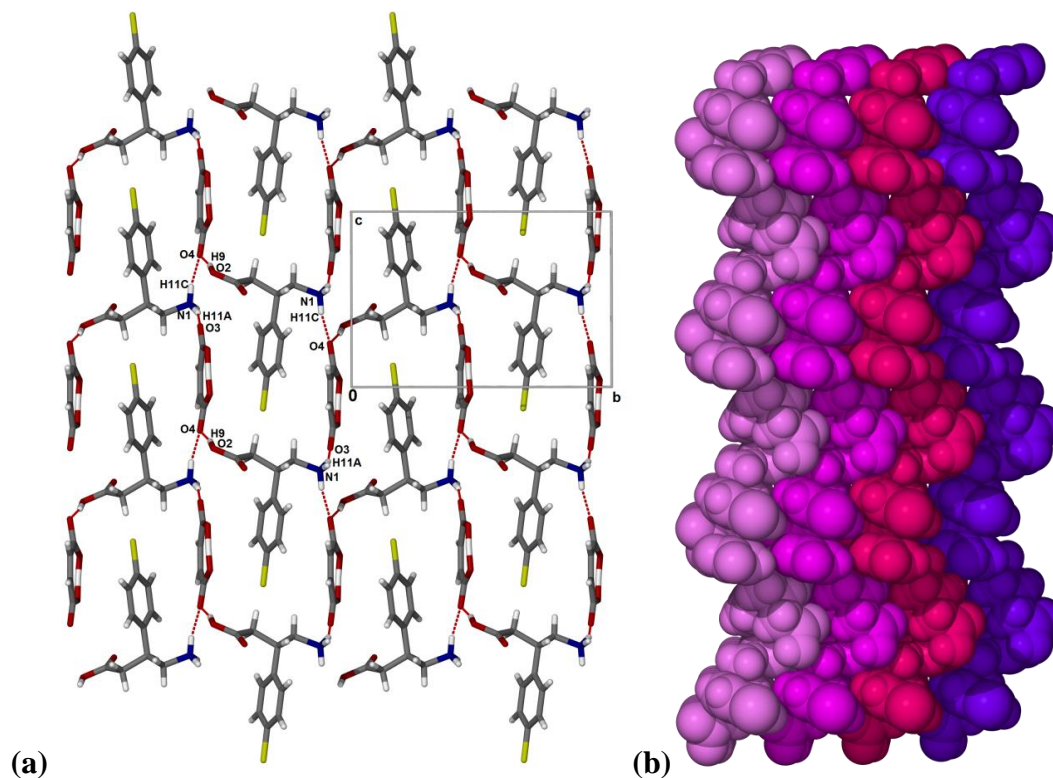
Figure 4.21 (a) Hydrogen bonded off-set brick type net of (BAC$^+$)(MA$^-$) down [100] and (b) their arrangement view down [001].

Table 4.7 Intermolecular interactions of (BAC$^+$)(MA$^-$)

D-H···A	d(D-H) (Å)	d(H···A) (Å)	d(D···A) (Å)	D-H···A (°)	Symmetry operator
O2-H9···O4	0.88	1.77	2.65	170	1-x,-1/2+ y,-z
O2-H9···O5	0.88	2.57	3.20	130	1-x, -½+y,-z
N1-H11A···O3	0.96	1.93	2.82	155	
N1-H11B···O3	0.94	2.56	3.45	160	-1+x, y, z
N1-H11B···O6	0.94	2.28	2.93	126	-1+x, y, z
N1-H11C···O4	0.91	2.04	2.86	149	x,y, 1+z
O5-H14···O6	1.21	1.21	2.41	176	
C3-H3···O1	0.95	2.42	3.36	169	1+x, y, z
C10-H10A···O1	0.99	2.59	3.48	149	1+x, y, z

4.2.3 Thermal analysis of crystals of baclofen 2(BAC⁺)(OA²⁻) and (BAC⁺)(MA⁻)

The DSC curve of 2(BAC⁺)(OA²⁻) salt (**Figure 4.22**) shows one endotherm corresponding to the melting point of the salt (T_{on}= 165.4°C, T_{peak}= 169.5°C). The melting point of the salt is located between the melting points of the two starting material, BAC (T_{on}= 205.5°C, T_{peak}= 210.4°C) and OA (T_{on}= 103.4°C, T_{peak}= 105.4°C).
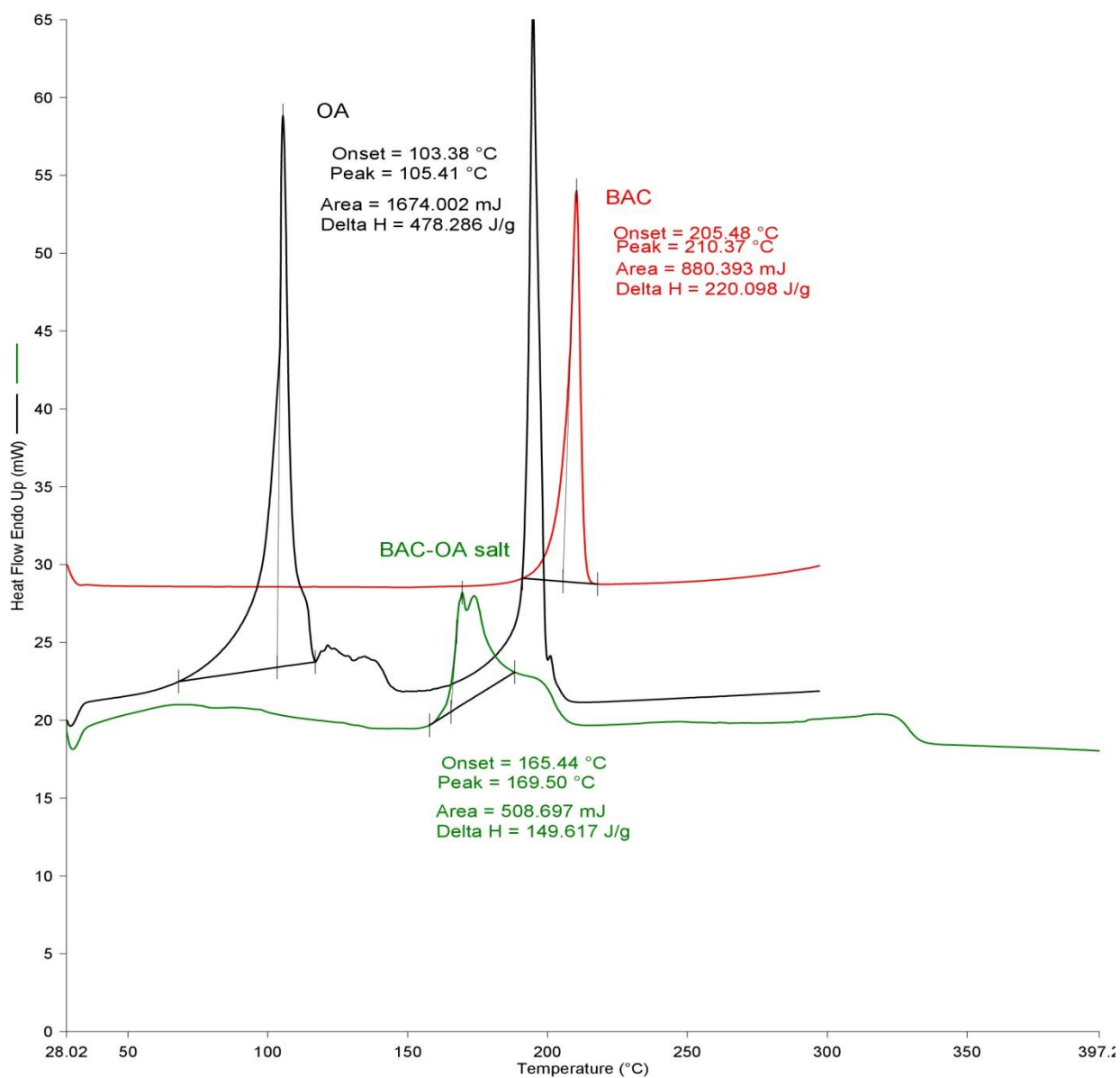
Figure 4.22 DSC curves of 2(BAC⁺)(OA²⁻).

The DSC curve of $(BAC^+)(MA^-)$ salt (**Figure 4.23**) shows one endotherm corresponding to the melting point of the salt (T_{on}= 180.1°C, T_{peak}= 186.5°C). The melting point of the salt is located before the melting points of the two starting material, BAC (T_{on}= 205.5°C, T_{peak}= 210.4°C) and MA (T_{on}= 151.5°C, T_{peak}= 153.3°C).
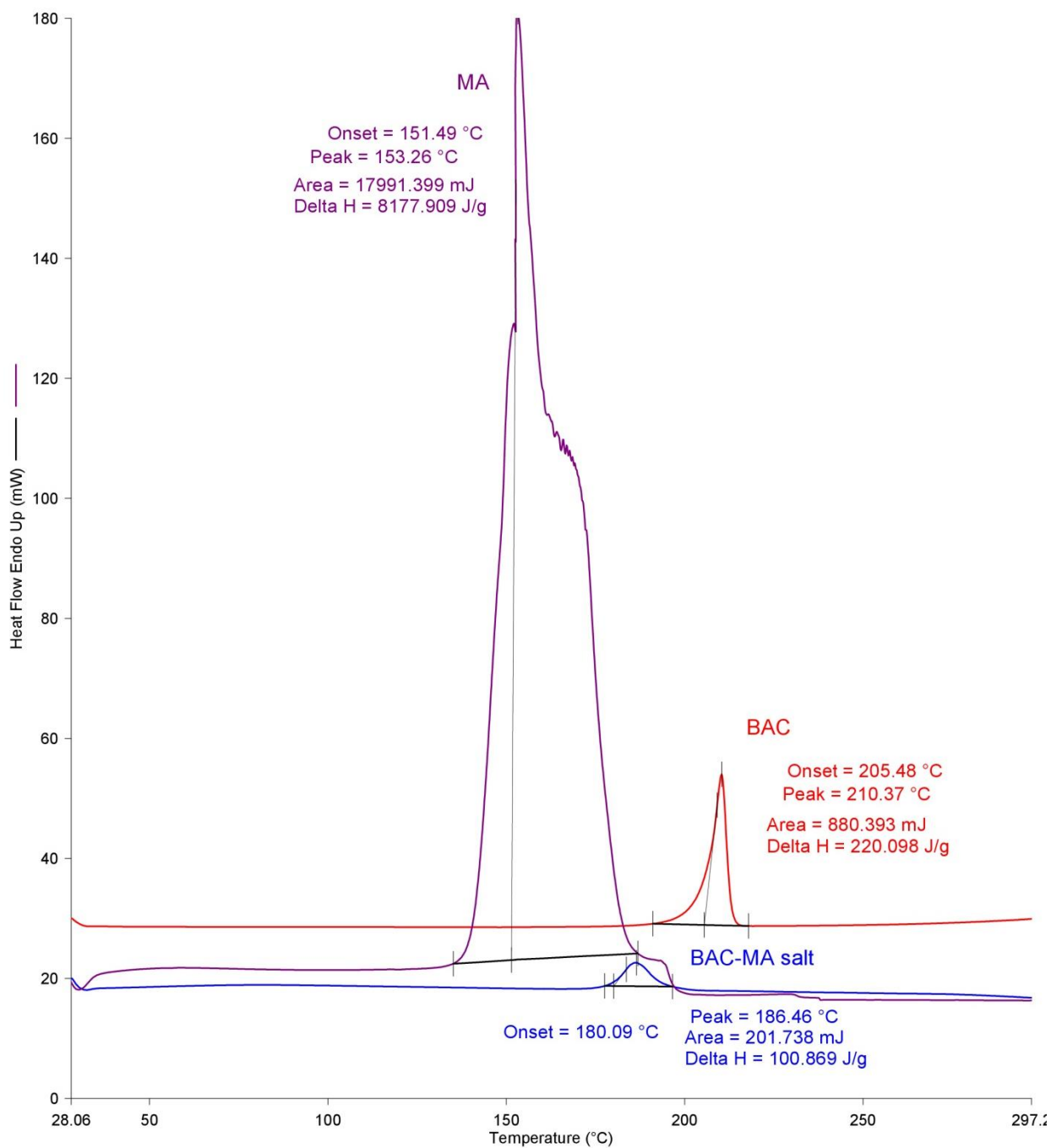
Figure 4.23 DSC curves of $(BAC^+)(MA^-)$.

4.2.4 Powder X-ray analysis of 2(BAC⁺)(OA²⁻) and (BAC⁺)(MA⁻)

Powder X-ray analysis was carried out to show that the structure detected by using one single crystal only (**Figure 4.24**, green- 2(BAC⁺)(OA²⁻) single crystal, calculated) is representative of the grinding product (**Figure 4.24**, blue- 2(BAC⁺)(OA²⁻)grinding). PXRD analysis was used to show that the 2(BAC⁺)(OA²⁻) salt obtained via slow evaporation from a minimal amount of methanol can be prepared via the environmentally friendly method, solvent drop grinding. Pure BAC and OA were ground with several drops of 1:1 ethanol/water and after 60 mins the PXRD pattern was collected (**Figure 4.24**, blue- 2(BAC⁺)(OA²⁻) grinding). This was compared to the starting pattern of the pure BAC and OA (**Figure 4.24**, light blue-BAC, purple- OA). The patterns for the single crystal and the ground material are not similar and clearly differ from the starting compounds, BAC and OA, therefore it may be concluded that the solvent drop grinding method is not suitable to produce the 2(BAC⁺)(OA²⁻) salt.
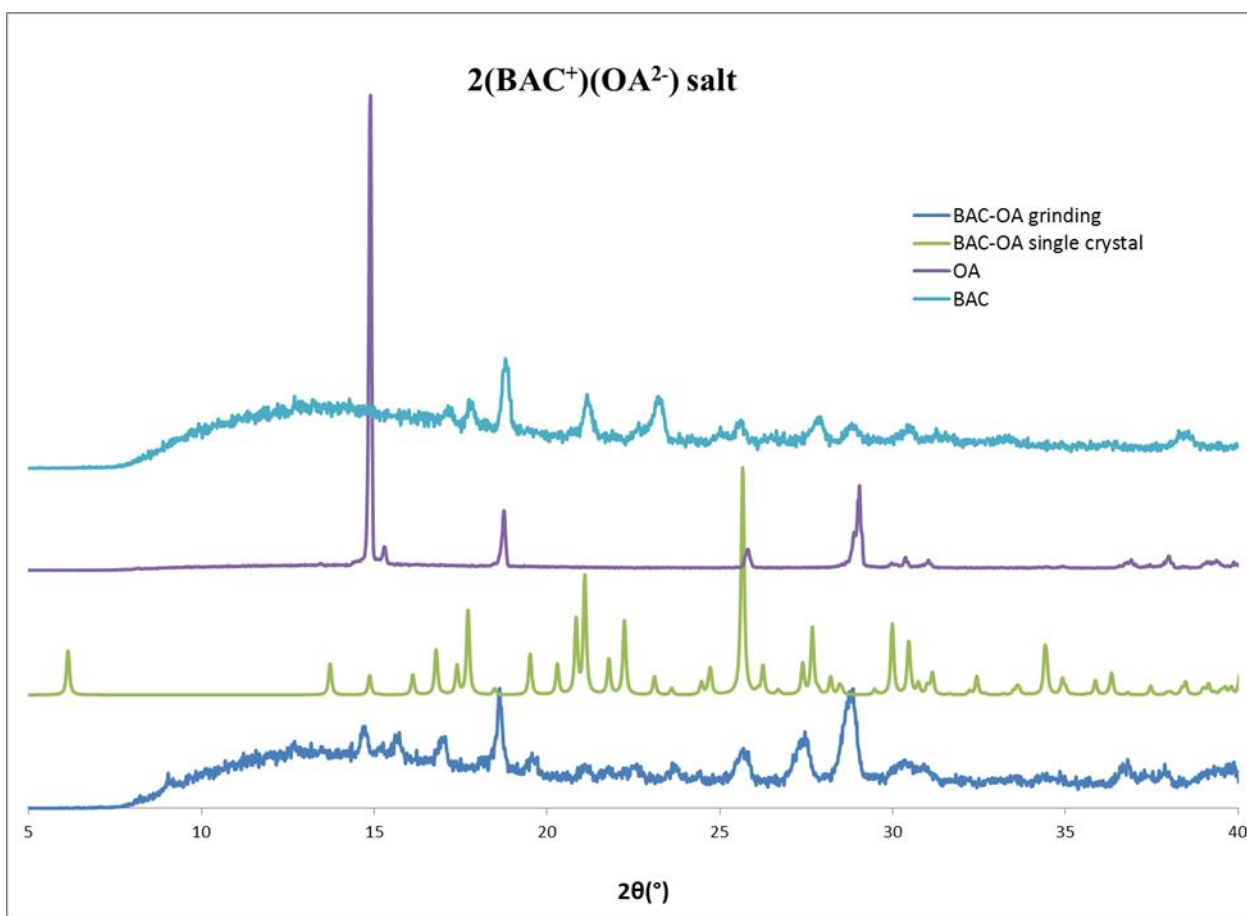
Figure 4.24 PXRD patterns of BAC (light blue), OA (purple), BAC•OA pattern generated from single crystal structure (green) and BAC•OA grinding (blue).

Pure BAC and MA were ground with a minimal amount of methanol and after 60 mins the PXRD pattern was collected (**Figure 4.25** blue-$(BAC^+)(MA^-)$ grinding). In a similar manner, it may be concluded that the salt of $(BAC^+)(MA^-)$ cannot be prepared via solvent drop grinding.
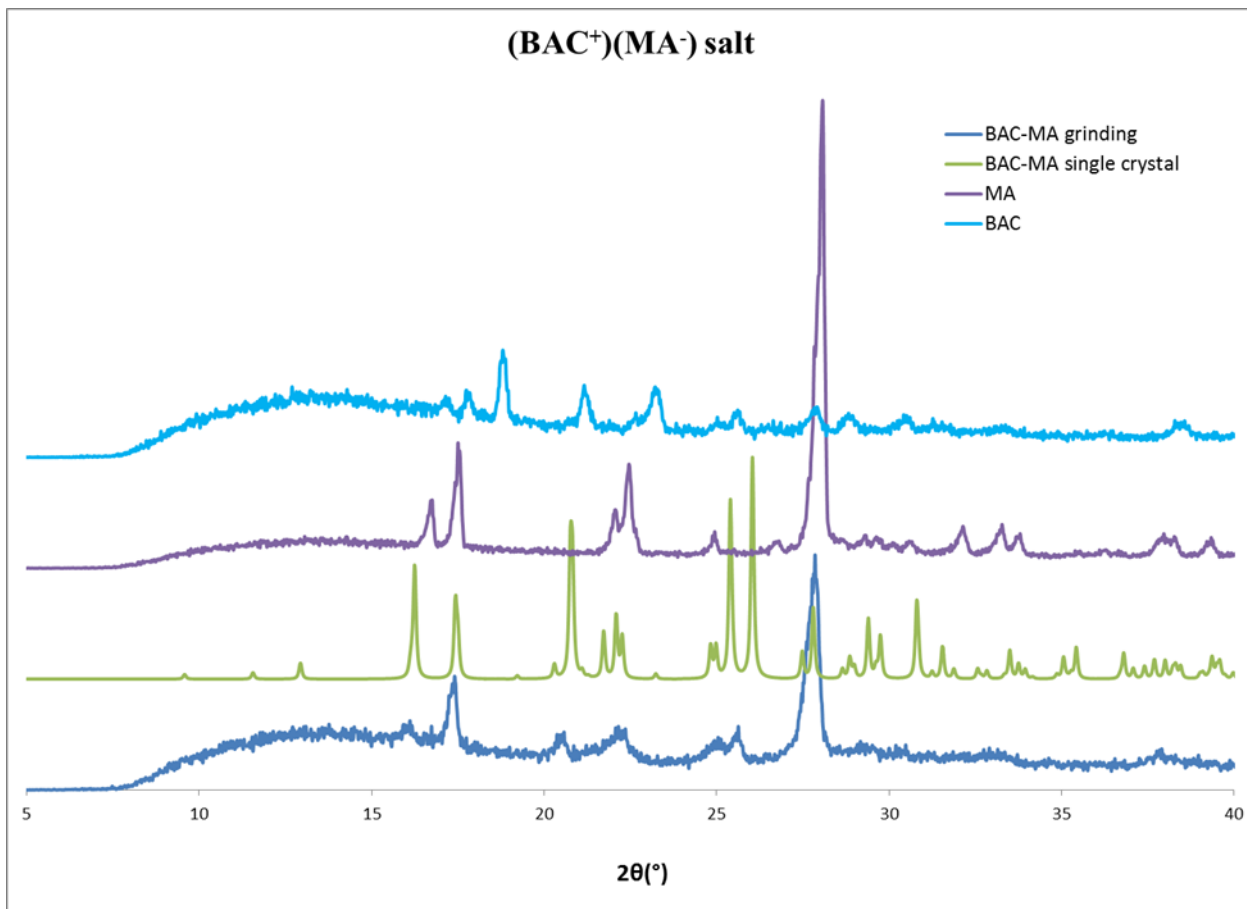
Figure 4.25 PXRD patterns of BAC (light blue), MA (purple), BAC•MA pattern generated from single crystal structure (green) and BAC•MA grinding (blue).

## 4.3 Salt of baclofen with p-toluene sulfonic acid $(BAC^+)(PTSA^-)$•IPA

The co-crystal of baclofen (BAC) and p-toluene sulfonic acid (PTSA) was prepared by dissolving 45mg (0.21 mmol) of BAC with 28mg (0.16 mmol) of PTSA in a minimal amount of isopropanol (IPA) until the solution became clear, and was left to crystallize at room temperature. Colourless crystals were obtained after several weeks.

### 4.3.1 Crystal structure analysis of (BAC$^+$)(PTSA$^-$)•IPA

A suitable crystal of (BAC$^+$)(PTSA$^-$)•IPA with dimensions 0.05×0.06×0.54 mm was subjected to single crystal data collection. The compound crystallizes in the monoclinic achiral space group P2$_1$/c (No.14) with one baclofen, one p-toluene sulfonic acid and one disordered isopropanol molecule in the asymmetric unit. The molecular formula is C$_{20}$H$_{28}$ClNO$_6$S. (**Figure 4.26**) The unit cell consists of four BAC molecules, four PTSA molecules and four isopropanol molecules (Z=4). The structure refined to R$_1$= 0.0680 and wR$_2$=0.1291 and the crystallographic data are summarized in **Table 4.8**. The hydrogen atoms on the carboxylic acid group and on the amine moiety were located in the electron density map and their coordinates refined freely. One proton has been transferred from the p-toluene sulfonic acid to the baclofen therefore it is a salt-solvate. The isopropanol (IPA) is disordered over two positions (C20, C22 and the related H atoms have 89% S.O.F while C19, C21 and the bonded hydrogens have S.O.F. of 11%). The main packing motif in the crystal is the hydrogen bonded 2D net in the [010] direction, shown in **Figure 4.27**. The main feature of this structure is the $R_6^6(26)$ ring formed via O2-H1⋯O6 (2.60 Å, 172°), O6-H6A⋯O3 (2.78 Å, 102°), N1-H11B⋯O5 (2.85 Å, 157°) hydrogen bonds and their symmetry generated counter parts. Another centrosymmetric ring motif $R_2^2(8)$ may be described with N1-H11A⋯O5 (2.89 Å, 135°) and N1-H11B⋯O5 (2.85 Å, 157°) hydrogen bonds. In the [100] direction C8-H8A⋯O1 (3.36 Å, 156°) and N1-H11C⋯O3 (2.76 Å, 164°) hydrogen bonds are connecting the layers together. (**Figure 4.27**) The intermolecular interactions of (**BAC$^+$**)(**MA$^-$**) are summarized in **Table 4.9**.
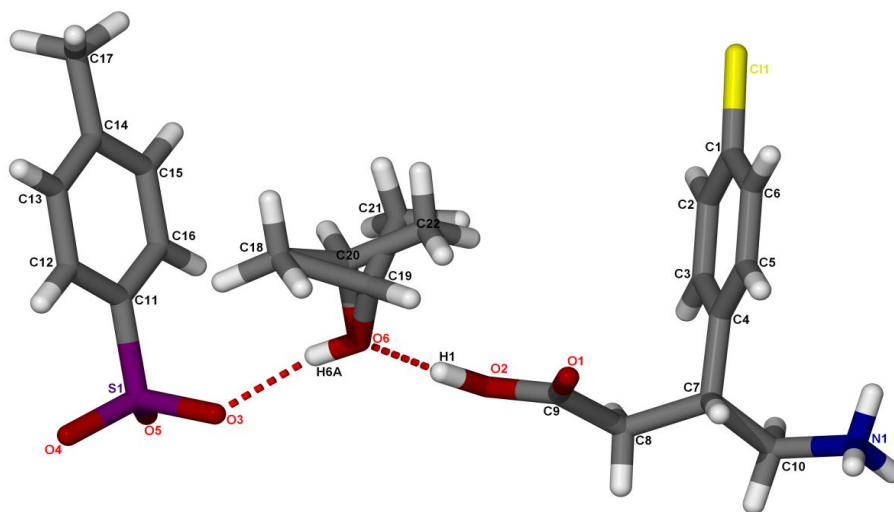
Figure 4.26 Asymmetric unit of (BAC$^+$)(PTSA$^-$)•IPA. Only heavy atoms are labelled for clarity.

Table 4.8 Crystal data of $(BAC^+)(PTSA^-)•IPA$

Crystal data	
Compound	$(BAC^+)(PTSA^-)•IPA$
Molecular formula	$C_{20}H_{28}ClNO_6S$
Formula weight(g.mol^{-1})	445.94
Crystal system	Monoclinic
Space group	$P2_1/c$ (No. 14)
a(Å)	5.4900(11)
b(Å)	13.400(3)
c(Å)	28.910(6)
α(°)	90.00
β(°)	90.90(3)
γ(°)	90.00
V(Å)	2126.5(7)
Z	4
ρcalc / g.cm^{-3}	1.393
μ(MoKα)/ mm^{-1}	0.315
F(000)	944
Crystal size (mm)	0.05×0.06×0.54
Temperature (K)	173(2)
Radiation [Å]	MoKα, 0.71073
Theta min-max[°]	1.41, 28.83
Dataset	-7:7;-17:17;-37:39
Final R indices [I>2.0 (I)]	R_1= 0.0680, wR_2=0.1291
R indices (all data)	R_1=0.1152, wR_2=0.1444
Tot., uniq.data, R(int)	5211, 3301, 0.0573
N_{ref}, N_{par}	5211, 284
S	1.059
Max. and av. Shift/error	0.00, 0.00
Min. and max. res. dens.	-0.396, 0.340
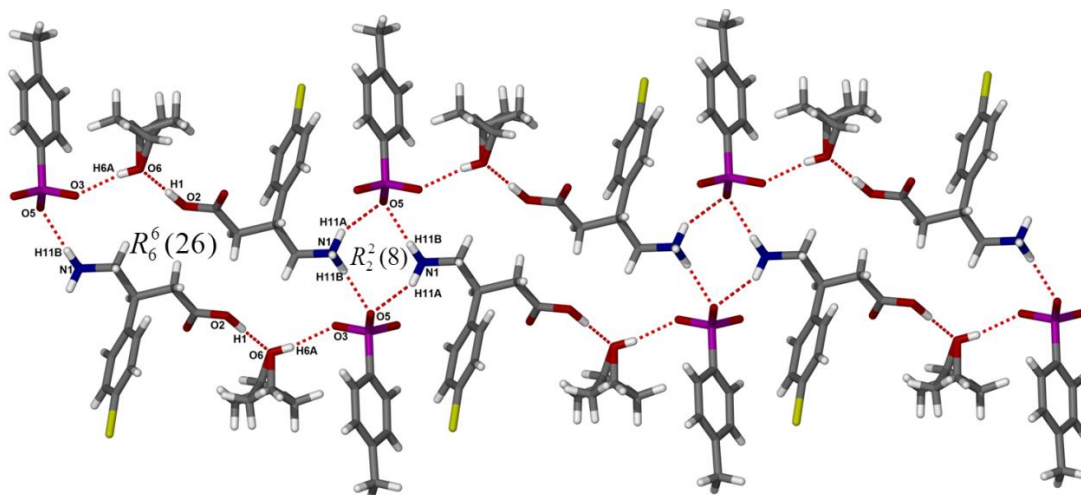
Figure 4.27 Hydrogen bonding in $(BAC^+)(PTSA^-)\cdot IPA$ down [100].
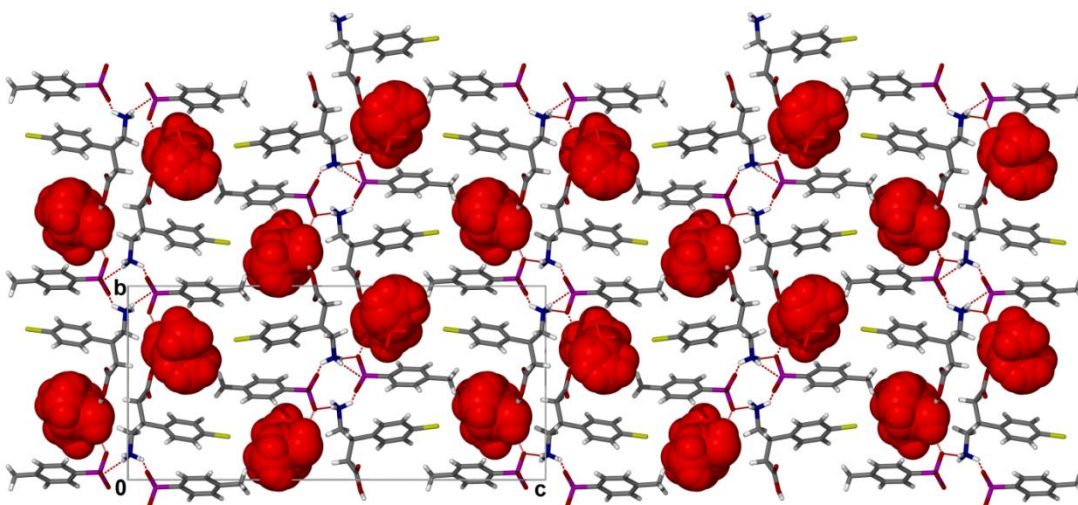
Figure 4.28 Crystal packing of $(BAC^+)(PTSA^-)\cdot IPA$ down [100]. The included isopropanol molecules are with red space filling model.

Table 4.9 Hydrogen bonds in $(BAC^+)(PTSA^-)\cdot IPA$

D-H⋯A	d(D-H) (Å)	d(H⋯A) (Å)	d(D⋯A) (Å)	D-H⋯A (°)	Symmetry operator
O2-H1⋯O6	0.98	1.63	2.60	172	-1+x, y, z
O6-H6A⋯O3	0.79	1.96	2.74	167	1-x, ½+y,1/2-z
N1-H11A⋯O4	0.91	2.44	2.78	102	1-x, -1/2+y,1/2- z
N1-H11A⋯O5	0.91	2.18	2.89	135	-x, -1/2+y,1/2- z
N1-H11B⋯O4	0.91	2.40	2.78	105	1-x,-1/2+ y,-1/2- z
N1-H11B⋯O5	0.91	1.99	2.85	157	1+x, ½-y, -1/2+z
N1-H11C⋯O3	0.91	1.87	2.76	164	x,1/2-y, -1/2+z
C3-H3⋯O1	0.95	2.39	3.33	171	1+x, y, z
C8-H8A⋯O1	0.99	2.43	3.36	156	1+x, y, z
C12-H12⋯O4	0.95	2.55	2.89	101	

4.3.2 Thermal analysis of (BAC⁺)(PTSA⁻)•IPA

TG was used to confirm the solvent ratio of the $(BAC^+)(PTSA^-)\cdot IPA$. The DSC curve of $(BAC^+)(PTSA^-)\cdot IPA$ crystals shows one endotherm corresponding to the melting point of the crystal (T_{on}= 169.6°C, T_{peak}= 171.3°C). The melting point of the salt is located between the melting points of the two starting material, BAC (T_{on}= 205.5°C, T_{peak}= 210.4°C) and PTSA (T_{on}= 101.5°C, T_{peak}= 106.8°C). (**Figure 4.29**)
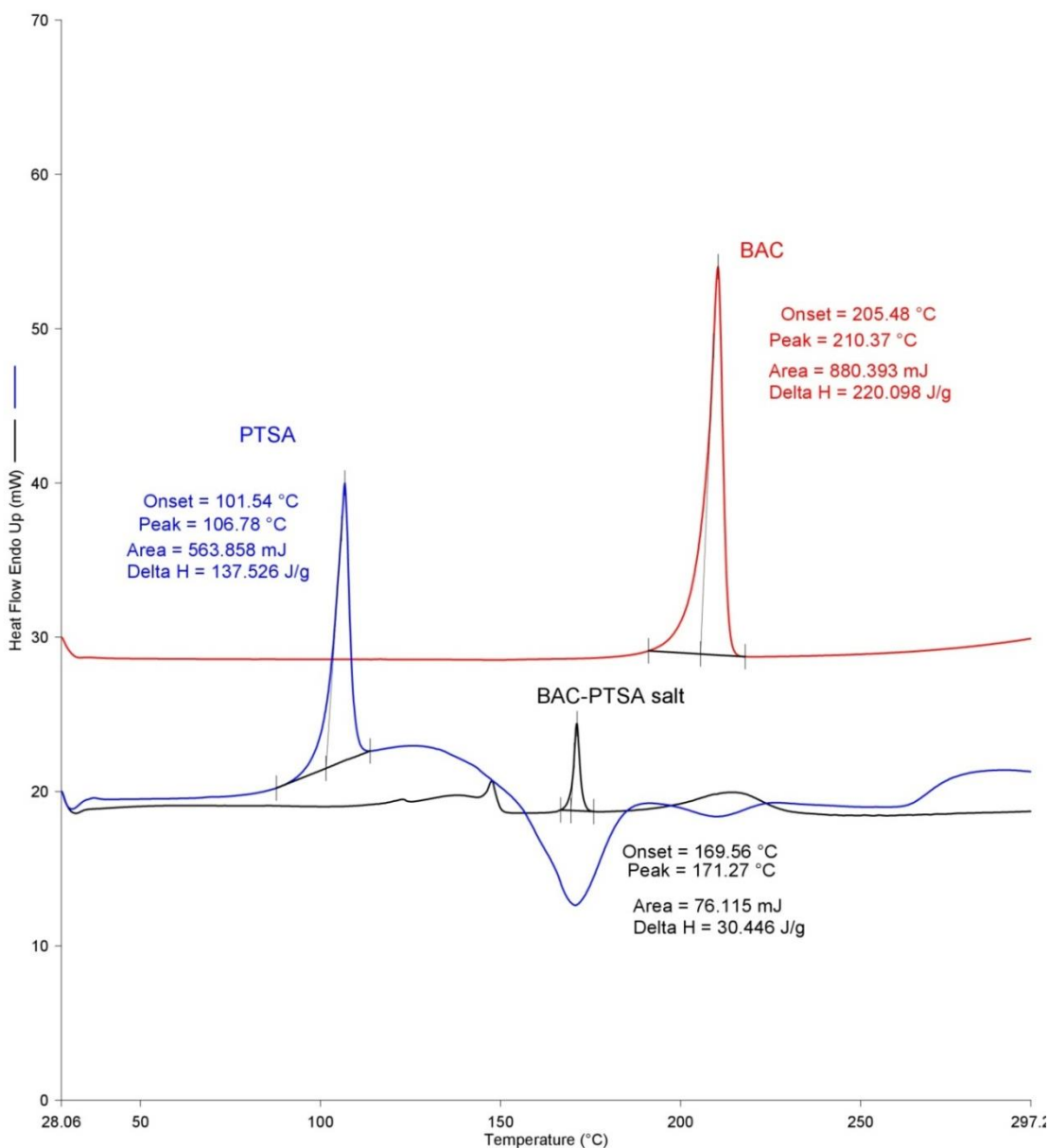
Figure 4.29 DSC curve of (BAC⁺)(PTSA⁻)•IPA

4.3.3 Powder X-ray analysis of (BAC⁺)(PTSA⁻)•IPA

Powder X-ray analysis was carried out to show that the structure detected by using one single crystal only (**Figure 4.30**, green- BAC•PTSA single crystal, calculated) is representative of the material obtained via grinding (**Figure 4.30**, blue-BAC•PTSA grinding). Pure BAC and PTSA were ground with several drops of isopropanol and after 60 mins the PXRD pattern was collected (**Figure 4.30**, blue- BAC•MA grinding). This was compared to the pattern of the starting materials, pure BAC and PTSA (**Figure 4.30,** light blue-BAC, purple- PTSA). The patterns for the single crystal and the ground material are somewhat similar and clearly differ from the starting compounds. However, the match is not perfect and several peaks related to BAC and PTSA are still noticeable, therefore the reaction occurs only partially.
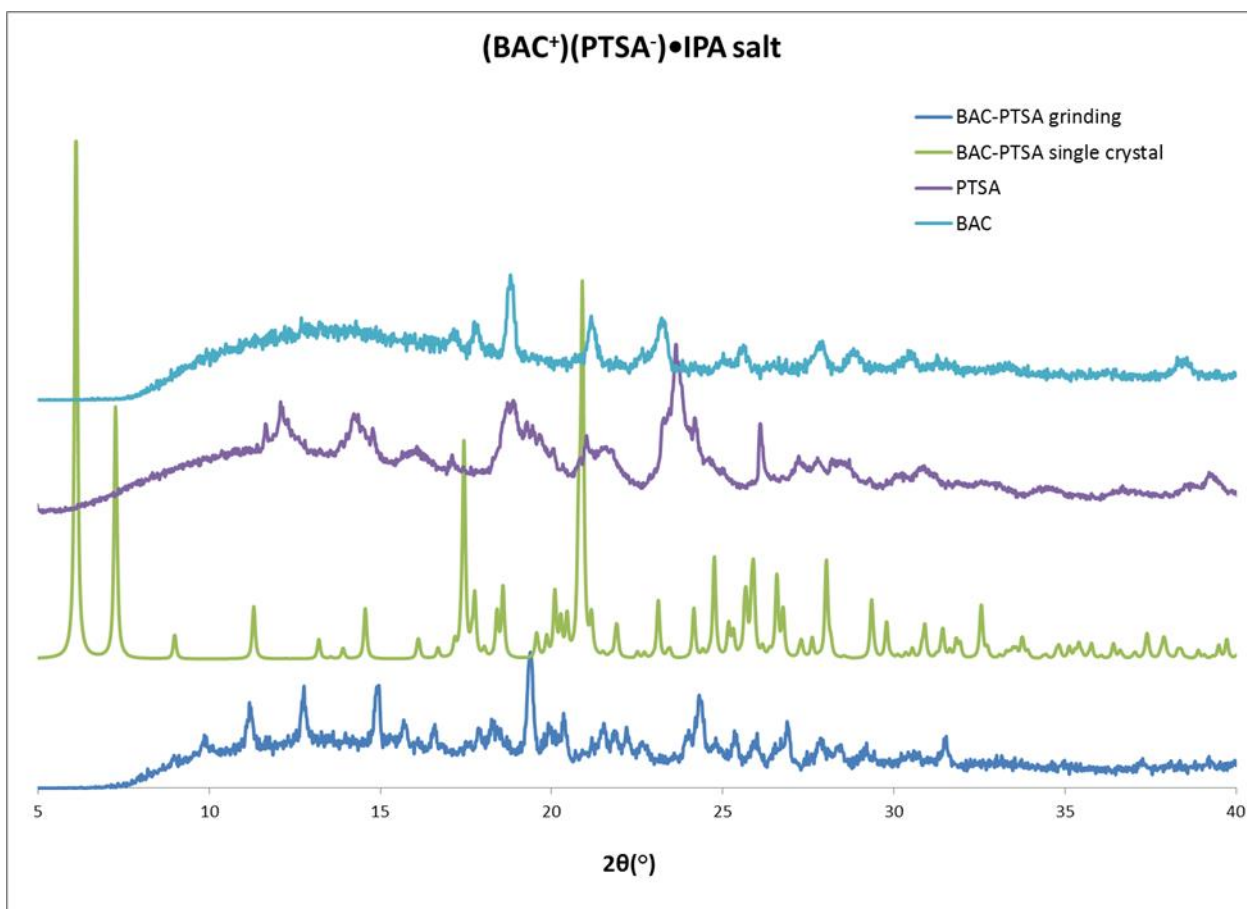
Figure 4.30 PXRD patterns of BAC (light blue), PTSA (purple), (BAC⁺)(PTSA⁻)•IPA pattern generated from single crystal structure (green) and (BAC⁺)(PTSA⁻)•IPA grinding (blue).

4.4 Conformational comparison of baclofen molecules

Baclofen has four torsion angles thus these are the source of the conformational freedom of baclofen. (**Figure 4.31a**) The rotation of the –CH$_2$-COOH/ –-CH$_2$-COO$^-$ moiety may be described by τ1, while the rotation of the –COOH/-COO$^-$ with τ2. The movement of the –NH$_2$/ –NH$_3^+$ group is defined by τ3 and the aromatic ring rotation relative to the amino acid functionality with τ4. The previously described six baclofen crystal structures contain seven different conformations of baclofen (BAC•BA has two symmetrically independent baclofen molecules in the asymmetric unit). All structures crystallized in achiral space groups with the exception of (BAC$^+$)(MA$^-$). That structure was solved with the S enantiomer based on the Flack parameter, therefore the torsion angles were measured on the S enantiomer in all crystal structures. In the case of salts, the carboxylate oxygen atoms are indistinguishable; therefore for the measurement of τ1 the smaller torsion angle was recorded. Also, the tilt of the aromatic ring (τ4) was described with the smaller torsion angle. The superimposed baclofen molecules, BAC•BA (molecule A: dark blue, molecule B: blue), BAC•PTA (violet), (BAC$^+$)(HNA$^-$) (magenta), 2(BAC$^+$)(OA^{2-}) (cyan), (BAC$^+$)(MA$^-$) (purple) and (BAC$^+$)(PTSA$^-$)•IPA (lilac) are shown in **Figure 4.31b**. The related torsion angles are summarized in **Table 4.10** and the ones with similar angles are shown with the same background.

(a)   **(b)**
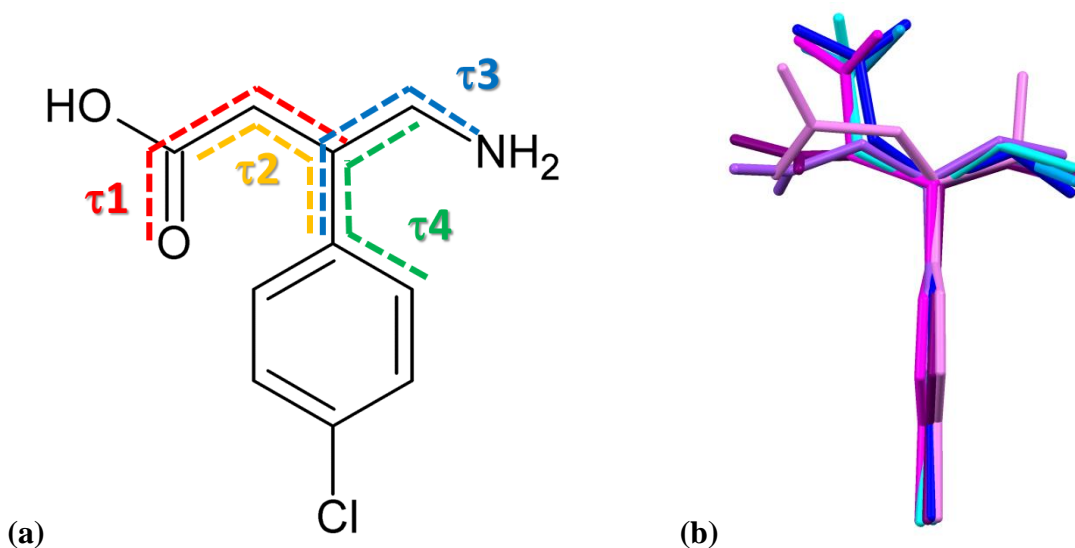
Figure 4.31 Graphical explanation of the discussed torsion angles of baclofen (a) and the superimposed 7 baclofen molecules from structures BAC•BA (molecule A: dark blue, molecule B: blue), BAC•PTA (violet), (BAC$^+$)(HNA$^-$) (magenta), 2(BAC$^+$)(OA^{2-}) (cyan), (BAC$^+$)(MA$^-$) (purple) and (BAC$^+$)(PTSA$^-$)•IPA (lilac).

Table 4.10 Related torsion angles of baclofen measured on the S enantiomer in all the structures. Similar angles are shown with the same background.

S enantiomer in compounds:	$\tau 1$ /° -CH$_2$COOH/- CH$_2$COO$^-$	$\tau 2$ /° -COOH/-COO$^-$	$\tau 3$ /° -NH$_2$/-NH$_3^+$	$\tau 4$ /° (aromatic tilt)
BAC•BA *Molecule A*	+164	+5	-57	-74
	C1A-C7A-C8A-C9A	C7A-C8A-C9A-O2A	C1A-C7A-C10A-N1	C2A-C1A-C7A-C10A
BAC•BA *Molecule B*	+168	+17	-57	-72
	C1B-C7B-C8B-C9B	C7B-C8B-C9B-O2B	C1B-C7B-C10B-N2	C6B-C1B-C7B-C10B
BAC•PTA	+83	-20	-175	+86
	C4-C7-C8-C9	C7-C8-C9-O2	C4-C7-C10-N1	C5-C4-C7-C10
(BAC$^+$)(HNA$^-$)	+167	-39	-61	-37
	C4-C7-C8-C9	C7-C8-C9-O1	C4-C7-C10-N1	C3-C4-C7-C10
2(BAC$^+$)(OA^{2-})	+165	-58	-67	-55
	C4-C7-C8-C9	C7-C8-C9-O2	C4-C7-C10-N1	C3-C4-C7-C10
(BAC$^+$)(MA$^-$)	+68	+11	-64	-57
	C4-C7-C8-C9	C7-C8-C9-O1	C4-C7-C10-N1	C3-C4-C7-C10
(BAC$^+$)(PTSA$^-$)•IPA	+64	+31	-75	-68
	C4-C7-C8-C9	C7-C8-C9-O1	C4-C7-C10-N1	C3-C4-C7-C10
CRBMZC10*	-84	+17	+168	+63
	C5-C3-C2-C1	C3-C2-C1-O2	C5-C3-C4-N1	C6-C5-C3-C4
RUWGOG *Molecule 1*	+51	+34	-176	-70
	C1-C7-C9-C10	C7-C9-C10-O6	C1-C7-C8-N1	C6-C1-C7-C8
RUWGOG *Molecule 2*	+72	+6	-168	-43
	C11-C17-C19-C20	C17-C19-C20-O8	C11-C17-C18-N2	C12-C11-C17-C18

*Angles were measured on the R enantiomer because the structure is chiral and were evaluated with the opposite values to generate a theoretical S enantiomer for clustering.

The CSD (Version 5.35 November 2013) contains only 4 structures of baclofen. Two of them (CRBMZB[4] and CRBMZC[2]) are the structures of S and R-baclofen hydrochloride respectively, but no 3D coordinates are presented therefore the molecular structure cannot be interpreted. The structure of the R-enantiomer was recollected at a later stage with 3D coordinates (CRMBZC10[5]). One inclusion compound of baclofen with ferulic acid hemihydrate has been also published (ROWGOG[6]) with 3D coordinates of the atoms. The torsion angles of these baclofen molecules are also included in **Table 4.10** for comparison. The very few structures cannot be a base of a statistical analysis; however it is interesting to note that the torsion angles are clustered. $\tau 1$ values are typically ~+165° or ~+65°, thus this suggests two preferred conformation for the –CH$_2$-COOH/ -–CH$_2$-COO$^-$ moiety. $\tau 2$ variations show almost free rotation of the –COOH/-COO$^-$ group; values vary from +5° to +34° and -17° to -58°. The –NH$_2$/ –NH$_3^+$ group shows less freedom of movement and the measured angles are close to ~-65° or ~-170°.

The tilt of the aromatic ring shows the smallest variation. All torsion angles vary between -37° and -74° with the exception of BAC•PTA. To summarize, baclofen presents acceptable torsional flexibility in the presented crystal structures, thus it may be concluded that this can be one of the reason of the successful co-crystallisation. The noticeable similarities in the crystal packing and the analogous hydrogen bonding networks suggest that the hydrogen bonding network is predictable to a certain degree and robust between baclofen and compounds with acid/ carboxylic acid functional groups. Also the adequate molecular flexibility will accommodate co-former molecules in a similar manner even with variable molecular size.

4.5 Intermolecular interactions of baclofen molecules in the multicomponent crystals

Hirshfeld surface analysis was conducted on all baclofen moieties found in the prepared crystals to map their intermolecular interactions with a more sophisticated method than a simple geometrical hydrogen bond analysis. The 3D Hirshfeld surfaces are demonstrated with a 2D representation, the so called fingerprint plot. (**Figure 4.32**) Two plots were generated for BAC•BA because that structure contains two molecules of BAC in the asymmetric unit. The visual comparison of the two molecules did not show significant differences; both molecules show strong hydrogen bonding interactions which are represented by the symmetrical spikes labelled ① on **Figure 4.32**. Fingerprint plots of BAC•PTA and $2(BAC^+)(OA^{2-})$ are very similar to BAC•BA in that the main feature of the plot is the symmetrical spikes related to hydrogen bond donor and acceptor functions of the molecule. All the remaining figures present slightly different hydrogen bond donor-acceptor behaviour hence the spikes are asymmetrical. This is due to the fact that the baclofen is protonated in these salt structures and therefore acts more as a hydrogen bond donor than an acceptor. This is the reason for the disappearance of the bottom spike which is the result of accepting hydrogens. However, $2(BAC^+)(OA^{2-})$ is also a salt, but the hydrogen bonding ability of the BAC is more similar to that of the co-crystals because of the different stoichiometry. The plot of $(BAC^+)(HNA^-)$ is distorted compared to the previous ones and show the 'chicken wings' feature, ② which is typical in crystals with $C_{aromatic}\cdots H$ interactions. A similar feature can be found on the plot of $(BAC^+)(PTSA^-)$•IPA. It is interesting to note that $(BAC^+)(MA^-)$ does not show this motif.

BAC•BA (molecule A)   BAC•BA (molecule B)   BAC•PTA   (BAC$^+$)(HNA$^-$)

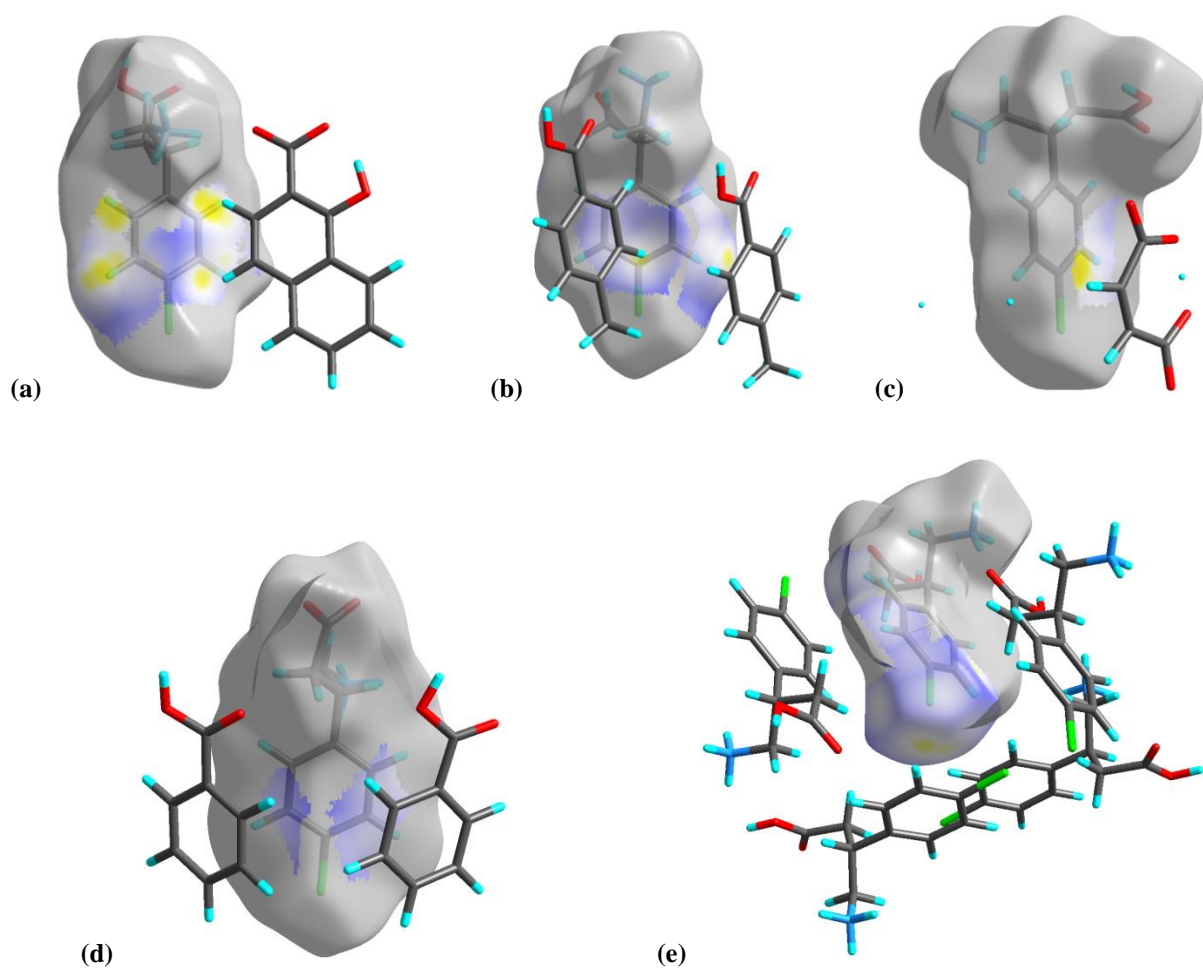2(BAC$^+$)(OA^{2-})   (BAC$^+$)(MA$^-$)   (BAC$^+$)(PTSA$^-$)•IPA
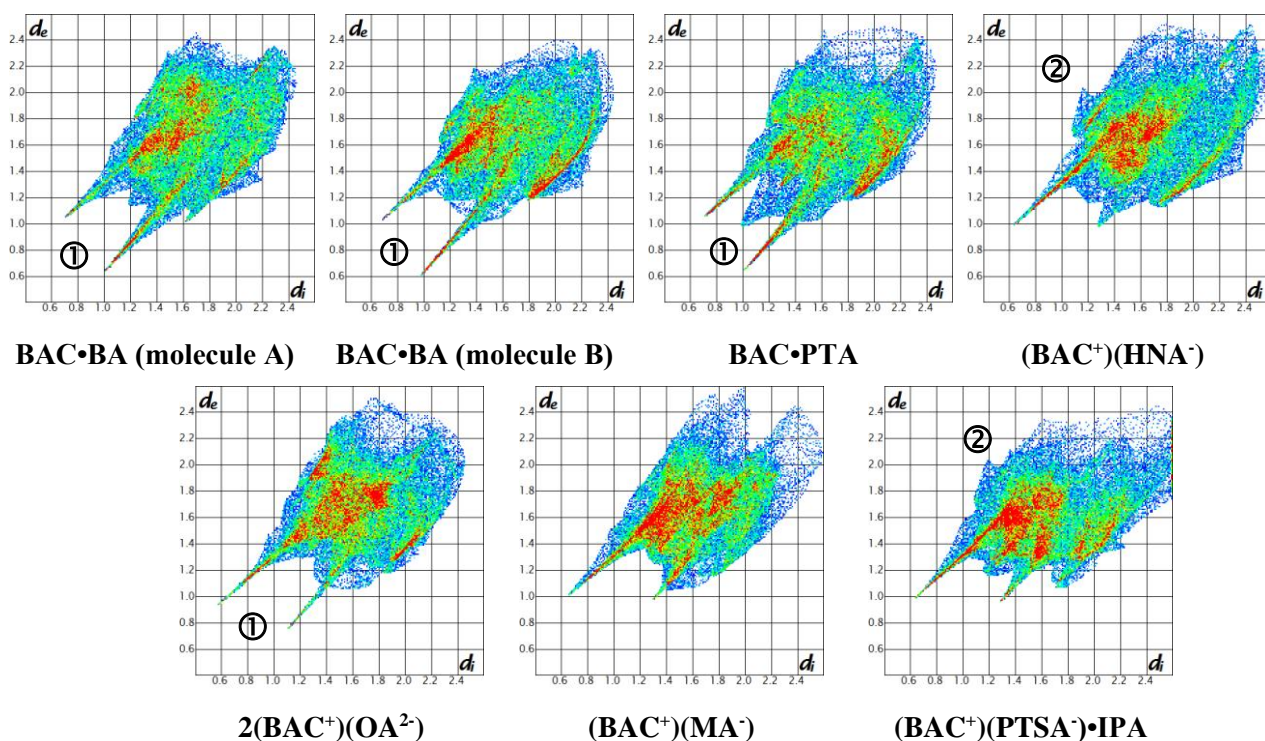
Figure 4.32 Fingerprint plots of Hirshfeld surfaces generated for baclofen moieties in the analysed multicomponent crystals.

Numerical comparison of the structures was conducted and the relevant intermolecular interactions of the baclofen moieties are presented in **Table 4.11**. The O⋯H interactions vary from 29% in 2(BAC$^+$)(OA^{2-}) to 38% in (BAC$^{+)}$(MA$^-$). The C⋯H % represent the C-H⋯π interactions in the crystals and its highest values were measured in (BAC$^+$)(HNA$^-$) and BAC•PTA. Indeed, subtle edge-to-face C-H⋯π interactions can be found in these two structures. (**Figure 4.33a** and **b**) The % of C⋯C interactions is the highest in (BAC$^+$)(MA$^-$) and for Molecule A in BAC•BA. These distances are informative typically about the π⋯π interactions. In the structure of (BAC$^+$)(MA$^-$) the maleic acid sp^2 carbons overlap with the aromatic ring of BAC while in BAC•BA the BAC moiety is off-set with a BA (Molecule D) (**Figure 4.33c** and **d**). The highest value for H⋯H interactions were measured for (BAC$^+$)(PTSA$^-$)•IPA. The Hirshfeld surface was calculated with the main component of the disorder isopropanol left in the structure therefore this % should be treated with caution. The Cl⋯H and the Cl⋯C interactions are the highest % in 2(BAC$^+$)(OA^{2-}), 18% and 4% respectively. The sigma hole, the electron deficient tip of the Cl is pointing towards neighbouring aromatic rings of BAC and its negative 'belt' is aligned with the π system of another BAC. (**Figure 4.33e**)

Table 4.11 Various intermolecular interactions of the baclofen moieties in the analysed crystal structures. (Their highest values are with bold.)

	(BAC$^+$)(MA$^-$)	(BAC$^+$)(PTSA$^-$) •IPA	BAC•PTA	(BAC$^+$)(HNA$^-$)	2(BAC$^+$)(OA^{2-})	BAC•BA (A)	BAC•BA (B)
O⋯H (%)	**38**	34	33	29	29	35	36
C⋯H (%)	6	14	**19**	**19**	10	16	16
C⋯C (%)	**3**	1	1	2	1	**3**	1
H⋯H (%)	30	**37**	31	34	33	31	31
Cl⋯H (%)	13	14	13	13	**18**	13	13
Cl⋯Cl (%)	0	0	1	0	1	1	0
Cl⋯C (%)	3	1	0	2	**4**	0	1

(a)   **(b)**   **(c)**

(d)   **(e)**

Figure 4.33 Interactions represented on Hirshfeld surfaces: (a) C-H⋯π interactions in (BAC$^+$)(HNA$^-$) and (b) BAC•PTA, C⋯C interactions in (c) (BAC$^+$)(MA$^-$) and (d) Molecule A in BAC•BA and Cl⋯H and the Cl⋯C interactions in (BAC$^+$)(OA$^-$) (e).

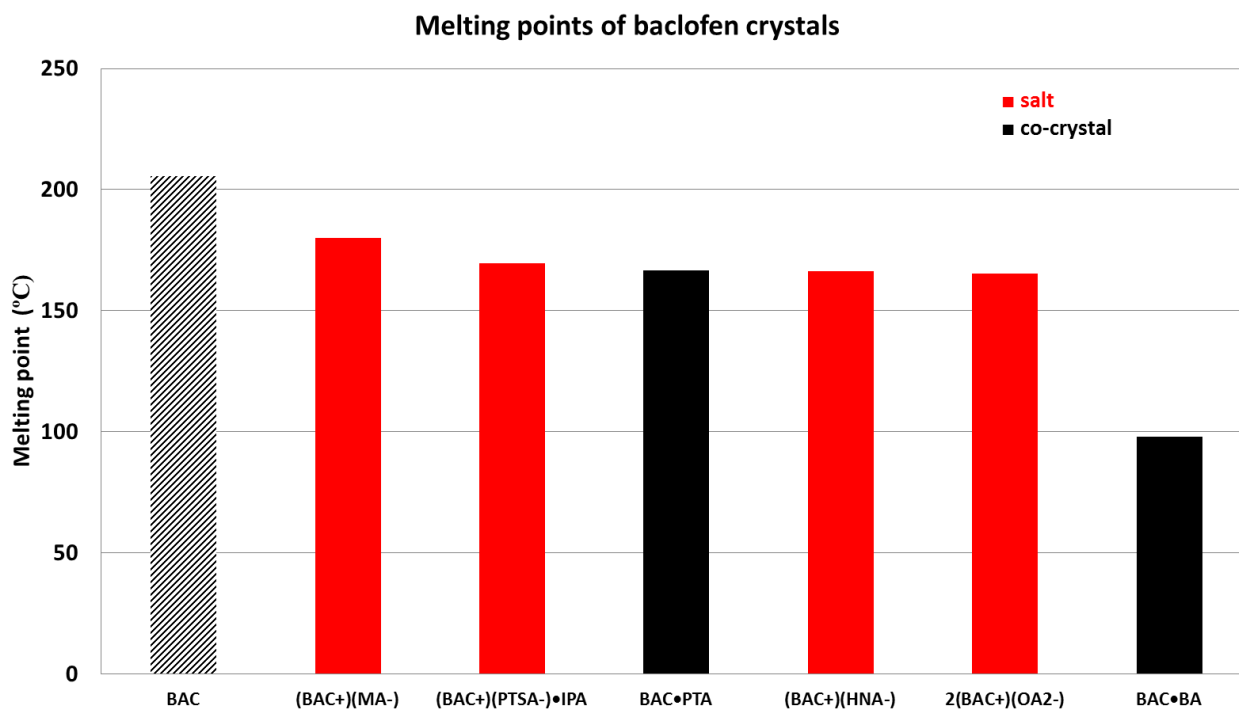## 4.6 Melting points of multicomponent baclofen crystals

The melting points of the baclofen crystals were recorded with DSC and the traces are presented in the relevant chapters. The values obtained are summarized in **Table 4.12** for clarity with the addition of the calculated Packing Indices (PI) and densities. It is clearly seen that the co-crystal/salt formation of baclofen resulted in crystals with lower melting points than baclofen itself ($MP_{BAC}=$ 205.5°C). The values of the melting point, the PI and the density do not necessary correlate. The lowest melting BAC•BA (98.1°C) has almost the same PI than BAC•PTA which melting point is 166.7°C. Also $2(BAC^+)(OA^{2-})$ melting point is almost identical with BAC•PTA, namely 165.4°C but its PI and density are one of the highest values, 72.8 and 1.502 g.cm^{-3}, respectively. However, $(BAC^+)(MA^-)$ has the highest melting point (180.1°C), the highest PI (73.7) and calculated density (1.517 g.cm^{-3}).

Table 4.12 Melting points, Packing Index and calculated density values for multicomponent crystals of baclofen. (Some outstanding values are coloured with red.)

compounds	Melting point (°C)	Packing Index	Density (g.cm^{-3})
BAC	205.4	-	-
BAC•BA	**98.1**	68.9	1.359
BAC•PTA	166.7	68.9	1.349
$(BAC^+)(HNA^-)$	166.4	68.8	1.386
$2(BAC^+)(OA^{2-})$	165.4	72.8	1.502
$(BAC^+)(MA^-)$	**180.1**	**73.7**	**1.517**
$(BAC^+)(PTSA^-)$•IPA *	169.5	-	1.393

* Packing Index cannot be calculated because of disordered structure.

In **Figure 4.34** the compounds are presented in decreasing order of their melting point values. The crystal structure of pure baclofen is unknown therefore its high melting point cannot be discussed with features of the intermolecular interactions. It is interesting to note that the nature of the structure, namely being a co-crystal or salt has no influence on the melting point. The two highest melting compounds are salts, $(BAC^+)(MA^-)$ and $(BAC^+)(PTSA^-)$•IPA, but the co-crystal BAC•PTA has virtually the same melting point as $(BAC^+)(HNA^-)$ and $2(BAC^+)(OA^{2-})$ salts. BAC•BA has the lowest melting point of all the compounds and this can be justified with the unusual stoichiometry of the crystal; the asymmetric unit consists of 2 BAC and 3 BA molecules.
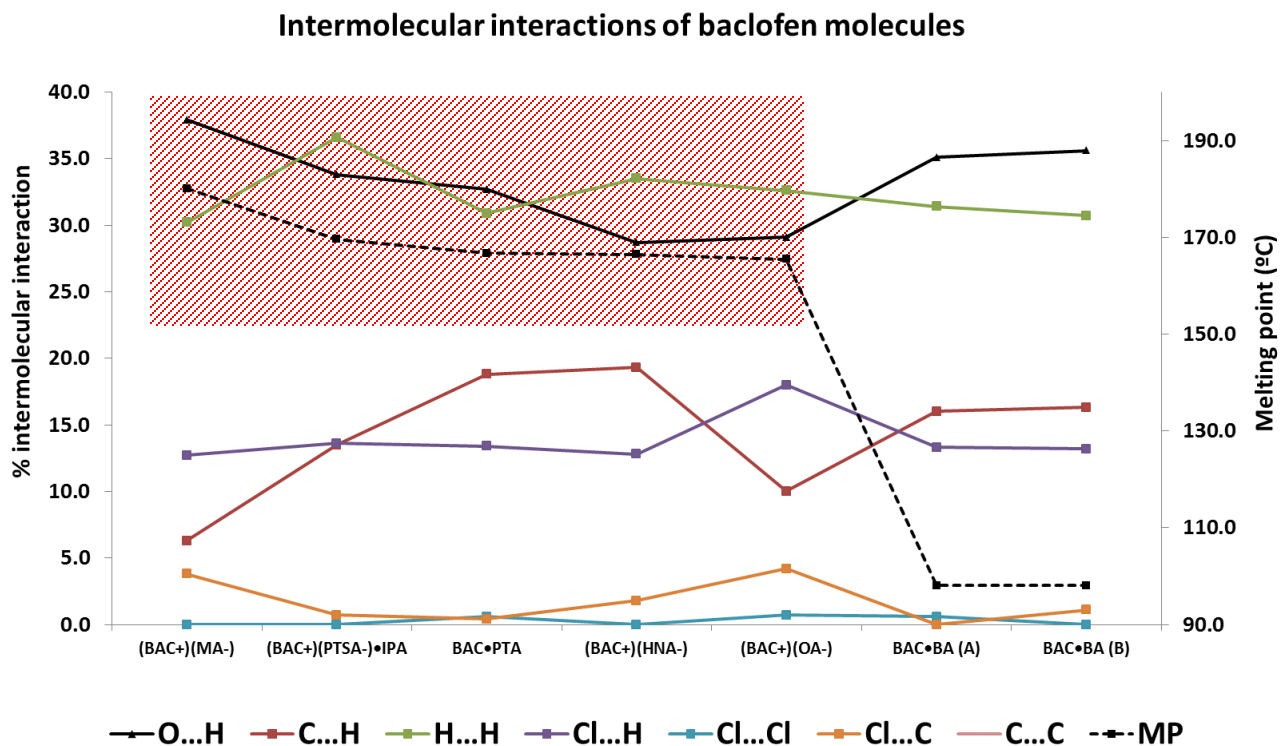
Figure 4.34 Melting points of BAC and its multicomponent crystals.

Unfortunately crystals have not been obtained yet from crystallisation experiments when BAC is exposed to racemic compounds and their relevant chiral forms, similarly to ETBIPY•racPSA and ETBIPY•(S)PSA (chapter 3). Therefore the effect of chirality cannot be investigated with the multicomponent crystals of baclofen.

The paucity of the baclofen crystals limited the solubility measurements. Great effort was made to produce more of these materials however no successful mass production was achieved during the limited time scale of the project. Therefore this part of the work is lacking the related solubility values.

The % of the various intermolecular interactions was aligned with the melting point of the crystals (**Figure 4.35**), however there was no correlation found between the calculated % interactions and the melting points for all the structures. It is interesting to note that if from the results the BAC•BA structure excluded, the correlation between the % O···H interactions and the melting points is 0.9023. (**Figure 4.35** red background) This value does not mean linear correlation between the O···H interactions and MP but suggests a kind of dependence.

In summary, it may be concluded that co-crystallisation of baclofen with mono- and dicarboxylic acids was successful and resulted in four salts and two co-crystals. The melting points and the % O⋯H interactions of BAC moieties show dependence between these values.

Intermolecular interactions of baclofen molecules

Figure 4.35 Various intermolecular interactions and the melting points of multicomponent crystals of BAC.

References:

[1] Calculator plugins were used for the structure property prediction and calculation, Marvin 6.3.0, 2014, ChemAxon (http://www.chemaxon.com)

[2] Etter, M.C., MacDonald, J.C. & Bernstein, J. 1990. Graph-set analysis of hydrogen-bond patterns in organic crystals. *Acta Cryst.* B46: 256-262.

[3] Jeffrey, G.A. 1997. *An Introduction to hydrogen bonding*. Chapter 3, Oxford University Press, Oxford.

[4] Chang, C.H., Yang, D.S.C., Yoo, C.S., Wang, B.C., Pletcher, J. & Sax, M. 1981. The crystal structures of (S) and (R) baclofen and carbamazepine. *Acta Crystallogr., Sec. A: Cryst. Phys. Diffr. Theor. Crystallogr.* 37, C71.

[5] Chang, C. H., Yang, D.S.C., Yoo, C.S., Wang, B.C., Pletcher, J., Sax, M. & Terrence, C.F. 1982. Structure and absolute configuration of (R)-baclofen monohydrochloride. *Acta Crystallogr. Sect.B: Struct. Crystallogr. Cryst. Chem.* 38: 2065-2067.

[6] Kavuru, P., Aboarayes, D., Arora, K.K., Clarke, H.D., Kennedy, A., Marshall, L., Ong, T.T., Perman, J., Pujari, T., Wojtas, L. & Zaworotko, M.J. 2010. Hierarchy of Supramolecular Synthons: Persistent Hydrogen Bonds between Carboxylates and Weakly Acidic Hydroxyl Moieties in Cocrystals of Zwitterions. *Cryst. Growth Des,* 10(8): 3568-3584.

Chapter 5

Summary and conclusion

5. Summary and conclusion

Active pharmaceutical ingredients with poor physicochemical properties are not automatic failures as drugs, because these properties may be altered via solid state modification, such as co-crystal or salt formation.

The prediction of certain properties, such as melting point or solubility of a new solid form, is still desired. The analysis of the relationship between the solubility and the melting point of a given multicomponent crystal is still an upcoming area of pharmaceutical and supramolecular research which is not fully understood. The common observation of no correlation between melting point and solubility of co-crystals and salts raises the question of what the connection is between these properties and how we can analyze and measure it.

The aim of this research was (i) to design and synthesize a series of model co-crystals where the API is replaced by a simple chemical unit with restricted secondary interaction possibilities and conformational motions, while the co-crystallising compound would be varied systematically and (ii) to synthesize a series of pharmaceutical co-crystals/salts in a similar manner.

In the first part, 4,4'-bipyridine (BIPY) and 1,2-bis(4-pyridyl)ethane (ETBIPY) were used to combine with a series of carboxylic acids as co-formers, such as p-toluic acid (PTA), rac-phenylbutyric acid (racPBA), racemic and S-phenylsuccinic acid (racPSA and S-PSA, respectively). These structurally related compounds were chosen to prepare the model co-crystals because of their ability to hydrogen bond via O-H···N interactions. Overall, five model co-crystals were obtained: BIPY•PTA, BIPY•racPBA, BIPY•racPSA, ETBIPY•racPSA and ETBIPY•(S)PSA. The single crystal structures, powder diffraction patterns, thermal behaviour, solubility (measured in water and ethanol) of these crystals were discussed. Analysis of BIPY co-crystals revealed reverse linear relationship between their melting points and their aqueous solubility. It was concluded that the BIPY co-crystals have similar polarity therefore their interactions with the solvent are expected to be similar. Thus the change in solubility should be the result of the crystal packing only and this is why it correlates with the melting point. The two co-crystals, ETBIPY•(rac)PSA and ETBIPY•(S)PSA have chemically the same building blocks, thus their polarity is the same

but their solubilities differ significantly. Therefore the only difference which can be related to the observed change in the solubility is their significantly different packing features, such as that ETBIPY•(rac)PSA contains strong hydrogen bonds between the molecular layers while in ETBIPY•(S)PSA there are no hydrogen bonds observed between the helices. The conclusion may be drawn that the introduction of a chiral building block may increase the solubility of the co-crystal via less efficient packing and hydrogen bonding network.

In the second part, co-crystals of baclofen (BAC, (RS) 4-amino-3-(4-chlorophenyl)-butanoic acid), were investigated. Six new multicomponent crystals of baclofen were prepared with mono- and dicarboxylic acids: two pharmaceutical co-crystals were obtained with benzoic acid (BAC•BA) and p-toluic acid (BAC•PTA) and four pharmaceutical salts with 1-hydroxy-2-naphthoic acid, $(BAC^+)(HNA^-)$, oxalic acid, $2(BAC^+)(OA^{2-})$, maleic acid, $(BAC^+)(MA^-)$ and p-toluene sulfonic acid, $(BAC^+)(PTSA^-)$•IPA. The single crystal, powder diffraction patterns and the thermal behaviour of these crystals were discussed. The analysis of the crystal structures revealed a packing motif, the $-COO/-COO^-\cdots-NH_2/-NH_3^+$ hydrogen bonded feature, which occurs in all six structures. These similarities in the crystal packing and the analogous hydrogen bonding networks suggest that the hydrogen bonding network is somewhat predictable and robust between baclofen and compounds with acid/ carboxylic acid functional groups. The torsional flexibility of baclofen may suggest that baclofen, as a host, is able to accommodate co-former molecules in a similar manner with variable molecular size. The % of the various intermolecular interactions was aligned with the melting point of the crystals and dependence was found between the % $O\cdots H$ interactions and the melting point values.

This thesis makes a contribution to supramolecular chemistry, co-crystal and salt formation studies of common and pharmaceutical compounds and the alteration of their physicochemical properties via solid state modification and it is hoped that will contribute to new research directions in the field of crystal engineering.